2005

Estimation of volumetric flow rate through a circular duct: Equal area versus Log-Tchebycheff method.

Md Ramiz Ahemad
University of Windsor

Estimation of Volumetric Flow Rate in a Square Duct:

Equal Area Versus Log-Tchebycheff Methods

by

Changjie Zhou

A Thesis

Submitted to the Faculty of Graduate Studies and Research

through the Department of Mechanical, Automotive and Materials Engineering

in Partial Fulfillment of the Requirements for

the Degree of Master of Applied Science at the

University of Windsor

Windsor, Ontario, Canada

2005

Your file Votre référence
ISBN: 0-494-09844-9
Our file Notre référence
ISBN: 0-494-09844-9

ABSTRACT

Accurate measurement of the volumetric airflow rates in a duct is critical to room comfort and energy saving in HVAC industry. Presently, the Equal Area and the Log-Tchebycheff methods are extensively used in practice. Both methods deduce the flow rate based on averaging discrete point velocities along the cross section while their difference is associated with the rules in specifying the measurement locations.

This study aims at evaluating the Equal Area and the Log-Tchebycheff methods in deducing airflow rate in a 0.46 m square duct up to 40 D_h long, over a range of Reynolds number from 10,000 to 500,000. The numerical investigation evaluated the two methods for ideal flow conditions in the absence of practical imperfections. The airflow was simulated in a three-dimensional space using the commercial CFD code FLUENT with the RNG k-ε turbulence model. Based on the simulated flow field, the volumetric flow rates were calculated according to the Equal Area and the Log-Tchebycheff methods. It was observed that the Equal Area method overestimated the flow rate by 3.5 ~ 4.7% while the Log-Tchebycheff method's values fell within –0.4 ~ 0.8% of the actual flow rates.

In addition to the numerical analysis, experiments were carried out in a blower-duct assembly where the physical non-idealities and measurement uncertainties were present. A hot-wire anemometry facility was used to measure point velocities and a Venturi meter was employed to acquire the reference flow rate. The Equal Area method overestimated the flow rate by 3 ~ 4.6% whereas the Log-Tchebycheff method underestimated the flow rate by 0.6 ~ 2.3%. The experimental results confirm the finding from the simulation that the Log-Tchebycheff method achieves a better accuracy in estimating the airflow rate.

To my –

Wife **Shuhui**

Son **Midong**

ACKNOWLEDGEMENTS

I would like to give my sincere gratitude to my supervisors, Dr. A. Fartaj and Dr. D. Ting, for their excellent supervision, guidance, and encouragement throughout this research work. I would also like to thank Dr. G. W. Rankin and Dr. R. Seth for participating as my thesis committee.

The excellent secretarial assistance offered by Ms. R. Gignac and Ms. B. Denomey in the MAME Department is appreciated. Thanks are extended to Mr. P. Seguin, Mr. R. Mavrinac, Mr. R. Tattersal, Mr. S. Budinsky and other staff in the Technical Support Center for their technical assistances throughout the study period. I express my gratitude to Dr. S. Olson, from TSI Inc., and Mr. R. Lang, from Lambda Square Inc., for their technical support on the experimental facilities.

I am very grateful to the supports and encouragements from the fellow students and friends, especially R. Liu, R. Ahemad, M. Islam, M. Khan, Z. Faruquee, J. Lu, W. Yang and L. Yang.

I express my gratitude to the University of Windsor for providing me with GA and Tuition Scholarship. The funding from ASHRAE (American Society of Heating, Refrigerating and Air-conditioning Engineers) and CAABC (Canadian Associated Air Balance Council) to conduct the experimental work are also appreciated.

Finally, I would like to express my sincere gratitude to my wife and son for their consistent understanding, support and dedication during my study. I am also grateful to my parents-in-law in encouraging and supporting my study during their visit.

TABLE OF CONTENTS

LIST OF FIGURES

LIST OF TABLES

NOMENCLATURE

Letters/Symbols

2-D	Two-dimensional
3-D	Three-dimensional
A	Area [m^2]
A/D	Analog to digital conversion
A_{SD}	The cross-sectional area of the square duct [m^2]
AABC	Associated Air Balance Council
A/D	Analog/Digital
AMCA	Air Movement & Control Association
ASHRAE	American Society of Heating, Refrigeration & Air Conditioning Engineers
atm	atmospheric pressure, 1 atm = 101,325 Pa.
a_{00}, a_{01}... a_{04}	Coefficients of the polynomial function of hot-wire calibration
a_k, a_ε	Coefficients in the RNG κ-ε model
B	Bias error
$B_{\overline{F}}$	Bias error for the variable F
BSI	British Standards Institution
CFD	Computational Fluid Dynamics
CTA	Constant temperature anemometer
$C_{1\varepsilon}$, $C_{2\varepsilon}$	Coefficients in κ-ε model
$C_{2\varepsilon}^*$	Coefficient used in the RNG κ-ε model
C_μ	Eddy-viscosity coefficient

D_C	The diameter of the circular pipe
D_h	Hydraulic diameter of the duct [m]
E	Voltage [Volt]
E_R	Voltage at the calibration point [Volt]
E_{off}/*Offset*	Offset voltage of the signal conditioner [Volt]
$E(t)$	The output signal as a function of the time from the anemometer circuit [Volt]
$E_G(t)$	The output signal as a function of the time from the signal conditioner [V]
F	A generic variable to denote any parameters used in experiment
$\overline{F}$	Mean value of the parameter F
f	Functional relationship
Gain	Amplification coefficient for the signal conditioner
G_k	Generation of turbulent kinetic energy due to the mean velocity gradients
G_b	Generation of turbulent kinetic energy due to buoyancy
g	Gravitational acceleration [m^2/s]
H, H_1, H_2	The side size for a square duct [m]
H_{sea}	The altitude to the sea level [km]
h_{Hg}	The height of the mercury column in the barometer [mm]
HVAC	Heating, Ventilation and Air Conditioning
h	The location of traverse point from one side of a square duct [m]
k	Turbulent kinetic energy [m^2/s^2]
LDA	Laser-Doppler-Anemometry
L	Length of the square duct [m]

L_C	Length of the circular duct [m]
ℓ	Length of the fluid column in the inclined manometer [m]
M	Mach number
N	Number of repeated measurements
n	Number of measuring points/error sources
P	Precision error
$P_{\overline{F}}$	Precision error of the mean for the parameter F
PDE	Partial differential equation
p_{atm}	Atmospheric pressure [Pa]
p	Mean pressure component [Pa]
$\tilde{p}$	Instantaneous pressure [Pa]
p'	Fluctuating pressure component [Pa]
Q	Volumetric flow rate [m^3/s]
Q_{STP}	Volumetric flow rate measured by Venturi meter at the standard temperature and pressure [m^3/s]
Q_{ven}	Volumetric flow rate measured by Venturi meter at the actual airflow condition [m^3/s]
RSS	Root-sum-square method in estimating uncertainty
RNG	Renormalization group theory
$r_{inclination}$	Inclination ratio of the inclined manometer
SMACNA	Sheet Metal and Air Conditioning Contract's National Association
S_F	Standard deviation of parameter F
$S_{\overline{F}}$	Standard deviation of the mean for the parameter F

S_k, S_ε	Source terms for discretized equations
T	Temperature [°C]
T_a	Airflow temperature [°C]
T_r	Room temperature [°C]
T_u	Turbulence intensity [%]
t	Time [s]
$t_{N-1,\ 95\ \%}$	The distribution coefficient at *N-1* degrees of freedom with 95% confidence level
Re	Reynolds number
TAB	Test and air balance
U_τ	Friction velocity [m/s]
$\widetilde{U},\widetilde{V},\widetilde{W}$	Instantaneous velocity components in the *X, Y, Z* directions respectively [m/s]
U, V, W	Mean velocity components in the *X, Y, Z* directions respectively [m/s]
u, v, w	Fluctuating velocity components in the *X, Y, Z* directions respectively [m/s]
U_{avg}	The average velocity of the duct cross section [m/s]
U_b	Bulk velocity [m/s]
U_C	The velocity at the center of the duct cross section [m/s]
U_{EA}	The average velocity deduced from the Equal Area method [m/s]
U_{eff}	Effective velocity calculated from the calibration equation [m/s]
U_i	The velocity component at a specific direction of the 3-D coordinate system ($U_1 = U,\ U_2 = V,\ U_3 = W$) [m/s]
U_j	The velocity component at each direction of the 3-D coordinate system

	$(U_1 = U,\ U_2 = V,\ U_3 = W)$ [m/s]
U_{LT}	The average velocity deduced from the Log-Tchebycheff method [m/s]
$\overline{u^2}, \overline{v^2}, \overline{w^2}$	Turbulence normal stresses [m^2/s^2]
$\overline{uv}, \overline{uw}, \overline{vw}$	Turbulence shear stresses [m^2/s^2]
X	Coordinate axis in the streamwise direction
x	Coordinate in the streamwise direction
Y	Coordinate axis in the cross-stream direction
y	Coordinate in the cross-stream direction
y_P	The normal distance from the wall to the centroid of the nearest cells
Y_m	The dilation dissipation term in consideration of fluid compressibility
y^+	Dimensionless normal distance to the wall
Z	Coordinate axis in the spanwise direction
z	Coordinate in the spanwise direction

Greek letters

β	The ratio of the throat diameter to the inlet pipe diameter of the Ventuir meter, in this study, $\beta = 0.688$
ε	Turbulent dissipation rate [m^2/s^3]
Λ	Turbulent length scale [m]
ϕ	Dependent variable
φ	Latitude [°]
ρ	Density [kg/m^3]

ρ_{fluid}	Density of fluid in the inclined manometer [m]
ρ_{Hg}	Density of mercury
τ_w	Wall shear stress [kPa]
μ	Dynamic viscosity [kg/m·s]
μ_t	Turbulent eddy-viscosity [kg/m·s]
ν	Fluid kinematic viscosity [m^2/s]
σ_k, σ_ε	Coefficients in κ-ε model
η_0	Coefficient in the RNG κ-ε model, $\eta_0 = 4.38$.
η	Coefficient in the RNG κ-ε model
ζ	Curve fit coefficient
Δp	Differential pressure [Pa]

Subscripts/Exponents

a	Air
b	Traverse points in the boundary layer region
C	Centerline
c	Traverse points in the central region
cf	Curve fit
Cal	Calibration
EA	Equal Area
i	Iteration number
LT	Log-Tchebycheff
max	The maximum value

min	The minimum value
read	Readability
STP	Standard temperature (20°C) and atmospheric pressure (103,125 P_a)
ven	Venturi meter

Prefix

Δ	Denotes the uncertainty of a quantity

CHAPTER 1 INTRODUCTION

A fundamental objective of a heating, ventilating, and air conditioning (HVAC) system is to maintain desirable environmental conditions within a space. One of the prominent requirements in achieving this goal is to provide adequate conditioned airflow by an air distribution system. The system is designed in a way that the right quantity of cycling airflow is distributed to each separate room in a building via ducts to maintain the room air quality. However, due to the complexity of a HVAC system, the actual operation often departs from the design conditions. In practice, after a HVAC system is installed in a building, it has to be properly commissioned, i.e., tested and balanced, before it is handed over to the building owner. The test and air balance (TAB) process involves measuring airflow rate within the distribution system, i.e., sub-mains, branches and terminals, and then adjusting the terminal equipment (e.g., damper position, fan speed) to achieve the design values. Similarly, during the operation of the building, test and air balance for the HVAC system have to be repeated periodically to ensure the continual operation at the design condition.

The objective of air balance is to check if the airflow rate is within the designed range and to ensure that the supply and discharge air for each conditioned room are equal. Otherwise, the pressure balance between the conditioned space and the outside environment cannot be achieved and there would be additional energy loss due to infiltration or exfiltration.

The testing and air balancing need to be performed at each duct branch. It is not economical to mount an in-line flow meter, such as an orifice, nozzle or Venturi meter, at each branch, to measure the corresponding volumetric flow rate. Moreover, the air velocity is seldom uniform across any section within a duct. In general, air tends to move slower toward the edges or corners and faster in the center for a rectangular duct. It is not accurate to assume the central point velocity to be equal to the mean velocity of the whole cross section for an air-handling duct with a relatively big size. This restricts the use of the single point measurement method in which the velocity of a specific point is measured and then multiplied by the cross-sectional area to acquire the volumetric flow rate.

The multi-point velocity traverse method is thus widely accepted in HVAC industries. In this method, the volume flow rate, Q, is the product of the mean velocity and the area of a specific cross section. The area is relatively easy to measure whereas the mean velocity is acquired by averaging several measurements along the cross section in which different rules are developed to specify the total number of measurement points and the measurement location for each point.

Due to the non-uniform velocity profiles, the points at which velocities are measured in order to determine the mean velocity must be carefully selected. There are a few techniques developed to determine these points. Presently the two most widely used methods, are the Equal Area and Log-Tchebycheff methods.

The Equal Area and Log-Tchebycheff methods are similar in dividing the flow cross section into several small equal-area elements. The point velocity is measured at a

specific point of each element. These measured velocities are simply averaged and multiplied by the total area to obtain the flow rate.

The Equal Area method defines the center of each element as the measurement location (Winternitz and Fischl, 1957; Ower and Pankhurst, 1977). On the other hand, the Log-Tchebycheff method defines measurement locations with the consideration of the shape of velocity profile. For fully developed turbulent flow in a duct, the velocity profile is nearly flat in the central region whereas it sharply drops at the near-wall region (Munson et al., 2002). In view of this, the Log-Tchebycheff method determines the measurement point for each element in a way that the velocity at that point represents the mean velocity of that element (ISO 3966 (E), 1977).

The Log-Tchebycheff method is expected to acquire better performance since the traverse points are determined from the velocity profile whereas the Equal Area method only considers the spatial average. However, the flow in practical situations normally departs from the ideal flow profile which is assumed in the Log-Tchebycheff method. According to Saxon (2001), it is entirely possible that both the Equal Area and Log-Tchebycheff methods acquire "wrong" results. Whether the Log-Tchebycheff method is more accurate than the Equal Area method remains a matter of debate. Therefore the effectiveness of both methods in estimating volumetric flow rate through a square duct is the principal focus of this study.

1.1 Motivation

The need to measure volumetric flow rates in ducts is common in HVAC industries. The multi-point velocity traverse methods are considered to be the best way to estimate the volumetric flow rate in a duct. Among them, the Equal Area and Log-

Tchebycheff methods are the two main methods currently employed. However there is an ongoing debate over which of these two methods is superior. Solving this question is essential to diminish the potential disagreement with respect to the volumetric flow measurement.

Resolving this debate is also beneficial to other industries. For instance, due to the environmental concern, the SO_2 emissions from nearly all fossil fuel-fired generating units have to be effectively monitored. However, Norfleet (1998) found that using the Equal Area method resulted in an overestimation of flow rate from 1.7% to 3.0% which could increase the cost for emission treatment for the power plants. The economic impact would be in excess of $ 250,000,000 for the utility industry in the next decade alone.

1.2 Objective

Since the rectangular duct is a common shape applied in HVAC industries, the main objective of this study is to investigate the accuracies of the Equal Area and the Log-Tchebycheff methods for volumetric flow rate measurement through a 0.46 m square duct. The considered parameters include the Reynolds number, which is based on the bulk flow velocity, and the downstream location, where the flow displays different velocity profiles. The investigation was carried out at the following conditions,

- Numerical simulations: Re of 10,000 ~ 500,000 and the maximum downstream location of 40 D_h.
- Experimental investigations: Re of 90,000 ~ 140,000 and the maximum downstream location of 10 D_h.

CHAPTER 2 LITERATURE REVIEW AND THE SCOPE OF THE CURRENT STUDY

The velocity traverse methods are extensively utilised for measuring volumetric flow rates in air distribution ducts and other engineering applications. The techniques have been the subject of research for many years. Presently, the debate among HVAC field focuses on two commonly used methods: the Equal Area and the Log-Tchebycheff methods.

To estimate the volumetric flow rate via the velocity traverse method, one has to obtain the velocity distribution in the ducts. The flow patterns in rectangular ducts have been extensively investigated during past decades. Several numerical investigations are done in this area by Gessner and Emery (1981), Demuren and Rodi (1984), Speziale (1987), Naimi and Gessner (1994), etc. These studies employed different turbulence simulation models, including the k-ε model, to predict the flow in a rectangular duct. In some other studies (Kim and Patel, 1993; Rokni et al., 1998), hot-wire anemometers or Laser-Doppler anemometers (LDA) were used to measure the flow profiles.

This chapter focuses on the review of previous studies dealing with the estimation of volumetric flow rate in a duct. First, a variety of velocity traverse methods developed during past decades are introduced. Second, the previous works in comparing the Equal Area and the Log-Tchebycheff methods are presented.

2.1 Point Velocity Measurement Location Determination Methods

Due to the non-uniform velocity profile in a duct, care has to be taken to determine the measurement locations to deduce the volumetric flow rate. There are several techniques developed to specify the measurement points. In the literature, various methods used by different authors include:

- the Equal Area method;
- the British Standards Institution (BSI) method;
- the Log-Linear method;
- the Method of Cubics;
- the Log-Tchebycheff method.

The details of each method are described below.

In the Equal Area method, the cross-sectional area of a rectangular duct is partitioned into a number of rectangular elements, each having an equal cross-sectional area. The point velocity is measured at the center of each element, and then the velocities are simply averaged and multiplied by the total cross-sectional area to obtain the flow rate (Ower and Pankurst, 1977). Compared to the single point measurement, it considers the non-uniformity of the actual velocity profile by multi-point averaging. This method is still the most common method in HVAC industries due to its fair accuracy and extreme simplicity.

However, the Equal Area method does not consider the velocity fall-off near the wall. Since the velocity drops abruptly to zero on the surface of the wall, there is a much higher velocity gradient in the near-wall region than in the central region of the duct. For the elemental subsections next to the wall, the velocities of the centers of partitioned

subsections are higher than the actual mean velocities of these subsections. This method thus results in an overestimation of the total flow rate. The British Standards Institution (BSI 1042, 1943; cited by Ower and Pankhurst, 1977) employed a method that made a modification for the divisions next to duct walls. It recommended that in each of such divisions, readings should be taken at one-sixth and five-sixths of the width or height of the division from the duct wall, in addition to the reading at the center of the division. Thus five readings will be taken in each corner division, and three in each of other wall divisions. It is obvious that this modification increases the number of measurement points and complicates the procedure.

Another arithmetic method was developed which was called the Log-linear method. This method was originally proposed by Winternitz and Fischl (1957) for circular ducts and it was later extended to rectangular ducts. This method assumes the velocity along the side of a rectangular duct to be logarithmic with respect to the distance from the wall. A variety of measurement points, combined with a weighting factor for each point, are used to estimate the average velocity of the cross section (ISO 3966 (E), 1977). This method considers the characteristics of velocity profile but is more complicated than the Log-Tchebycheff method, as introduced later.

The Method of Cubics, which is a numerical integration method, appeared to be an alternative method with sufficient accuracy (Kinghorn et al., 1973; ISO, 1977). This method does not specify the measurement locations. Instead, it specifies that the velocity distribution between any two successive measurement points is a cubic polynomial function of the dimensionless location along the duct side. A mathematical integration is taken along a curve fitted velocity profile to calculate the flow rate. The main advantage

of this technique lies in the fact that it does not specify the location for each measurement point. However, it involves quite a large computational effort. It is rarely used today due to its complexity.

Tchebycheff, a Russian mathematician, developed and published the Log-Tchebycheff method in the ISO Standard 3966 (E) (1977). This method uses a similar technique to the Equal Area method, except that instead of the point velocity measured at the center of each subsection, it is taken at a point corresponding to the mean velocity of that subsection. To locate such a specific point for each subsection, the velocity distribution, as a function of the distance from the wall, was assumed to be logarithmic in the outermost subsections and polynomial in the other subsections (ISO 3966 (E), 1977). In this way, the mean of the traverse point velocities corresponds to the overall mean velocity of the cross section. It attempts to capture the sharp velocity gradients in the near-wall region by positioning the measurement point in each outmost subsection closer to the duct wall than the center of that subsection. The traverse point locations for this method are defined in various standards (ISO 3966 (E), 1977; ASHRAE 111, 1988; AABC, 2002; etc.).

Presently, the Equal Area and the Log-Tchebycheff methods are two main methods in estimating the volumetric flow rate in rectangular ducts. As a conventional method, the Equal Area method is still the principal method due to its simpleness and reasonable accuracy. On the other hand, the Log-Tchebycheff method has drawn attention due to its potential to achieve higher accuracy than the Equal Area method (ASHRAE 111, 1988).

The AABC (Associated Air Balance Council), an association of independent test and air balance (TAB) agencies with the publications of national standards on TAB procedures, recommends the use of the Equal Area method. However, it also includes the Log-Tchebycheff method as an alternative method. Moreover, organizations such as American Society for Testing and Materials (ASTM D3464, 1996), American Society of Mechanical Engineers (ASME, 1971), support the Equal Area method without mentioning the Log-Tchebycheff method.

ASHRAE (American Society of Heating, Refrigerating, and Air-Conditioning Engineers), a worldwide dominant organization in leading the HVAC industry and making technical and practice standards, prefers the Log-Tchebycheff method. In ASHRAE standard 111 (1988), it recommends the Log-Tchebycheff method for ducts over the size of 0.46 m (18 inch). It has no preference between the two methods for ducts under this size, presumably due to the fact that the difference of the measurement locations between these two methods is of the order of measurement uncertainty.

The International Organizations for Standardization (ISO 3966 (E), 1977) lists the options of the Equal Area method, the Log-Linear method, the integration method (i.e. the Method of Cubics), and the Log-Tchebycheff method. It does not mention which method is superior. The Sheet Metal and Air Conditioning Contractor's National Association (SMACNA, 1983), supports both the Equal Area and the Log-Tchebycheff methods without any preference.

2.2 The Equal Area versus the Log-Tchebycheff Methods

The Log-Tchebycheff method is expected to give better performance than the Equal Area method. However, the assumed velocity profile in the Log-Tchebycheff

method only matches the fully developed flow conditions at high Reynolds numbers. In practice, due to the limitation of the straight duct length and unavoidable disturbance, traverse measurements are normally not carried out with the fully developed flow. Thus, debates have arisen as to whether the Log-Tchebycheff method really results in higher accuracy than the commonly used Equal Area method in estimating the flow rate in practical applications.

Macferran, a mechanical engineer, described his preference on the Log-Tchebycheff method in two publications (Macferran, 1999(a); Macferran, 1999(b)). Based on tests on a 1.22 m $\times$ 0.30 m rectangular duct on three separate days, he drew a conclusion that the flow rate measured by the Log-Tchebycheff method was "correct" while the Equal Area method was "wrong". His investigation, however, was rather superficial and inaccurate and generated considerable criticism.

In response to Macferran's concluding statement (Macferran, 1999(a)), Saxon (2001), a member from Air Movement & Control Association (AMCA), stated that there is no preference of one method over another in AMCA. Saxon also mentioned since the actual velocity profile always departs from an ideal "D" shape, i.e. fully developed flow profile, the accuracy of the Log-Tchebycheff method would diminish. He pointed out that since there is no reference flow rate sensed by a proven technique in Macferran's experiment, both methods would probably be "wrong" under field conditions.

Baumgartner (2001) addressed some incorrectness concerning Macferran's experimental procedure and data presentation. He analytically detected flow rates based on a normally used power law velocity profile. The calculation showed that the flow rates deduced from the Equal Area and the Log-Tchebycheff methods have a difference less

than 3%, which is industrially acceptable. He then concluded that it is not necessary to replace the Equal Area method with the Log-Tchebycheff method.

Although failing to justify his statement, Macferran proposed an interesting topic in the HVAC community and has probably promoted the application of the Log-Tchebycheff method. Attempting to evaluate these two methods, Klaassen and House (2001) carried out experiments on a 0.7 m × 0.5 m duct section, which was part of an existing HVAC system. They tested three measurement planes located at 1.2 D_h, 2.4 D_h downstream of a fan outlet and 1.2 D_h downstream of a 90° elbow, where D_h is the hydraulic diameter of the duct. A turning vane was installed in the elbow to condition the flow. The reference flow rates were acquired from a high-resolution equal–spaced traverse measurement. The experiment was performed at velocities of 5.08, 7.62, 10.16 and 12.7 m/s. To one's surprise, the results did not show clear difference of the flow rates deduced from the Equal Area and the Log-Tchebycheff methods. The reason was probably due to the fact that the three measurement planes were too close to upstream disturbances (a fan and an elbow), that is, their maximum distance of 2.4 D_h was significantly less than the normally required 7.5 D_h (ASHRAE 111, 1988). Since the measurement planes were so close to the upstream obstruction, the rounded shape of the velocity distribution did not form, as assumed in the Log-Tchebycheff method. Thus the gap between two traversing methods was insignificant due to the un-recovered velocity profile after obstructions.

In the same year, Richardson (2001) conducted an experimental investigation concerning this issue and published his data. In the experiment, the tested duct sizes were 1.22 m × 0.31 m and 0.61 m × 0.61 m respectively. A nozzle was used to sense the

reference flow rate. It showed that the flow rate acquired from the Equal Area method had a maximum overestimation of 4.6% from the reference flow rate, whereas the Log-Tchebycheff method had a maximum variance of 2.2%. The differences between the two methods were not more than 2.5%. Compared to Klaassen and House (2001), the measurement planes were a little further from the inlet disturbance (3.75 and 3 D_h for two different ducts respectively). However, they were still too close to the disturbance according to ASHRAE 111 (1988) or other standards.

2.3 Scope of the current study

The question about whether the Log-Tchebycheff method can offer a better accuracy in estimating the airflow rate in a duct has generated considerable debate. It is thus necessary to resolve this question in order to accurately estimate the volumetric flow rate. The previous investigations (Macferran 1999(a); Klaassen and House, 2001; Richardson, 2001), as mentioned above, are incomplete.

In the present study, the performance of the Equal Area and the Log-Tchebycheff methods was evaluated based on the airflow in a square duct. The size of the square duct was selected to be 0.46 m (18 inch) since it is frequently encountered in practice.

A numerical study was carried out with the use of commercial Computational Fluid Dynamics (CFD) software FLUENT. It aimed at evaluating the accuracies of the Equal Area and the Log-Tchebycheff methods theoretically where ideal flow conditions without real-life imperfection were assumed. The simulated duct length was 40 times the hydraulic diameter, D_h, where the flow was nearly fully developed. The investigated bulk velocity, U_b, was in the range of 0.3 ~ 15 m/s, which covers almost the whole range of practical applications (McQuiston and Parber, 1994). The corresponding Reynolds

numbers, based on U_b and D_h, were found in the range of 10,000 ~ 500,000. Following the simulated flow profiles, the Equal Area and the Log-Tchebycheff methods were used to deduce the volumetric flow rate at different Re and streamwise locations.

On the second part of this research work, the experimental study was carried out to verify the numerical results and, at the same time, to evaluate the performance of both methods under practical situations. In the experimental investigation, a blower-duct assembly was constructed to generate the desired airflow. A Venturi flow meter was employed to sense the reference flow rate and a hot-wire anemometry system was used to measure the velocity profile. The Equal Area and the Log-Tchebycheff methods were evaluated at different Re and downstream locations. The investigated velocities were in the range from 3 m/s to 5 m/s, which are in the lower range of HVAC applications. The corresponding range of Reynolds numbers was from 90,000 to 140,000. Three streamwise locations from the inlet of the square duct, 3.4 D_h, 6.5 D_h, and 9.6 D_h, were also examined in this study.

CHAPTER 3 SIMULATION OF SQUARE DUCT FLOW

In this chapter the CFD method was used to predict the distribution of airflow in a square duct, based on which, the Equal Area and the Log-Tchebycheff methods were employed to estimate the volumetric airflow rate. The finite volume technique is extensively used in Computational Fluid Dynamics. This method first divides the calculation domain into discrete control volumes, each containing a grid point, and then differential equations are integrated across each control volume to construct algebraic equations for the discrete dependent variables, such as velocities and pressure. The variables between two neighboring grids are interpolated based on a piecewise profile, which depends on the specific scheme used. In this study, the second order scheme, which includes the second order term of a Taylor series expansion of partial differential equations (PDE), was employed to construct algebraic equations. This study assumes the following characteristics for the airflow in a square duct,

- the flow is in turbulence region;
- the flow is steady;
- the airflow is incompressible, since, $M < 0.3$ (Munson et al., 2002);
- it is isothermal flow where both the air and the duct walls are kept at 20°C.

With the above assumptions, the governing equations are described below.

3.1 Governing Equations

The governing equations for the dependent variables, such as velocity and pressure, are derived from the conservation laws of mass and momentums. Thus, the mass conservation equation, known as the continuity equation; and the momentum balance equations, known as the Navier-Stokes equations, are used upon each control volume in the form of PDEs. In a three-dimensional domain, the continuity and momentum equations can be described in a tensor notation as below.

Continuity:

$$\frac{\partial(\widetilde{U}_j)}{\partial x_j} = 0 \quad , \tag{3-1}$$

Momentum:

$$\rho \widetilde{U}_j \frac{\partial \widetilde{U}_i}{\partial x_j} = -\frac{\partial \widetilde{p}}{\partial x_i} + \mu \frac{\partial^2 \widetilde{U}_i}{\partial x_j \partial x_j} \quad , \tag{3-2}$$

where $\widetilde{U}_j$ is the velocity component at each direction of the 3-D domain, $\widetilde{U}_i$ is the velocity component at a specific direction of the 3-D domain, $\widetilde{p}$ is the pressure, ρ is the density, μ is the dynamic viscosity.

The left-hand side of the momentum equation is convection or inertia term. On the right-hand side, the first term is pressure-stress term and the second term is viscous diffusion term. Since there are no fluctuation terms in velocities and pressure for laminar flow, the ensemble average of above equations for laminar flow has the same formula as their instantaneous equations. Thus the laminar flow has only four mean flow variables, *U, V, W* and *p*, which can be solved by four equations in a three dimensional space, i.e.

one continuity equation and three momentum equations in the X, Y, Z directions respectively.

However, since turbulent flow is characterized by random fluctuation of the velocities and pressure at each point of the flow field, the Reynolds decomposition method (Reynolds, 1900) was introduced based on which the instantaneous flow characteristic scales, $\widetilde{U},\widetilde{V},\widetilde{W},\widetilde{p}$, are decomposed into the mean flow scales, U, V, W, p and fluctuating flow scales, u, v, w, p'. Their tensor notations are described below,

$$\widetilde{U}_j = U_j + u_j \ , \tag{3-3}$$

$$\widetilde{p} = p + p' \ . \tag{3-4}$$

Substituting these into Equations (3-1) and (3-2) and taking ensemble average give,

$$\frac{\partial U_j}{\partial x_j} = 0, \tag{3-5}$$

$$\rho U_j \frac{\partial U_j}{\partial x_j} = -\frac{\partial p}{\partial x_i} + \frac{\partial}{\partial x_j}(\mu \frac{\partial U_i}{\partial x_j} - \rho \overline{u_i u_j}) \ . \tag{3-6}$$

The following equations can be attained in steady 3-D turbulent problem,

Continuity equation:

$$\frac{\partial U}{\partial x} + \frac{\partial V}{\partial y} + \frac{\partial W}{\partial z} = 0 \ . \tag{3-7}$$

X-direction momentum equation:

$$\rho\left(U\frac{\partial U}{\partial x} + V\frac{\partial U}{\partial y} + W\frac{\partial U}{\partial z}\right) = -\frac{\partial p}{\partial x} + \frac{\partial}{\partial x}\left(\mu\frac{\partial U}{\partial x} - \rho\overline{u^2}\right) + \frac{\partial}{\partial y}\left(\mu\frac{\partial U}{\partial y} - \rho\overline{uv}\right) + \frac{\partial}{\partial z}\left(\mu\frac{\partial U}{\partial z} - \rho\overline{uw}\right) \tag{3-8}$$

Y-direction momentum equation:

$$\rho\left(U\frac{\partial V}{\partial x} + V\frac{\partial V}{\partial y} + W\frac{\partial V}{\partial z}\right) = -\frac{\partial p}{\partial y} + \frac{\partial}{\partial x}\left(\mu\frac{\partial V}{\partial x} - \rho\overline{uv}\right) + \frac{\partial}{\partial y}\left(\mu\frac{\partial V}{\partial y} - \rho\overline{v^2}\right) + \frac{\partial}{\partial z}\left(\mu\frac{\partial V}{\partial z} - \rho\overline{vw}\right) \tag{3-9}$$

Z-direction momentum equation:

$$\rho\left(U\frac{\partial W}{\partial x}+V\frac{\partial W}{\partial y}+W\frac{\partial W}{\partial z}\right)=-\frac{\partial p}{\partial z}+\frac{\partial}{\partial x}\left(\mu\frac{\partial W}{\partial x}-\rho\overline{uw}\right)+\frac{\partial}{\partial y}\left(\mu\frac{\partial W}{\partial y}-\rho\overline{vw}\right)+\frac{\partial}{\partial z}\left(\mu\frac{\partial W}{\partial z}-\rho\overline{w^2}\right). \quad (3\text{-}10)$$

Compared to the tensor notation form of Equation (3-2), there are additional terms on the right-hand side of the momentum equations, in the tensor notation form, $-\rho\overline{u_i u_j}$. They are called Reynolds stress terms which represent the mean transport of fluctuating momentum by the turbulent velocity fluctuations. It exchanges momentum between the turbulent and the mean flow.

Turbulent flow introduces six additional terms of Reynolds stresses, they are $\overline{u^2}, \overline{v^2}, \overline{w^2}$ and $\overline{uv}, \overline{uw}, \overline{vw}$. The introduction of the Reynolds stresses after decomposition of the turbulent fluctuating variables brings the closure problem, one has to find additional relationship between the mean flow variables and the turbulent components. There is a wide range of methods used to do this, varying from the most simple zero-equation models to the much more complex seven-equation Reynolds-stress model.

3.2 Turbulence model

In simulating the turbulent airflow in a square duct, there are several options of turbulence model. According to Naimi and Gessner (1994), the seven-equation Reynolds stress model (RSM) results in a high accuracy of results. This model includes six differential transport equations to calculate each Reynolds stress term, $-\rho\overline{u_i u_j}$, and an additional scale-determining equation. Thus, the Reynolds-averaged momentum equations (Equations (3-7) to (3-10)) can be solved. However, the computational cost of this model is expensive since this model introduces seven additional equations.

On the other hand, the two-equation k-ε model significantly reduces the computational cost, yet retaining a good overall performance. In this model the Reynolds stress terms are solved by the Boussinesq assumptions (Launder and Spalding, 1974). Two separate transport equations, one for the turbulent kinetic energy (k) and one for the dissipation rate (ε) of k, allows the turbulent velocity and length scale to be determined. This model was first proposed by Launder and Spalding (1972), presently named as the Standard k-ε model.

The standard k-ε model achieves notable successes in calculating a variety of confined flow where the Reynolds shear stresses are most important (Wilcox, 1994; Damodaran et al., 1995). However, several authors, including Speziale (1987), Gessner and Emery (1981), Rokni et al. (1998), mentioned that the standard k-ε model is not accurate in simulating rectangular duct flow due to the anisotropy of the Reynolds normal stress, which does not satisfy the requirements of the Boussinesq assumptions. In 1986, a new modification of the standard k-ε model, using a rigorous statistical technique called "renormalization group" (RNG) method, was developed by Yakhot and Orszag (1986). It is proved to be more accurate than the standard k-ε model for a wide variety of flows and is included in several commercial CFD packages, including FLUENT (Version 6.2, 2003). One feature of the RNG k-ε model is that it significantly improves the accuracy for flow with anisotropic stresses. This model was used to simulate the rectangular duct flow by Barton et al. (1991, cited by Naimi and Gessner, 1994).

In the current study, both the Standard k-ε and RNG k-ε models were used in the trial simulation phase. It was found that the RNG k-ε model has better agreement with

available experimental data. The RNG k-ε model was thus used for all cases of the current simulation. The details of this model are given in Appendix A.

3.3 Computational domain and boundary conditions

A three-dimensional (3-D) numerical simulation was performed for airflow through a 0.46 m (H) square duct at standard temperature (20°C or 293K) and pressure (101,325 Pa) using the commercial CFD code FLUENT (Version 6.2, 2003). Due to the symmetry characteristics, the simulation was performed over a quadrant of the duct cross section; as portrayed in Figure 3.1. According to Demurn and Rodi (1984), no definite conclusion can be drawn as to whether the square duct flow with the Reynolds number of 250,000 is fully developed at 84 D_h downstream of a uniform inlet. However, the center line velocity will reach its peak value around 40 D_h and then slowly drop by less than 5% by 84 D_h. Due to the limitation of computational cost, a length of 40 D_h was used in the current simulation.

In this study, the simulated range of Reynolds numbers, is from 10,000 to 500,000,

$$\mathrm{Re} = \frac{\rho U_b D_h}{\mu} \quad , \tag{3-11}$$

where ρ is the density and μ is the dynamic viscosity of air.

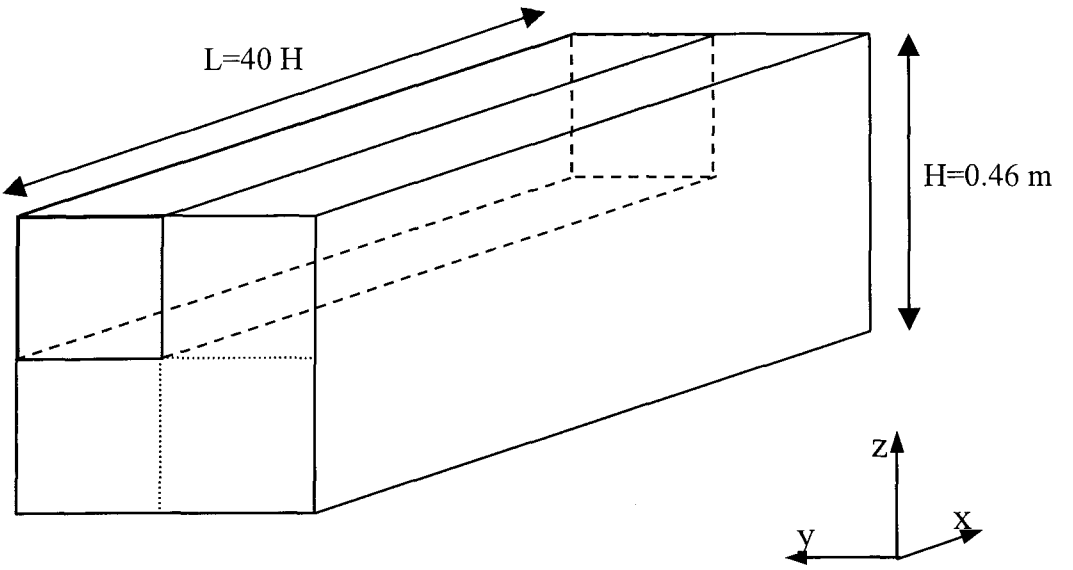

Figure 3.1 Schematic diagram of flow geometry (the upper right quadrant was taken as the calculation domain).

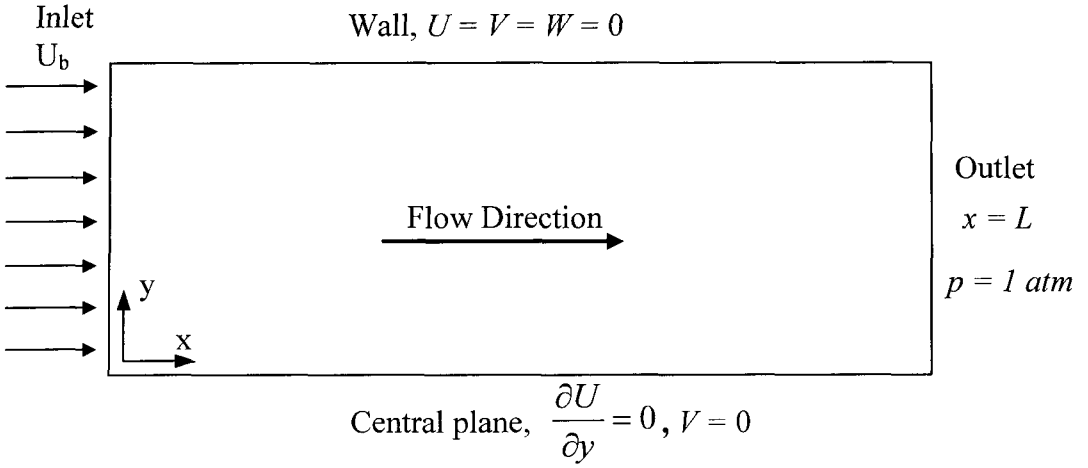

Figure 3.2 The top view (*X-Y* plane) of the computational domain and boundary conditions.

Figure 3.2 portrays the top view of the computational domain and boundary conditions (X-Y plane). The right view (X-Z plane) has a similar form with the Y-axis changed to Z-axis. The boundary conditions in the computational domain thus consist of inlet, outlet, symmetric central planes and wall surfaces. They were dealt with as follows,

(a) Velocity inlet

Velocity inlet boundary conditions were applied to define the velocity and scalar properties of the flow at the inlet. The flow with a uniform velocity U_b enters the duct along the streamwise direction (X axis); that is,

$$U = U_b,\ V = W = 0 \text{ at } x = 0,\ 0 \le y < H/2,\ 0 \le z < H/2 \tag{3-12}$$

(b) No-slip walls

No-slip wall boundary conditions were applied in the present numerical simulation, i.e. the velocities on the inner surface of walls are equal to zero,

$$U = V = W = 0 \text{ at } y,\ z = H/2,\ 0 \le x \le L. \tag{3-13}$$

(c) Central planes

Symmetry of reflective boundary conditions were adopted on the two central planes of the duct, that is, for the horizontal central plane ($y = 0$) as shown on Figure 3.2,

$$\frac{\partial U}{\partial y} = 0 \text{ and } V = 0 \text{ at } y = 0,\ 0 \le x \le L,\ 0 \le z < H/2. \tag{3-14}$$

Similarly, the boundary condition for the vertical plane ($z = 0$) is,

$$\frac{\partial U}{\partial z} = 0 \text{ and } W = 0 \text{ at } z = 0,\ 0 \le x \le L,\ 0 \le y < H/2. \tag{3-15}$$

(d) Pressure outlet

The pressure at the outlet surface was assumed to be constant with the value of atmospheric pressure. That is,

$$p = 1\ atm = 101{,}325\ Pa, \text{ at } x = L,\ 0 \le y \le H/2,\ 0 \le z \le H/2. \tag{3-16}$$

In addition, the initial turbulent parameters at the inlet, including the relative turbulence intensity T_u, turbulence length scale Λ, turbulent kinetic energy k and turbulence dissipation rate ε, are required before the iteration process. The turbulence intensity T_u is defined as the ratio of the root-mean-square of the fluctuating velocities to the mean velocity. FLUENT (Version 6.2, 2003) recommends the initial input of T_u as a function of the Reynolds number as below,

$$T_u = 0.16(\mathrm{Re})^{-1/8} \times 100\%. \tag{3-17}$$

The turbulence length scale (Λ), is a physical quantity related to the size of eddies that contains the energy in turbulent flows, which is defined to correspond to D_h,

$$\Lambda = 0.07\, D_h. \tag{3-18}$$

The turbulent kinetic energy (k) is the kinetic energy per unit mass of the turbulent fluctuations. The turbulent dissipation rate (ε) is defined as the rate of conversion of turbulence into heat by molecular viscosity. They are determined by T_u and D_h as follows,

$$k = \sqrt{\frac{3}{2}}(U_b T_u)^2, \tag{3-19}$$

$$\varepsilon = C_{\mu}^{3/4} \frac{k^{3/2}}{\Lambda}, \tag{3-20}$$

where C_{μ} is the eddy-viscosity coefficient. The default value of 0.0845 was used in the current study (FLUENT Version 6.2, 2003).

3.4 Discretization

The computational domain and the governing partial differential equations were discretized before simulation. GAMBIT (Version 2.2, 2004), a preprocessing software, was utilized to build the geometry and generate mesh. The structured hexahedral cells were applied to discretize the computational domain into small control volumes.

The mesh scheme has to capture the complex flow structure in the domain, especially in the boundary layers. The presence of the friction between the flow and the duct wall generates a non-uniform flow distribution. Normally the boundary layer flow can be divided into three layers. In the innermost layer immediately beside the wall, the flow is almost laminar, and the (molecular) viscosity plays a dominant role in momentum and mass transfer. This layer is called the viscous layer. In the outer layer, or the fully turbulent layer, turbulence plays a major role. Finally, there is a buffer layer between the viscous layer and the fully turbulent layer where the effects of molecular viscosity and turbulence are equally important.

The grid spacing normal to the wall needs to be sufficiently fine to resolve the steep velocity gradients (Rokni et al., 1998). Since the velocity changes significantly at the near-wall region whereas the profile is relatively flat at the central region, non-uniform grid was employed on the cross-sectional plane. Figure 3.3(a) portrays a sample mesh with the 30 × 30 grids on a quadrant of the cross section. Since the variation of

flow is relatively slow along the streamwise direction, the mesh is allowed to be coarser at this direction to reduce the computational cost. This is crucial in the present study since the computational domain in the streamwise direction is very long, at 80 times that in the cross-sectional direction (a quadrant of the duct). A uniform grid spacing of 0.1 D_h, as recommended by Gessner and Jones (1965), was applied in this study. Figure 3.3(b) depicts a small section of mesh at the X-Y plane.

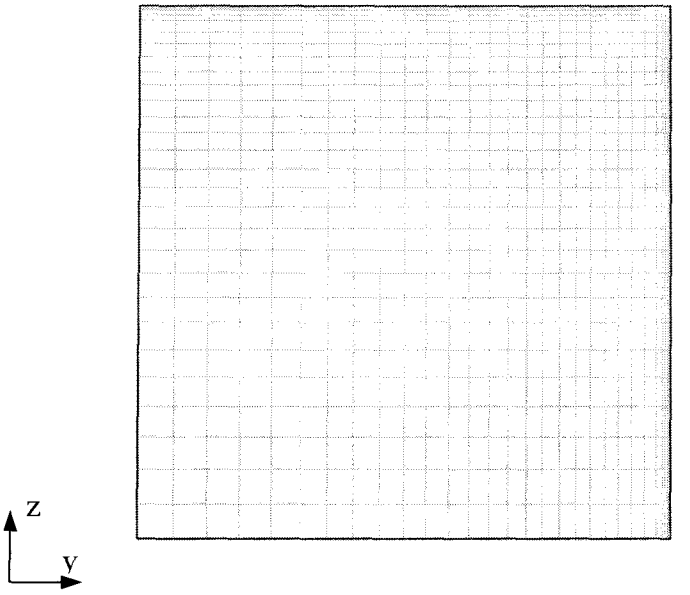

(a) 30 × 30 non-uniform mesh on the cross sectional plane.

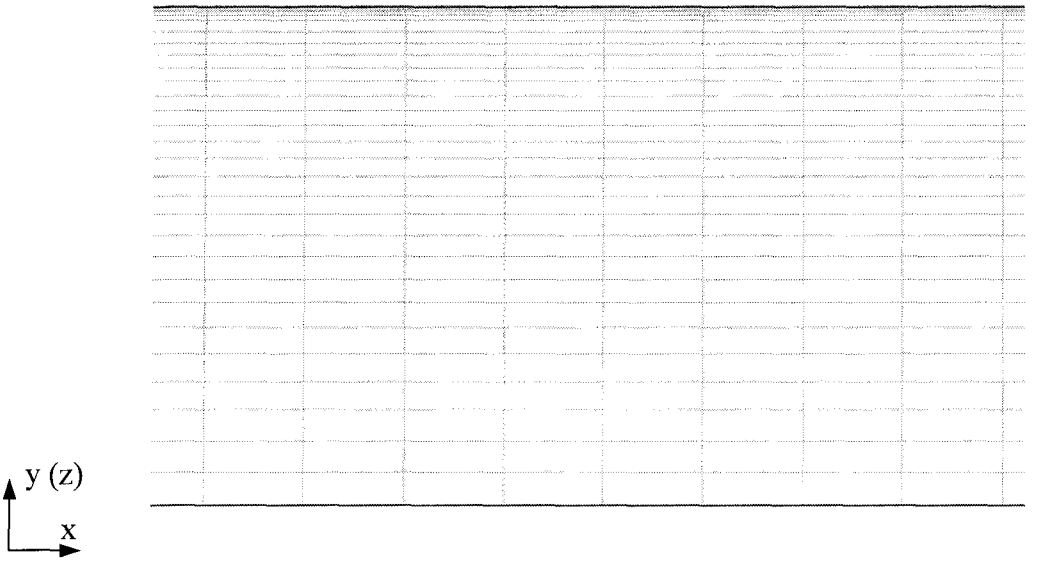

(b) A small section of the 400 mesh grids along the streamwise direction.

Figure 3.3 Sample mesh of 400 × 30 × 30. (a) 30 × 30 non-uniform mesh on the cross sectional plane; (b) A small section of the 400 mesh grids along the streamwise direction.

The RNG k-ε model is only valid in the fully turbulent region and not effective at the near-wall region where the viscous effect is important. A common method is to use a semi-empirical wall function to simulate the viscosity-affected regions, i.e. the viscous layer and the interim buffer layer. FLUENT (Version 6.2, 2003) provides two options of wall function: the Standard and the Enhanced Wall Functions. The Standard Wall Function can extend the solution over the buffer layer whereas the Enhanced Wall Function can extend the turbulence modeling further beyond the viscous layer. Since the Enhanced Wall Function has a better estimation of flow in the near-wall region, this study employed the Enhanced Wall Function to resolve the flow until the viscous layer.

To apply the Enhanced Wall Function, at least one mesh line has to be located in the viscous layer. This was realized by constructing very fine boundary layer mesh and calculating the dimensionless distance between the first mesh line and the nearest wall, y^+, which is defined as,

$$y^+ = \frac{\rho u_\tau y_P}{\mu}, \tag{3-21}$$

where u_τ is the friction velocity, y_P is the normal distance from the centroid of the nearest cell to the wall. The y^+ value is normally observed to be under 5 in the viscous layer (Munson et al., 2002; FLUENT Version 6.2, 2003).

The convergence criterion for solved variables was setup as,

$$\left| \frac{\phi^{i+1} - \phi^i}{\phi^i} \right| \leq 10^{-5} . \tag{3-22}$$

where ϕ^i represents the value of variables at i^{th} iteration.

3.5 Grid independence

The discretization process involves certain amount of errors. The error arose from the discretization process can be minimized through the investigation of mesh independence, i.e. increasing the mesh density until the solution does not change with further mesh refinement. Since a 3-D model with very fine grid normally takes a much higher computational cost, a 2-D model with the domain of 18.4 m × 0.23 m was first investigated to find the suitable mesh size. This mesh scheme was then extended to a 3-D model. The domain and the boundary conditions of the 2-D trial simulation are similar to 3-D model. It can be referred as the *X-Y* plane of the 3-D model, as portrayed in Figure 3.2.

The 2-D domain was first constructed with a mesh of 400 × 30 grids, i.e. 400 grids along the streamwise (*X*) direction and 30 grids along the lateral (*Y*) direction. Then the grids were doubled along each direction step by step, up to 800 × 60 grids. The results were then compared with each other. Figure 3.4(a) portrays the profiles of the streamwise velocity along the duct central line (the symmetry boundary) at a Reynolds number of 10,000. Correspondingly, the mesh independence along the lateral direction was also examined by plotting the velocity profiles along the outlet boundary, as portrayed in Figure 3.4(b). It shows that in each direction the velocity profiles with different meshes agree very well. It can be concluded that the 400 × 30 grids can produce an approximately mesh-independent result.

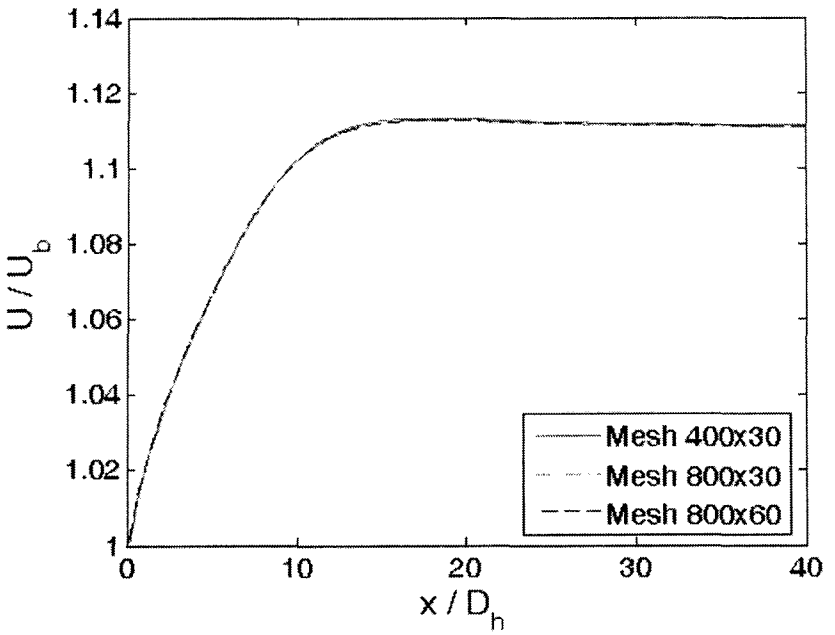

(a) Velocity profile along the central line.

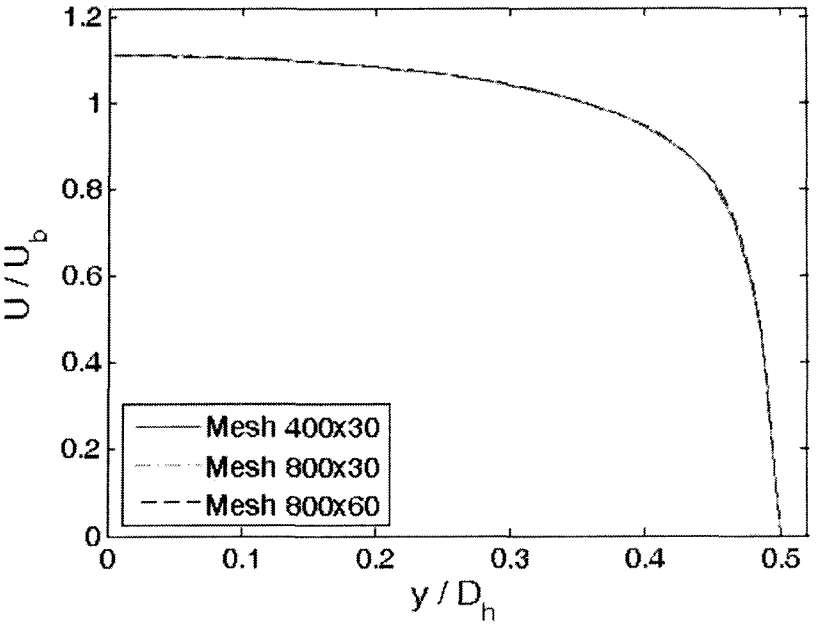

(b) Velocity profile along *Y*-axis at outlet.

Figure 3.4 Effect of mesh on the velocity profile for 2-D simulation at Re of 10,000. (a) Velocity profile along the central line; (b) Velocity profile along *Y*-axis at the outlet.

Therefore, the mesh scheme was applied to a 3-D domain with 30 grids applied to the spanwise (Z) direction as well. The mesh scheme for the 3-D domain was thus 400 × 30 × 30 hexahedral cells. To eliminate the potential variation of the mesh independence due to the mesh expansion from 2-D to 3-D, a double check was carried out by refining the mesh at the transverse plane to 45 × 45 grids. The results agreed well between these two meshes, as portrayed in Figure 3.5. To save the computational cost, the mesh with 400 × 30 × 30 grids was chosen as the final mesh scheme.

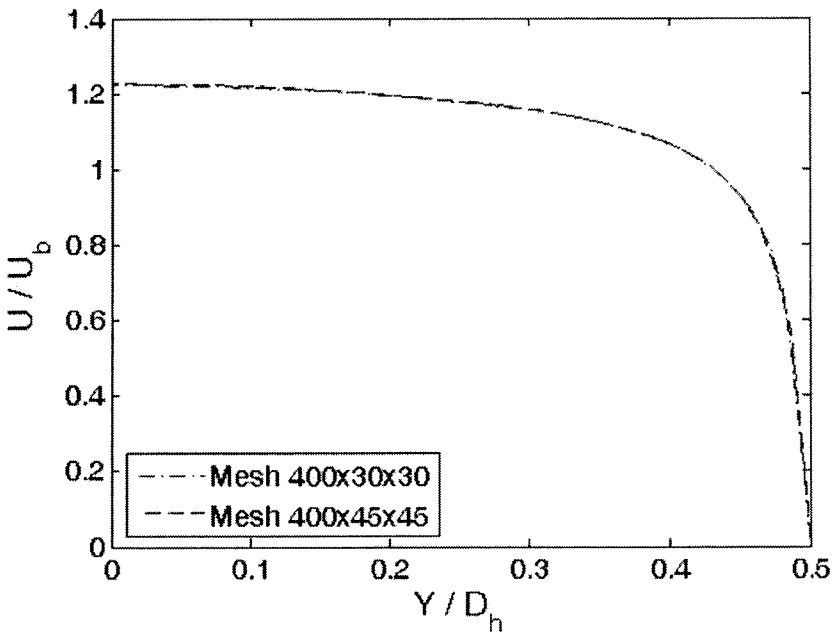

Figure 3.5 Effect of mesh on the velocity profile along Y axis at the outlet for 3-D simulation at Re of 10,000.

CHAPTER 4 EXPERIMENTAL SETUP AND PROCEDURES

The numerical investigation of airflow within a square duct provides an ideal flow without practical disturbances, also velocity values are acquired arithmetically such that no measurement uncertainty is considered. In order to evaluate the Equal Area and the Log-Tchebycheff methods in estimating the volumetric airflow rate under field conditions, a duct-blower test bench with relevant test facility was constructed in Room 103, Essex Hall, University of Windsor. This chapter describes the test bench and instrumentation facility, along with experimental procedures.

The schematic of the experimental setup is shown in Figure 4.1. It comprises of a centrifugal air blower, an in-line Venturi flow meter with upstream and downstream settling pipes, square test duct, hot-wire anemometer system, etc. The blower supplied airflow to the test duct, while the Venturi meter acquired the actual flow rate through the duct. A Meriam® inclined manometer was used to sense the differential pressure (Δp) across the Venturi meter. The TSI IFA® 300 constant temperature anemometer (CTA), combined with an 1192 automatic traversing mechanism, was used to measure the instantaneous velocity. A TSI VelociCalc® 8345 hand-held thermal anemometer, as an instrument employed in the HVAC industry, was used to sense the time-average velocity as may be acquired by a technician in practice. The details of the experimental setup are

described as below.

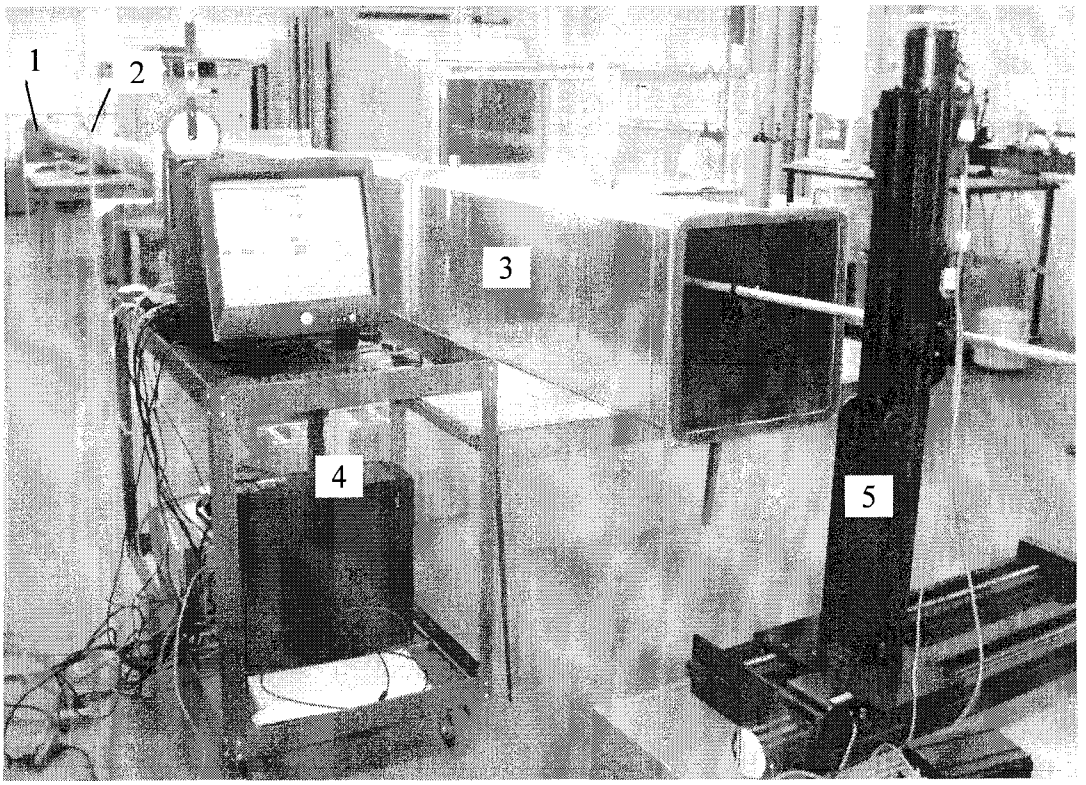

Figure 4.1 An overview of the experimental setup. (1) Blower; (2) Venturi meter; (3) Square duct; (4) CTA; (5) Traversing mechanism.

4.1 The test duct and air cycling facility

The airflow was measured in a blower-duct assembly. Figure 4.2 depicts the schematic of the flow facility. The total length of the test bench reaches 15.94 m when all the square duct sections are mounted. The details are as follows.

The centrifugal blower was used to generate airflow in the duct. It was driven by a 3.7 kW motor with a constant speed of 1750 rpm. A gate damper at the inlet of the blower was used to control the air flow rate. The exit of the blower was contracted into a circular

shape with an inner diameter of 0.26 m.

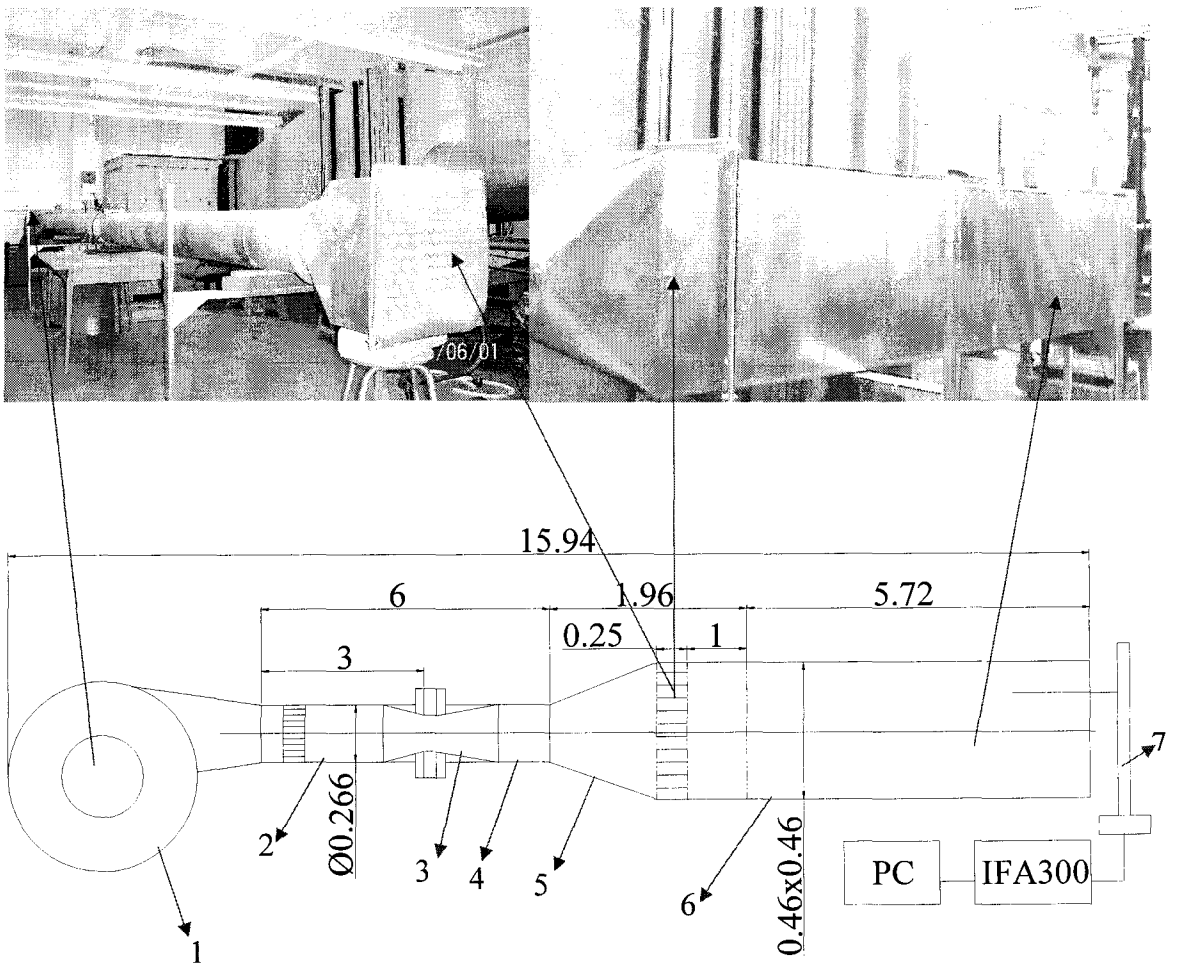

Figure 4.2 Schematic of the experimental setup (drawn not to scale). (1) Blower; (2) Upstream settling pipe combined with flow conditioner A; (3) Venturi flow meter; (4) Downstream settling pipe (5) Transitional section combined with flow conditioner B; (6) Square duct; (7) Automatic traversing mechanism.

A Venturi meter (Model 2300) made by Lambda Square Inc. was mounted in-line after the exit of the blower to measure the reference flow rate. The throat diameter of the Venturi meter is 0.183 m. The throat-to-pipe ratio, β, is 0.688. The reasons to select the

Venturi meter as the standard flow meter are its higher accuracy and excellent pressure recovery after the throat (Munson et al., 2002; ISO 5167-1, 2003) compared to commonly used Orifice and Nozzle flow meters. The setup of the Venturi meter and the inclined manometer is portrayed in Figure 4.3.

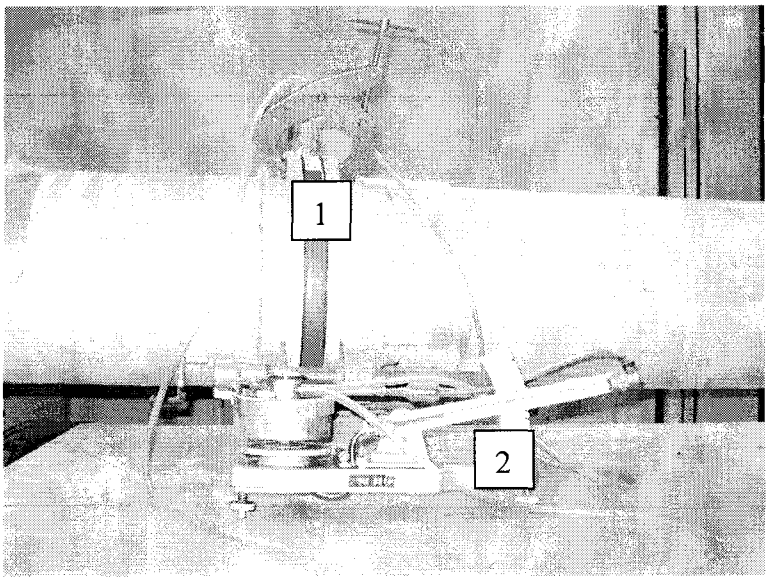

Figure 4.3 Venturi meter and inclined manometer. (1) Venturi tube (located inside the pipe); (2) Inclined manometer.

The principle behind the Venturi meter is the Bernoulli Equation which assumes steady, incompressible and non-swirl flow condition. According to the measured air velocity and the corresponding Mach number, the airflow was considered incompressible. In the present study, two 3 m (L_C) straight circular pipes with a diameter of 0.266 m (D_C, L_C = 11.3 D_C) were installed both upstream and downstream of the Venturi meter to minimize the swirling motion of airflow. A flow conditioner (Serial A) was placed 0.5 m (approximately 2 D_C) downstream of the blower exit attempting to make the flow more

uniform. The flow conditioner A includes a tube bundle with 278 circular tubes having a inner diameter of 0.018 m and length of 0.13 m. Metal screens, made of 0.3 mm wires with a spacing of 2.4 mm, were placed at the two ends of the tube bundle to hold those small tubes and to aid in conditioning flow.

After the Venturi tube the pipe was expanded to a square cross section which was connected to the test duct. A flow conditioner (Serial B) was placed after this expansion and preceding the test duct attempting to make the flow more uniform at the inlet of the test duct. As mentioned by several authors (Bradshaw et al., 1964; Laws and Livesey, 1978; Scheiman et al., 1981 and Lindgren et al., 2002), the combination of a tube bundle and multiple pieces of screens is very effective and widely used in uniforming internal flow. After several trials, the conditioner was finally constructed of a straw-filled tube bundle and three screens. The details are as follows.

The tube bundle is 0.25 m long. It was constructed of 120 small PVC tubes with an inner diameter of 0.035 m and a thickness of 0.004 m. Small plastic straws with a diameter of 0.004 m and a length of 0.28 m, were filled inside each tube, as shown in Figure 4.4. The main function of the straw-filled tube bundle is to restrict the cross-stream fluctuations.

Two metal screens, one made of 0.3 mm wires with a spacing of 2.4 mm and another woven by 0.3 mm wires with a spacing of 0.6 mm, were installed immediately upstream and downstream of the tube bundle. One of the objectives was to keep the tube bundle from moving. Their main function, is to break up larger eddies into smaller ones

and thus reduce the mean non-uniformity and turbulence fluctuations.

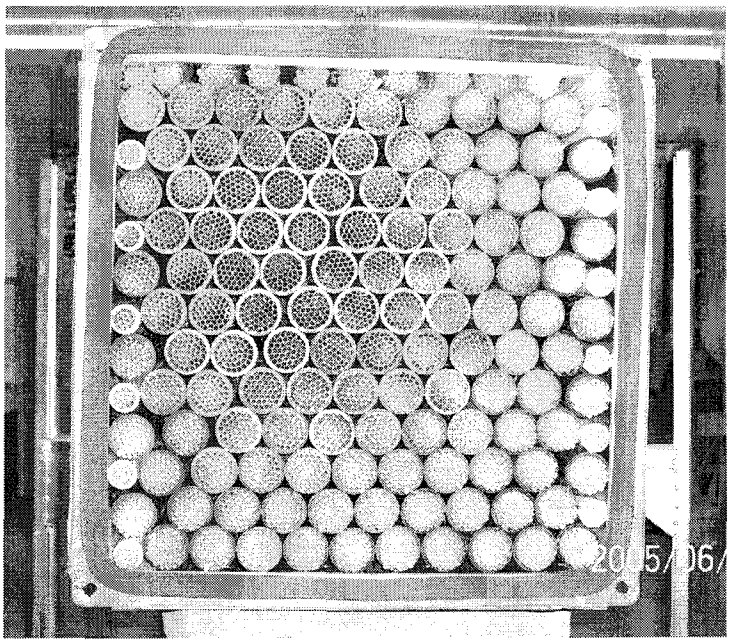

Figure 4.4 The cross-sectional view of the flow conditioner B.

The preliminary test shows that the flow downstream of the second screen was not close to uniform flow. Therefore the third screen, which has the same specification as the second one, was added 1 m downstream of the second screen. The downstream flow was found to be quite uniform, where the ratio of the maximum to the minimum velocity at the cross section 0.15 m downstream was under 12%.

The square test duct was fabricated by galvanized steel with a thickness of 1.2 mm. It comprises of four 1.43 m sections. These sections were connected each other via flanges with sealing foam in between. The actual dimensions of the cross section were measured to be 0.462 (Width, H_1) by 0.458 m (Height, H_2), which is not an exact square cross section but in this investigation treated as such with 1% error.

4.2 Hot-wire data acquisition instrumentation

The whole package of the TSI hot-wire instrumentation is shown in Figure 4.5. It is composed of a 1201 single normal hot-wire probe, an 1192 automatic traversing mechanism, an IFA® 300 CTA with an internal signal conditioner, an ADCPCI-8 A/D converter, a Dell® personal computer, an 1129 calibrator and an OMEGA® Type-T thermocouple. The specifications of each device are described in the following subsections.

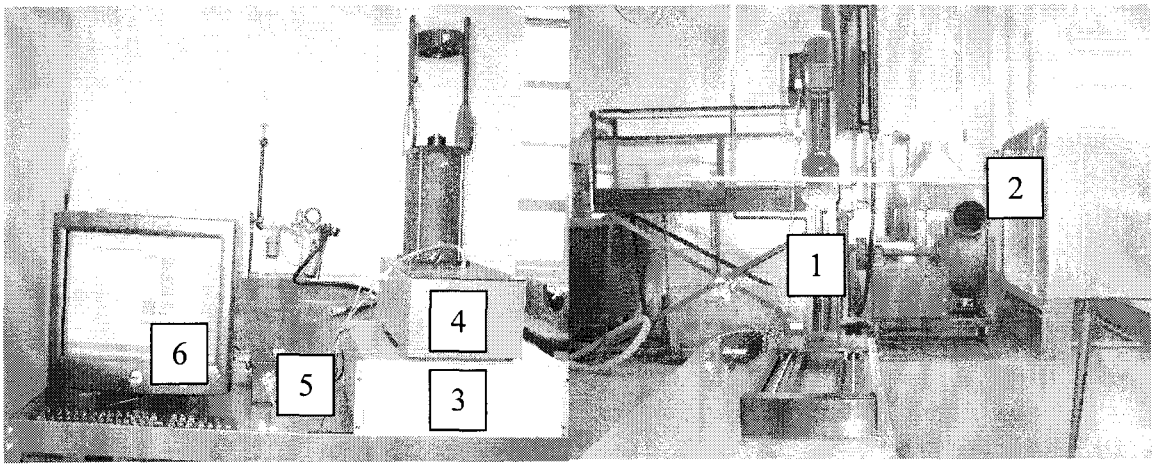

Figure 4.5 The hot-wire data acquisition instrumentation. (1) Traversing mechanism; (2) hot-wire probe (attached on traversing mechanism); (3) CTA; (4) Calibrator; (5) Pressure transducer; (6) Computer.

4.2.1 The single normal hot-wire probe

In this study, the instantaneous airflow velocities were measured using a TSI 1201 single normal hot-wire probe. It is constructed of a platium-coated tungsten wire with a

diameter of 3.8 μm. The probe senses the cooling effect of a moving gas stream passing over an electrically heated sensor. This cooling effect or heat transfer rate is correlated to the velocity of the gas stream based on the principle of energy conservation.

4.2.2 Hot-wire anemometer

The hot-wire anemometer used in the current study is an IFA® 300 CTA module. The control circuit for hot-wire anemometry is in the form of a Wheatstone bridge circuit consisting of four electrical resistances, one of which is the sensor, as shown in Figure 4.6. The sensor is heated to the operating temperature at 250°C. When it is placed in the flow, it is cooled by the fluid with a lower temperature. With the increase/decrease of air velocity, the heat transfer rate would increase/decrease correspondingly, causing the temperature of the sensor to depart from the operating temperature. To maintain the sensor at the operation condition, the current and then the voltage via the sensor are adjusted. Furthermore, a differential amplifier was used to amplify this voltage signal (TSI, 2002(a)). The bridge or amplifier output voltage is an indication of flow velocity. Due to the influence of the fluid velocity on the rate of heat transfer from the heated sensor to the flowing fluid, the power input to the sensor provides a measure of the flow velocity.

The acquired signal is then fed to a signal-conditioning unit before it is sent to the A/D converter and the central computer. It works to improve the accuracy at measured velocity range and match the range of the output voltage signal with the input voltage

range of the A/D converter. In the case that a nonlinear voltage signal with small fluctuations is fed into the A/D converter, there may exists a large error for the fluctuating part. In order to minimize the error and match the fluctuating part of the hot-wire signal to its voltage range, the offset voltage, E_{off}, which is about the mean value, is subtracted from the direct hot-wire signal, a *Gain* function is then applied to the signal to amplify the remaining part. The output signal $E_G(t)$ of the signal conditioner, is thus expressed as below,

$$E_G(t) = Gain\ (E(t)-E_{off}). \tag{4-1}$$

The *Offset* circuit can subtract up to 10 Volts from the bridge output in 10 mV steps. The *Gain* function can amplify the resulting signal up to 1000 times.

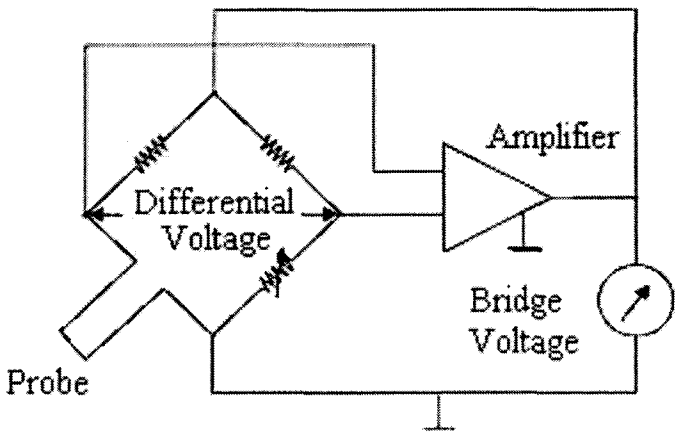

Figure 4.6 Schematic of the bridge circuit for a hot-wire sensor.

The CTA also integrates filtering circuits. A high pass filter is used when only velocity fluctuation measurements are needed since mean voltage information and thus the actual mean velocity is removed from the signal. A low-pass filter allows the removal

of high frequency signals which are out of range of interest (TSI, 2000).

4.2.3 A/D converter

The ADCPCI-8 A/D converter converts the analog signal from the signal-conditioning unit into digital signal. It is ideally suited for the specified requirements of thermal anemometer signals. The voltage range is -5 ~ 5 V. With a 12-bit outfit, the A/D converter has a digital resolution of 2.5 mV.

4.2.4 Temperature and pressure compensation

The thermal anemometer is based on the heat transfer between the hot-wire sensor and fluid medium. When the fluid temperature is different from that of calibration condition, a correction has to be made. The current IFA 300 system has a thermocouple circuit integrated inside the CTA unit with a plug-in connector. An OMEGA® Type-T thermocouple is placed at the exit of the square duct to sense the air temperature.

The CTA program also includes the compensation for the variation of atmospheric pressure. An external barometer was setup to indicate the atmospheric pressure. Its value is required to input during each calibration or measurement process.

4.2.5 THERMALPRO™ software

THERMALPRO™ software gives complete control over the operation of the anemometer system. Its function can be divided into four discrete sections: control, calibration, data acquisition, and analysis. The communication between the CTA,

calibrator, traversing mechanism and computer is realized via RS-232-C serial communication cables.

4.3 Calibration of single normal hot-wire probe

The calibration is critical to the accuracy of hot-wire measurement. Since the correlation of the anemometer voltage output to the air velocity is sensitive to external environment, the calibration process has to be carried out before any test to establish a current velocity-voltage correlation. During the measurement process, the hot-wire probe senses the air velocity (U) and produces a voltage signal (E) via the anemometer. This signal is conditioned and then compared to the calibrated correlation curve. Thus the voltage signal is re-converted to velocity information.

In this study, the velocity-voltage correlation of the hot-wire probe was expressed as a fourth order polynomial curve fit,

$$U = a_{00} + a_{01}E + a_{02}E^2 + a_{03}E^3 + a_{04}E^4, \tag{4-3}$$

where a_{00}, a_{01}, a_{02}, a_{03}, a_{04} are relevant coefficients.

The schematic of the calibration process using a Model 1129 calibrator is portrayed in Figure 4.7. The supply air is filtered and adjusted to a gage pressure no less than 207kPa (30 psi), and then the air pass through the calibrator and exit through a nozzle. The probe is positioned above the exit nozzle. The potential core of the jet flow from the nozzle exit is assumed to be uniform with a turbulence level less than 0.5%. The sensor is cooled by the jet and the corresponding voltage, E_R, is acquired by the

anemometer. At the same time, the reference velocity inside the potential core is determined by the pressure drop across the nozzle. A pressure transducer with the range of 0.4 ~ 99 mmHg was used to sense the differential pressure, Δp. The calibrator has a capacity to calibrate the velocity over a range of 0 ~ 150 m/s. In order to accurately calibrate the hot-wire sensor at low velocity range, two secondary nozzles with different velocity ranges were provided by TSI.

The secondary nozzle was installed at the base of the settling chamber. The pressure drop across the secondary nozzle was measured and related to the velocity emerging from the exit nozzle. The reason to use the secondary nozzle is to obtain relatively high pressure difference when the velocity of the free jet (emerging from the exit nozzle) is low.

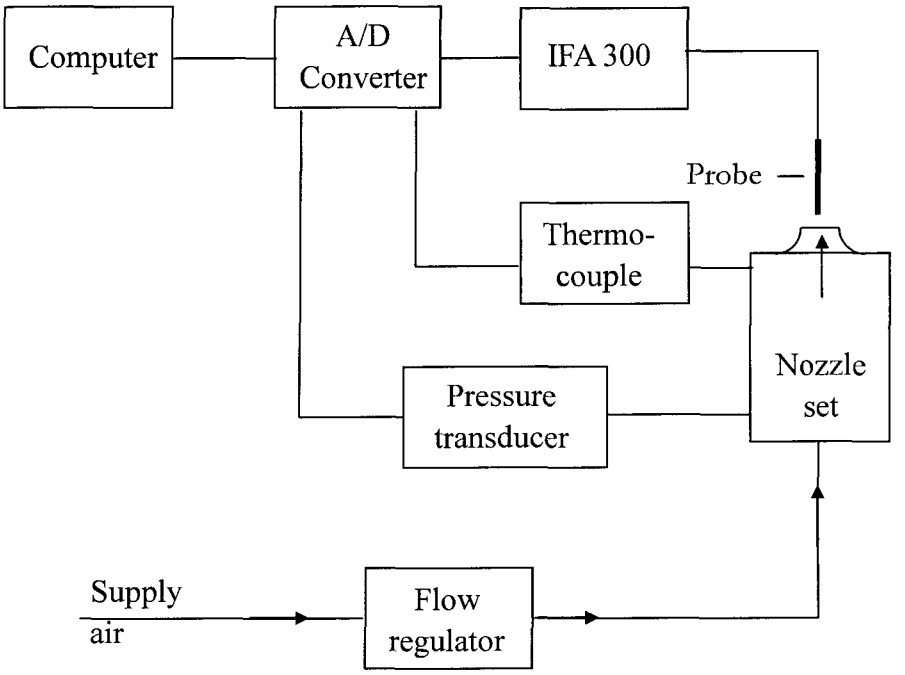

Figure 4.7 Schematic of the hot-wire calibration process.

An air volume booster was used to control the calibration flow at different velocity values. A set of calibration points (U_R, E_R), 17 points for the current study recommended by TSI (2003), were acquired to curve fit the *U-E* correlation within the applied velocity range. The calibration is carried out automatically with the application of the THERMALPRO software.

4.4 Selection of turbulence measurement parameters

To decide the suitable turbulence measurement parameters, i.e. the sampling frequency and time, Measurements were taken at a specific location with varied sampling frequencies and time whereas maintaining other conditions same. Table 4.1 depicts the time-mean velocities measured at a specific location with different sampling frequencies and time. It appears to be no obvious difference where the maximum variation of the mean velocity is 0.6%. The current study used a sampling frequency of 20 kHz and time of 6.55 s to take the traverse measurement.

Table 4.1 Selection of turbulence measurement parameters.

Serial No.	1	2	3	4	5
Frequency (Hz)	10	10	20	20	20
Time (s)	3.28	13.1	3.28	6.55	13.1
U_{mean} (m/s)	2.857	2.851	2.862	2.865	2.868

4.5 Traverse measurement locations

The point velocities at discrete points were measured by the hot-wire system. Accurate measurement locations were achieved by attaching the sensor on the arm of the computer-controlled traversing mechanism. The measurement (relative) origin was setup at the upper-left corner with 0.03 m normal distance to both side walls. However, to ease the data analysis process, the display (absolute) coordinate was setup at the center of the duct cross section, as shown in Figure 4.8.

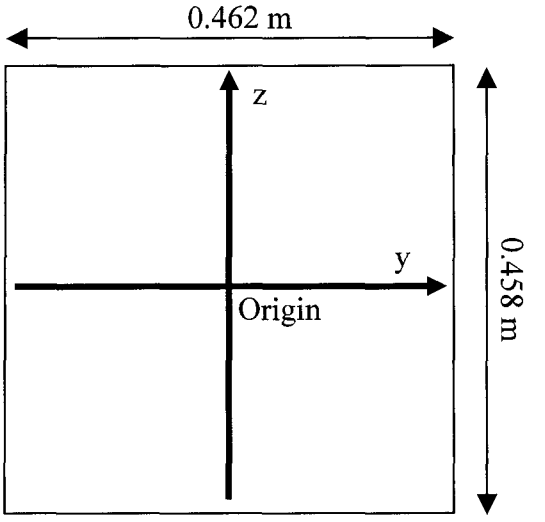

Figure 4.8 The display coordinate of the traverse measurement.

To investigate the influence of the velocity profile to the accuracy of the volumetric flow rate deduced from discrete point velocities, an 11 × 11 traverse grid was used based on which the point velocities were measured. Thus the velocity profiles along the duct cross section were obtained. The measurement locations are given in Table 4.2. The grid spacing is 0.05 m except that those points beside duct walls have 0.025 m

distance to their neighboring points at the normal directions. This is due to the fact that there are higher velocity gradients at the near-wall regions than at the central region.

Table 4.2 The 11 × 11 velocity traverse grid along the cross-sectional plane.

Coordinate	Location (m)
y	0, ±0.05, ±0.1, ±0.15, ±0.2, ±0.25, ±0.275, ±0.3
z	0, ±0.05, ±0.1, ±0.15, ±0.2, ±0.25, ±0.275, ±0.3

The dimensionless traverse locations for the Equal Area and the Log-Tchebycheff methods are defined in Standards (ISO 3966 (E), 1977; ASHRAE 111, 1988). With the specific duct dimensions in the current study, the locations for traverse points are defined in Table 4.3.

Table 4.3 Locations for the Equal Area and the Log-Tchebycheff methods along the cross-sectional plane.

Traverse method	Coordinate axis	Position (m)				
		1	2	3	4	5
Equal Area	y	-0.173	-0.058	0.058	0.173	-
	z	-0.172	-0.057	0.057	0.172	-
Log-Tchebycheff	y	-0.197	-0.098	0	0.098	0.197
	z	-0.195	-0.097	0	0.097	0.195

4.6 Measurement of reference flow rate

The Venturi meter was calibrated by the supplier. Figure 4.9 portrays the corresponding Q-Δp curve fit at the standard temperature and pressure conditions (STP, i.e. $T = 20°C$ and p_{atm} = 101,325 Pa). In the calibrated flows range of 0 ~ 1.2 m^3/s, it also has the equation form as follows,

$$Q_{ven,STP} = 0.03779\sqrt{\Delta p}\,, \tag{4-3}$$

where the units of Δp and Q_{STP} are Pa and m^3/s respectively.

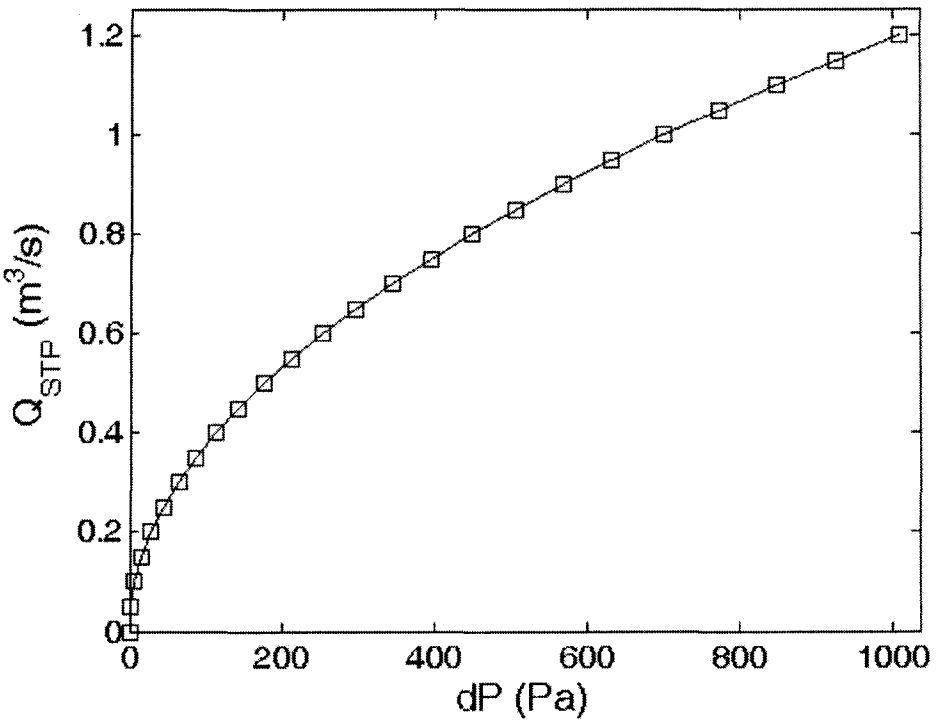

Figure 4.9 Calibration curve for the Venturi meter.

The calibration curve shows the Q–Δp correlation at standard temperature and atmospheric pressure (STP), i.e. 20°C for room temperature and 101,325 Pa for atmospheric pressure. During the actual measurement process, the actual environmental

condition departed from the standard condition. According to AABC (1989), a density correction factor, C_ρ, has to be introduced to determine the airflow rate. The equation for C_ρ and Q_{ven} are expressed as,

$$C_\rho = \sqrt{\frac{\rho_{STP}}{\rho}}, \tag{4-4}$$

$$Q_{ven} = C_\rho Q_{ven,STP}. \tag{4-5}$$

An inclined manometer was used to indicate the differential pressure across the Venturi tube, as portrayed in Figure 4.3. The fluid used to indicate ΔP is Meriam® Red Oil Model 923RO. It has a density of 827 kg/m^3. The scale has a range of 0 ~ 0.2 m with the resolution of 0.001 m. Its inclination ratio can be setup as 1:2, 1:5 or 1:25 according to the value of Δp.

In this study the Reynolds number was based on the mean velocity within the duct and its hydraulic diameter D_h. The actual dimensions of the duct are 0.462 m × 0.458 m and D_h was calculated to be 0.46 m. The mean velocity was acquired by dividing the reference flow rate with the cross-sectional area of the square duct (A_{SD}). Thus the Reynolds number is expressed as,

$$\mathrm{Re} = \frac{\rho\left(\frac{Q_{ven}}{A_{SD}}\right)D_h}{\mu}. \tag{4-6}$$

4.7 Velocity check by a hand-held anemometer

In HVAC industry, some hand-held instruments are widely used to take velocity

traverse measurement, such as hand-held thermal anemometer or Pitot-static tube. The advantages of them are their handy and inexpensive feature with an industrial acceptable accuracy. In this study, a TSI 8345 VelociCalc® hand-held anemometer was used to measure the velocity profile along the horizontal center line ($y = 0$) and the results were compared with that measured by the HWA system. It has an accuracy of 3% of reading and velocity range of 0 ~ 30 m/s (TSI, 2002(b)).

CHAPTER 5 RESULTS AND DISCUSSIONS

Both numerical and experimental investigations were carried out on the evaluation of the Equal Area and the Log-Tchebycheff methods in estimating the volumetric flow rate in a 0.46 m square duct. The numerical study investigated the airflow with the Reynolds number ranging from 10,000 to 500,000. The flow entered the duct with a uniform velocity, and exited as a nearly fully developed flow at 40 D_h. The Equal Area and the Log-Tchebycheff methods were compared and evaluated within the investigated flow regime. The experimental study was to verify the numerical results and, at the same time, evaluate the performance of both methods under practical situations. The experiment was carried out at Re of 90,000 ~ 150,000 with a maximum duct length of 9.6 D_h.

The outline for this chapter is as follows. Section 5.1 describes the results of the numerical study, Section 5.2 discusses the experimental results, and Section 5.3 conducts the comparison between the experimental and simulation data.

5.1 Simulation results

Based on the investigated range of Reynolds numbers (10,000 ~ 500,000), the airflow in the square duct is in the turbulent regime. The numerical study was carried out using commercial code FLUENT where the RNG k-ε model was employed as the turbulence model. The simulation results were compared with previously obtained results available in the literature, which included, the normalized centerline velocity and the

transverse velocity distribution. Based on the simulated flow fields, the Equal Area and the Log-Tchebycheff methods were applied to estimate the volumetric flow rates.

5.1.1 Flow field

When the airflow with a uniform velocity profile enters into a square duct, a boundary layer in the near-wall region will form and develop gradually. Consequently, the flow profile will develop to different shapes at different downstream locations until it becomes fully developed at a specific location. In the current simulation study the flow development process in a 0.46 m square duct with 40 D_h straight length was observed.

5.1.1.1 The normalized center line velocity U_C/U_b

Uniform velocity was assumed at the inlet of the simulated duct. When free flow enters into a duct, due to the wall friction and viscous effect, the flow velocity flow in the near-wall region will gradually decrease the velocity in the central part will increase. Thus the maximum velocity is acquired at the center of the cross section. The development of the flow may be represented by the variation of streamwise velocity along the duct central line, U_C.

The investigation of Gessner and Emery (1981) shows that at the Reynolds number of 250,000, the streamwise velocity at the center line (U_C) increases monotonically up to about 40 D_h downstream, where it reaches the maximum value. Further downstream, it decreases slightly until 84 D_h by less than 5% of the bulk velocity, U_b. No conclusion was drawn as to whether the flow was fully developed at this location. Due to the insignificant variation of flow profile and the limitation of computational resource, this study only extended the simulation until 40 D_h.

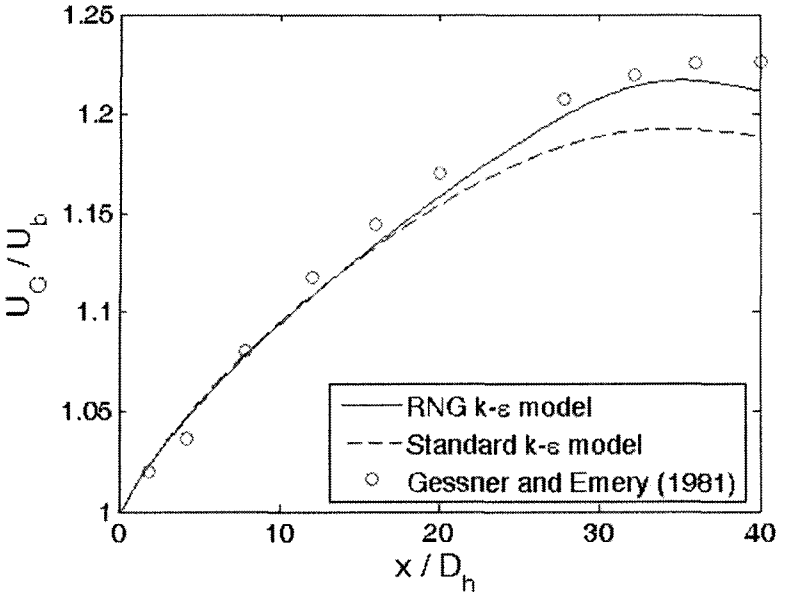

Figure 5.1 Dimensionless center line velocity (U_C /U_b) compared with published data at Re of 250,000.

It has to be noticed that in this study the bulk velocity in the duct was considered to be equal to the inlet velocity U_b. However, the bulk velocity calculated from the integration technique using FLUENT, i.e. the integrated volume flow rate divided by cross-sectional area, shows that there is a maximum variation of 0.25% of the inlet velocity at different downstream locations. This came from the numerical discretization error. Since this error is small it was neglected in this investigation.

Figure 5.1 portrays the simulated center line velocity, U_C, normalized by the bulk velocity, U_b, at the Reynolds number of 250,000. The simulations were carried out by the Standard and RNG k-ε turbulence models respectively and the results were compared with the experimental data by Gessner and Emery (1981), which was taken from the experiment on a 0.254 m square duct. It shows that the RNG k-ε model has a better agreement with the experimental data except that it reaches the peak value at 35.2 D_h

whereas the experiment reaches the peak value at 40 D_h. Comparatively, the Standard k-ε model has a lower peak velocity. Since the RNG k-ε model has a better agreement with experiment than the Standard k-ε model in predicting the mean flow field, it was selected to carry out all simulations in this study.

5.1.1.2 Velocity distribution along the transverse direction

One of the most important characteristics for the flow field is the streamwise velocity distribution along the cross-sectional plane. Due to the friction between the wall and the airflow, the maximum velocity is acquired at the center (U_C) of the cross section and then it gradually decreases to zero on the wall surface (the no-slip boundary condition). Figure 5.2 portrays the velocity along the wall bisector ($y = 0$) at the outlet at Re of 250,000, compared to the experimental data of Gessner and Emery (1981). The simulation result agrees well with the experimental data.

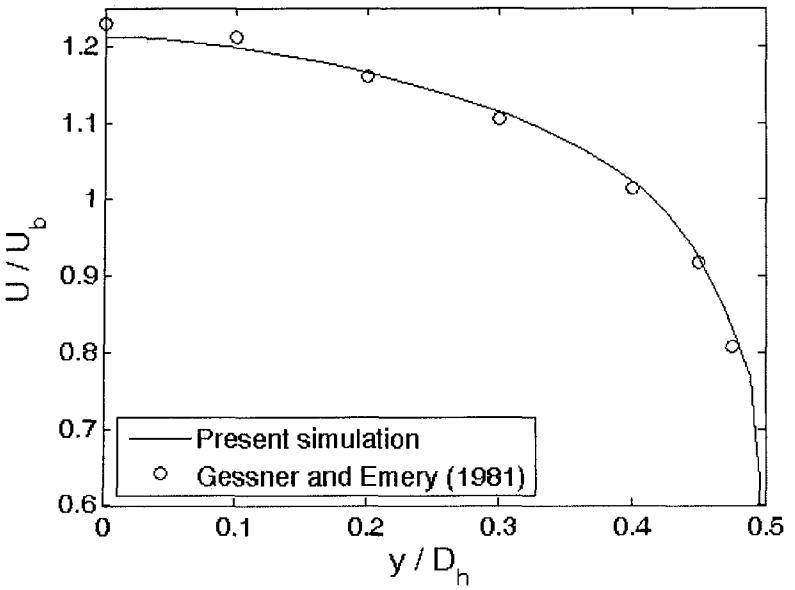

Figure 5.2 Comparison of the velocity profile along Y-axis at the outlet with published data at Re of 250,000.

Figure 5.3 depicts simulated velocity profiles along Y axis at the outlet with various Reynolds numbers. Slight differences can be observed among these profiles. The velocity distribution along the wall bisector becomes progressively flatter with increasing Reynolds number.

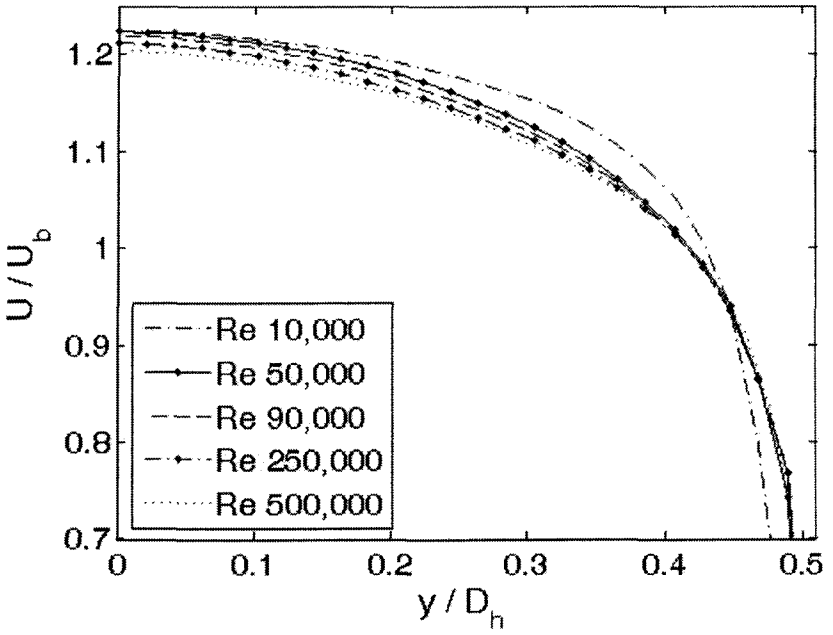

Figure 5.3 Simulated velocity profiles along Y-axis at the outlet.

Figures 5.4 and 5.5 portray the velocity profile along a quadrant of the cross section at the downstream locations of 6.5 D_h and the outlet respectively. At the location of 6.5 D_h (Figure 5.4), the velocity profile at near-wall region was rounded due to the boundary layer effect. It also can be observed that the velocities at the central region is nearly identical. This demonstrates that the flow is in developing situation. On the other hand, the airflow at the outlet (Figure 5.5) was very close to fully developed flow conditions, as mentioned in Chapter 3. The normalized center point velocity (U_C /U_b) is over 1.2.

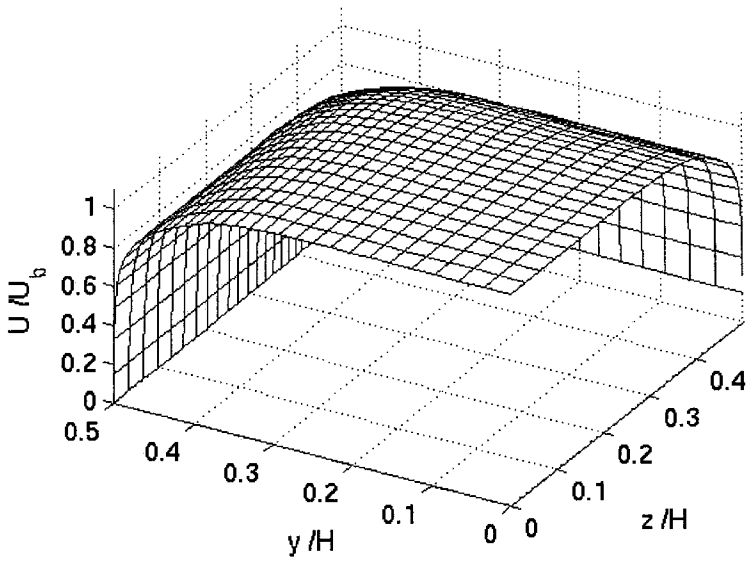

Figure 5.4 Dimensionless velocity profile at 9.6 D_h downstream and Re of 90,000.

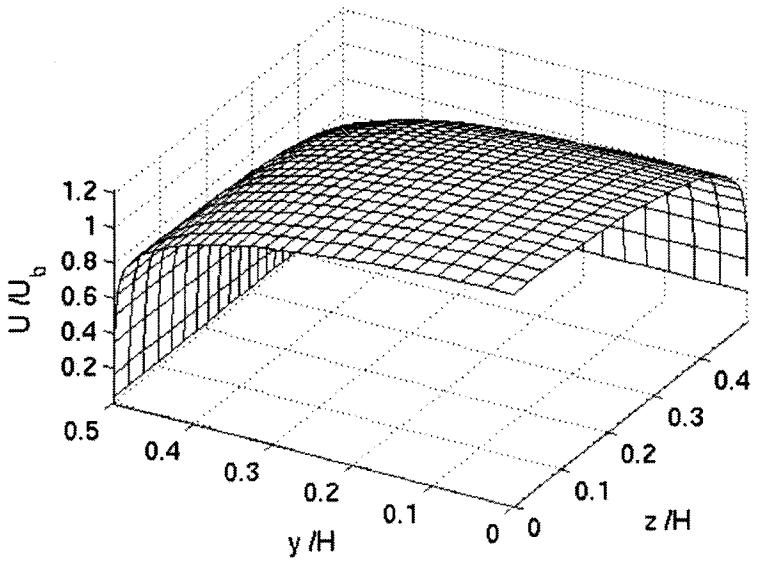

Figure 5.5 Dimensionless velocity profile at the outlet (40 D_h) and Re of 90,000.

5.1.2 Volumetric flow rate estimation

Based on the simulated velocity profile, the average velocity of the duct cross section can be estimated according to the Equal Area (U_{EA}) and the Log-Tchebycheff (U_{LT}) methods. Since the volumetric flow rate is the product of the average velocity and the cross-sectional area, which is a constant (A_{SD} = 0.2116 m), the volumetric flow rate (Q) thus can be estimated.

5.1.2.1 Locations of traverse points

The velocity traverse locations for the Equal Area and the Log-Tchebycheff methods are prescribed in various kinds of standards (ISO 3966 (E), 1977; ASHRAE 111, 1988; AABC, 2002). Table 5.1 depicts the traverse locations for a 0.46 m square duct. The center of the cross section was defined as the origin and the coordinate axes can be referred to Figure 4.9. There are totally 16 points specified for the Equal Area method and 25 points for the Log-Tchebycheff method.

Table 5.1 Locations for the Equal Area and the Log-Tchebycheff methods along the duct cross section.

Traverse method	Coordinate axis	Position (m)				
		1	2	3	4	5
Equal Area	y	-0.173	-0.058	0.058	0.173	-
	z	-0.173	-0.058	0.058	0.173	-
Log-Tchebycheff	y	-0.196	-0.098	0	0.098	0.196
	z	-0.196	-0.098	0	0.098	0.196

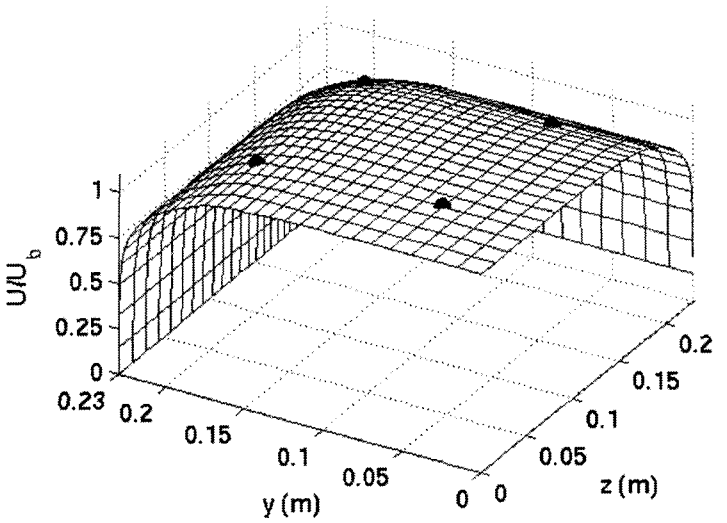

(a). The Equal Area method.

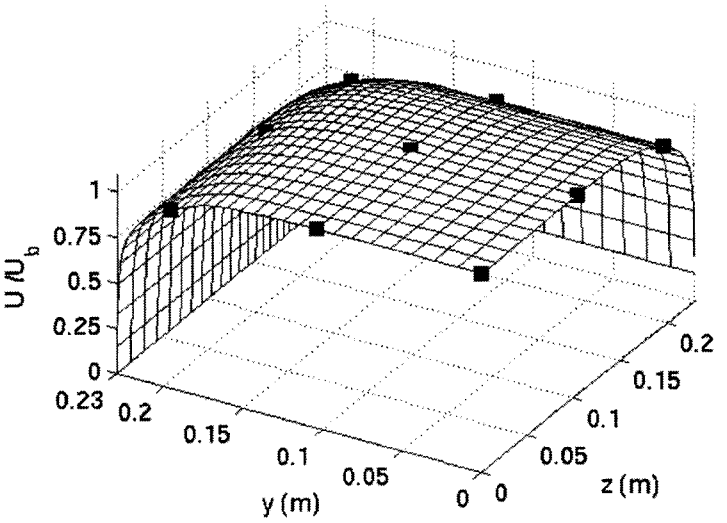

(b) The Log-Tchebycheff method.

Figure 5.6 The traverse locations corresponding to the dimensionless velocity profile at 6.5 D_h downstream and Re of 90,000. (a) The Equal Area method; (b) The Log-Tchebycheff method.

Figure 5.6 depicts the traverse locations for the Equal Area and the Log-Tchebycheff methods corresponding to the dimensionless velocity profile at Re of 90,000, 6.5 D_h downstream of inlet. On a quadrant of the cross section, there are 4 points for the Equal Area method and 9 points for the Log-Tchebycheff method displayed on the figure.

5.1.2.2 Effect of Reynolds number on accuracies of the Equal Area and the Log-Tchebycheff methods

As mentioned earlier, the flow at the outlet is very close to fully developed flow. Since the Log-Tchebycheff method deduces the traverse locations based on fully developed flow profile and the Equal Area method has no assumption on the velocity distribution, the comparison between the Equal Area and the Log-Tchebycheff methods at the outlet provides a critical evaluation of these two methods.

Figure 5.7 portrays the average velocities calculated from the Equal Area (U_{EA}) and the Log-Tchebycheff (U_{EA}) methods with different Re at the outlet, normalized by the bulk velocity U_b. Note that there is a numerical discretization error of 0.25% for U_b, as mentioned earlier. Since the average velocities (U_{EA}, U_{LT}) are proportional to the volumetric flow rates (Q_{EA}, Q_{LT}). The error calculated form Equation (5-1) is an indication of the accuracy of the estimated volumetric flow rate.

$$error = \frac{U - U_b}{U_b} \times 100\% . \qquad (5\text{-}1)$$

It can be seen that at the investigated Reynolds numbers, for each method, the variation of the relative error is very small with respect to different Reynolds numbers. The Equal Area method overestimates the flow rate by 3.5 ~ 4% while the Log-Tchebycheff method can achieve an accuracy of –0.4 ~ 0.8%.

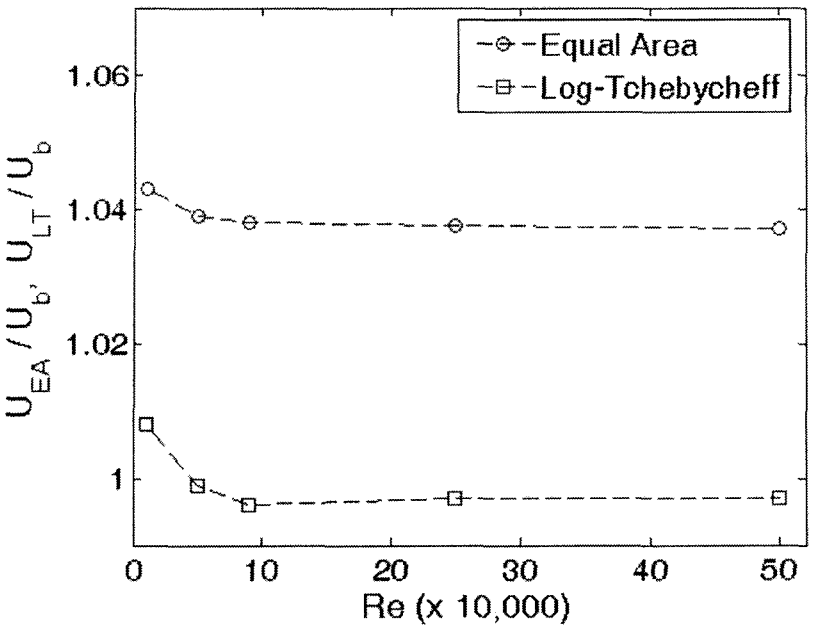

Figure 5.7 The accuracies of the Equal Area and the Log-Tchebycheff methods in deducing average velocities at the outlet.

5.1.2.3 Effect of downstream Location

Both the Equal Area and the Log-Tchebycheff methods are widely used in HVAC and other industries. The ideal application for the Log-Tchebycheff method is that the flow satisfies the fully developed flow condition. However, the flow in practice is seldom fully developed due to real-life disturbances. Practically, traverse measurements are often taken at 6 ~ 10 D_h downstream of any disturbance where the measurement results are considered to be acceptable (SMACNA, 1983). To find the effect of downstream location on the accuracy of the volumetric flow rate, the Equal Area and the Log-Tchebycheff methods were conducted at 3.4 D_h, 6.5 D_h, 9.6 D_h and 40 D_h (outlet) respectively. The average velocities (U_{EA} and U_{LT}) were calculated as Table 5.2.

Table 5.2 The effect of downstream locations on accuracies of traverse methods in deducing the average velocity.

Re		10,000	50,000	90,000	250,000	500,000
U_b (m/s)		0.33	1.64	2.96	8.22	16.43
3.4 D_h	U_{EA} (m/s)	0.347	1.724	3.081	8.556	16.986
	U_{LT} (m/s)	0.336	1.670	2.996	8.437	16.826
6.5 D_h	U_{EA} (m/s)	0.342	1.707	3.078	8.570	17.203
	U_{LT} (m/s)	0.333	1.652	2.972	8.297	16.649
9.6 D_h	U_{EA} (m/s)	0.341	1.711	3.087	8.606	17.193
	U_{LT} (m/s)	0.330	1.644	2.963	8.228	16.503
40 D_h	U_{EA} (m/s)	0.339	1.698	3.072	8.527	17.008
	U_{LT} (m/s)	0.331	1.64	2.948	8.196	16.381

Figure 5.8 portrays the variation of the dimensionless average velocities along the streamwise location at Re of 250,000. It can be seen that at 3.4 D_h downstream, the difference between the Equal Area and the Log-Tchebycheff methods is relatively small (1.5%). This is because at this location, the boundary layer is thin, the velocity profile is relatively uniform, so the velocity differences among traverse points are small, so the differences of average velocities and flow rates between the two methods are small. When the flow moves further downstream, the boundary layer develops to be thicker in which the velocity decreases while the velocity gradient increases. The flow profile is closer to the fully developed profile which is the assumption of the Log-Tchebycheff method. Thus U_{LT} /U_b decreases and the accuracy of the Log-Tchebycheff methods

increases. Since the Equal Area method divides the cross section into 16 subsections and the traverse points are located at the center of each subsection, the mean velocities in those 12 near-wall subsections are lower than the velocities of the corresponding traverse points. Therefore, the mean velocity of the whole cross section is lower than the average value of all traverse point velocities. The Equal Area method thus overestimates the volumetric flow rate.

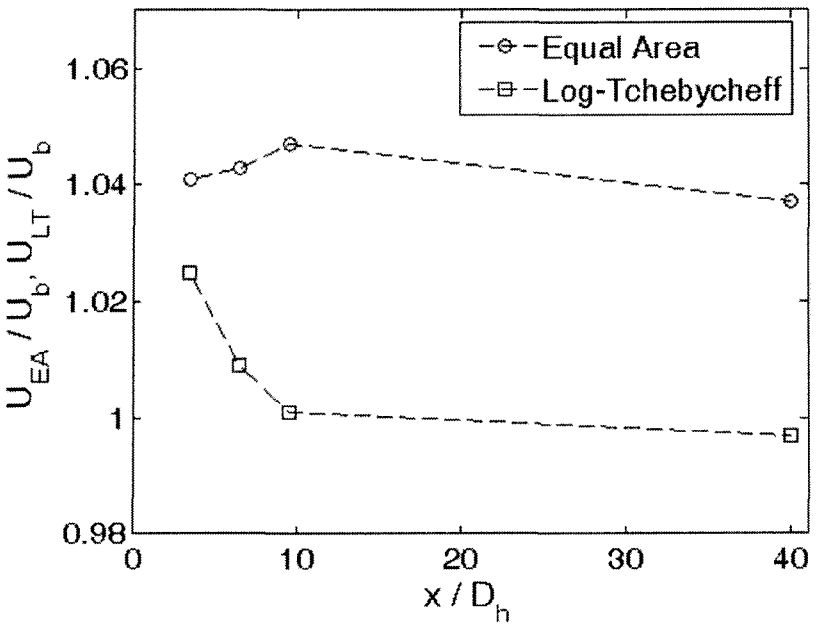

Figure 5.8 The accuracies of the Equal Area and the Log-Tchebycheff methods in deducing average velocities at different downstream locations at Re of 250,000.

It can be noticed that the accuracy changes little after 9.6 D_h compared to that at the immediate downstream location (3.4 D_h). This coincides with the fact that industrial standards do not require the traverse plane to be more than 10 D_h downstream. It can be concluded that after 6.5 D_h downstream, the Equal Area method overestimates the flow

rate by 3.5 ~ 4.7% while the Log-Tchebycheff estimates the flow rate with the deviation of –0.4 ~ 0.8% from the actual flow rate.

5.2 Experimental Results

The hot-wire anemometer system with an automatic traversing mechanism was employed to carry out velocity traverse measurements. According to the standard (ASHRAE 111, 1988), the traverse measurement plane was defined at 2.5 D_h upstream of the duct exit. In addition, to diminish the blockage effect of the traversing column, the traversing mechanism was placed 0.5 m (1 D_h) upstream of the exit.

The traverse measurements were performed at the duct inlet and three downstream locations by mounting different numbers of duct sections. At each cross section, an 11 × 11 traverse grid was followed to measure velocity profiles. Moreover, traverse measurements were performed at each downstream location following a 4 × 4 traverse grid according to the Equal Area method and a 5 × 5 traverse grid according to the Log-Tchebycheff method. The volumetric flow rates based on both methods were calculated and evaluated.

The flow at three Reynolds numbers, namely, 90,000, 115,000 and 140,000, were examined at each cross section. Due to the difficulty in precisely controlling the flow rate and Re, which were realized by adjusting the gate damper at the inlet of the blower, the actual Re, slightly deviated from the nominal Re. the examined flow was referred to its nominal Re in this study.

5.2.1 Flow profiles

The velocity profiles were acquired by measuring point velocities following an 11 × 11 traverse grid as defined in Section 4.5. The display coordinate is shown in Figure 4.8 where the origin is located at the center of the plane. The grid spacing is 0.025 m or 0.05 m along both the horizontal (Y) and vertical (Z) axis. The uncertainty of locating measurement points within the duct is 0.003 m along the coordinate axes. The uncertainty of measuring point velocities by the hot-wire system is 1.3% without considering the spatial uncertainty.

5. 2.1.1 Flow conditions at the inlet

A flow conditioner, constructed of a straw-filled tube bundle and three pieces of screens, was employed attempting to make flow more uniform at the inlet of the test square duct. It was found that the time-mean velocity of the incoming flow was steady with a fluctuation below 0.43%, as detailed in Appendix D.5. To check the uniformity of the velocity distribution at the inlet, the traverse measurement was performed at 0.15 m downstream of the last screen. Hence the cross section at this location was considered as the flow inlet. The flow was measured at the actual Reynolds numbers of 90,336, 115,860 and 143,676.

Figures 5.9 – 5.11 portray the measured velocity profiles at the inlet. The flow displays similar characteristics with varied Reynolds numbers. The uniformity of the velocity profiles is well behaved. Table 5.3 depicts the maximum (U_{max}), minimum (U_{min}) and the spatial-averaged (U_{avg}) velocities of the inlet plane. The maximum relative velocity difference ($(U_{max}-U_{min})/U_{avg}$) is an effective factor to indicate the velocity

uniformity of the cross section. It has a maximum value of 11.8% at Re of 90,336 and then decreases with the increase of Reynolds number. Several trials were conducted to achieve this result by repeatedly modifying the flow conditioner B with different combinations of tube bundle, screens and straws.

Table 5.3 The mean flow field at the inlet

Re	U_{avg} (m/s)	U_{max} (m/s)	U_{min} (m/s)	$(U_{max}-U_{min})/U_{avg}$ (%)
90,336	3.14	3.31	2.94	11.8
115,860	4.02	4.23	3.78	11.2
143,676	4.99	5.11	4.61	10

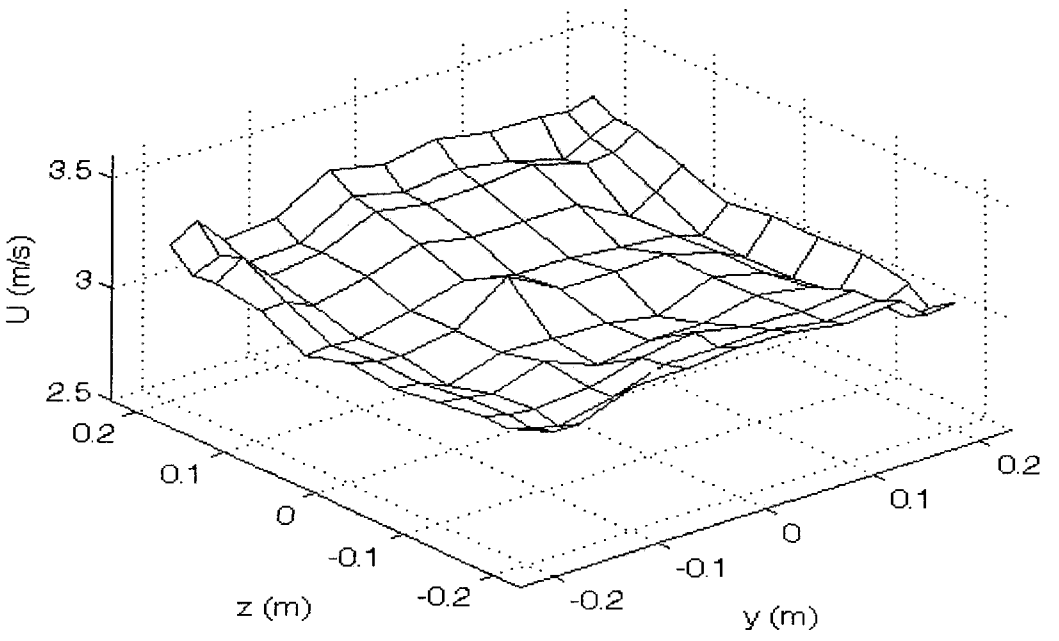

Figure 5.9 The inlet velocity profile at Re of 90,336.

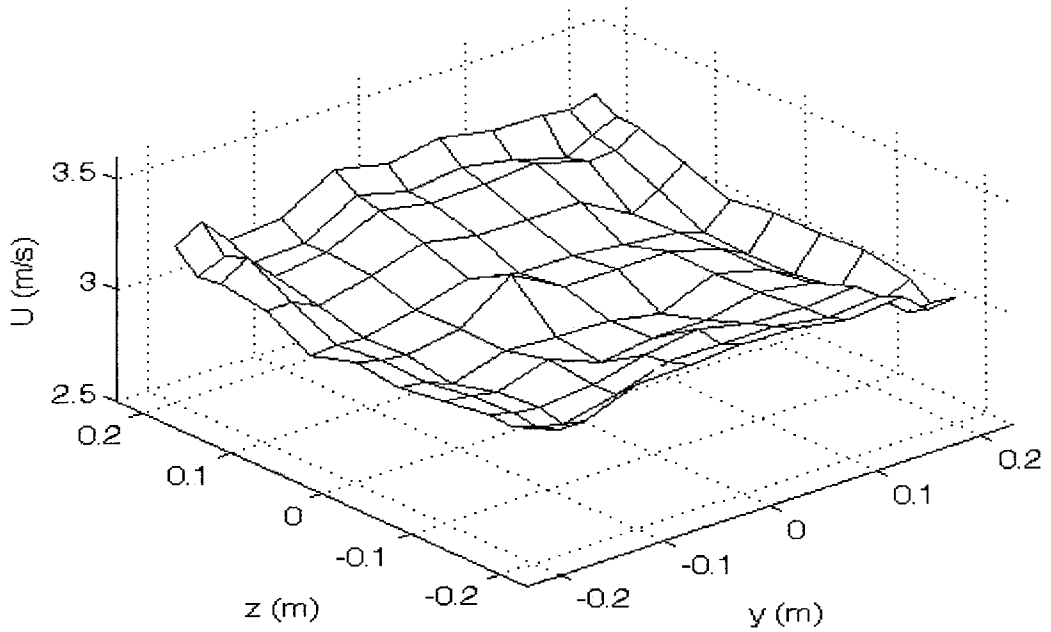

Figure 5.10 The inlet velocity profile at Re of 115,860.

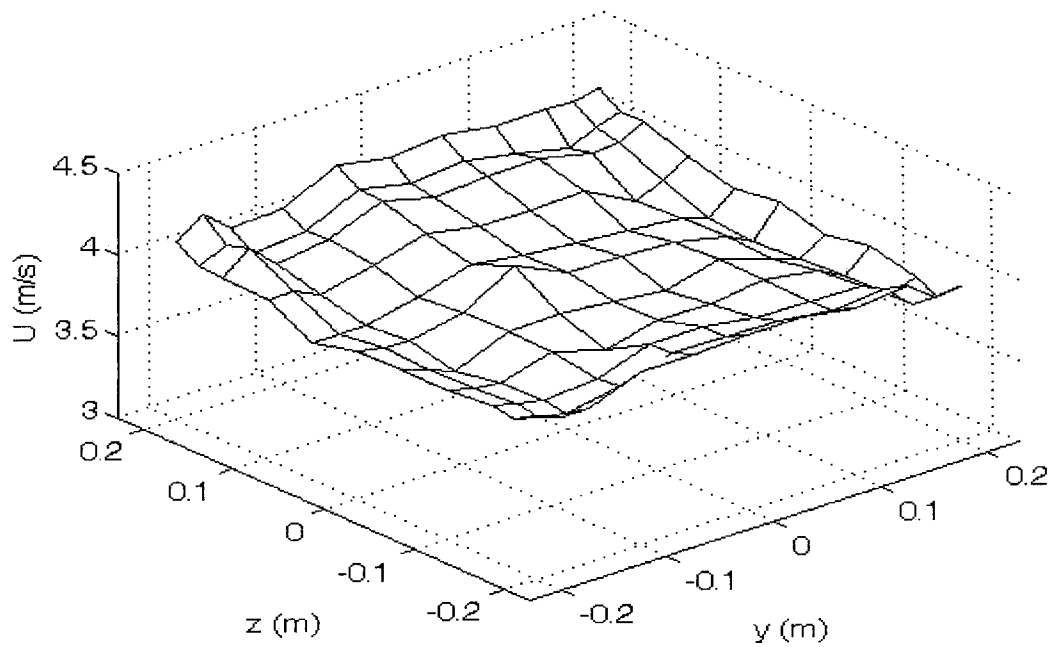

Figure 5.11 The inlet velocity profile at Re of 143,676.

5.2.1.2 Flow profiles at different downstream locations

The traverse measurements were carried out at three downstream locations: 3.4 D_h, 6.5 D_h and 9.6 D_h. At each cross section, three flow conditions with various Reynolds numbers were measured. Figure 5.12 portrays the development of the velocity profiles at the nominal Reynolds number of 90,000 (90,396, 90,835 and 89,721). At 3.4 D_h downstream, there is only a slight variation of the velocity profile compared to that at the inlet (Figure 5.9). This is mainly due to the fact that the traverse plane is so close to the inlet that the boundary layer is very thin and does not significantly influence the velocities of traverse points. Further downstream, a large velocity drop can be observed at the near-wall region (Figures 5. 12(b) and 5. 14(c)). At the 6.5 D_h downstream, the velocities on the first outmost traverse lines drop significantly. When flow moves further downstream to 9.6 D_h, the velocities on the second outmost traverse lines appear to drop largely, too.

Figure 5.13 portrays the velocity profiles at the nominal Reynolds number of 115,000 at varied downstream locations. Figure 5.14 depicts the velocity profiles at the nominal Reynolds number of 140,000. The characteristics of their flow development process are very similar to that at Re of 90,000.

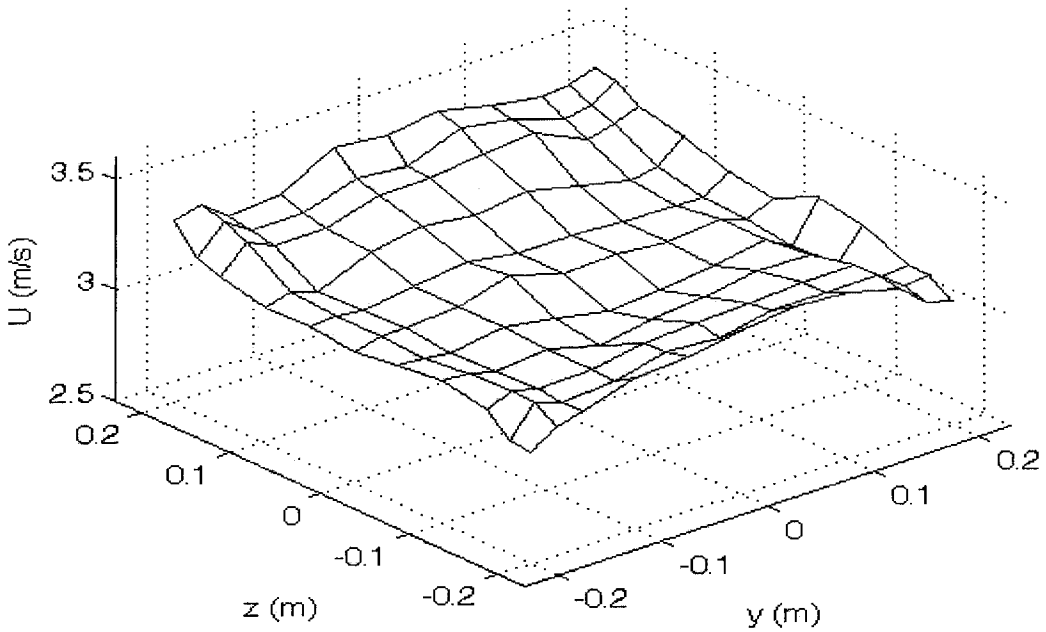

Figure 5.12 (a) The velocity profile at 3.4 D_h downstream and Re of 90,396.

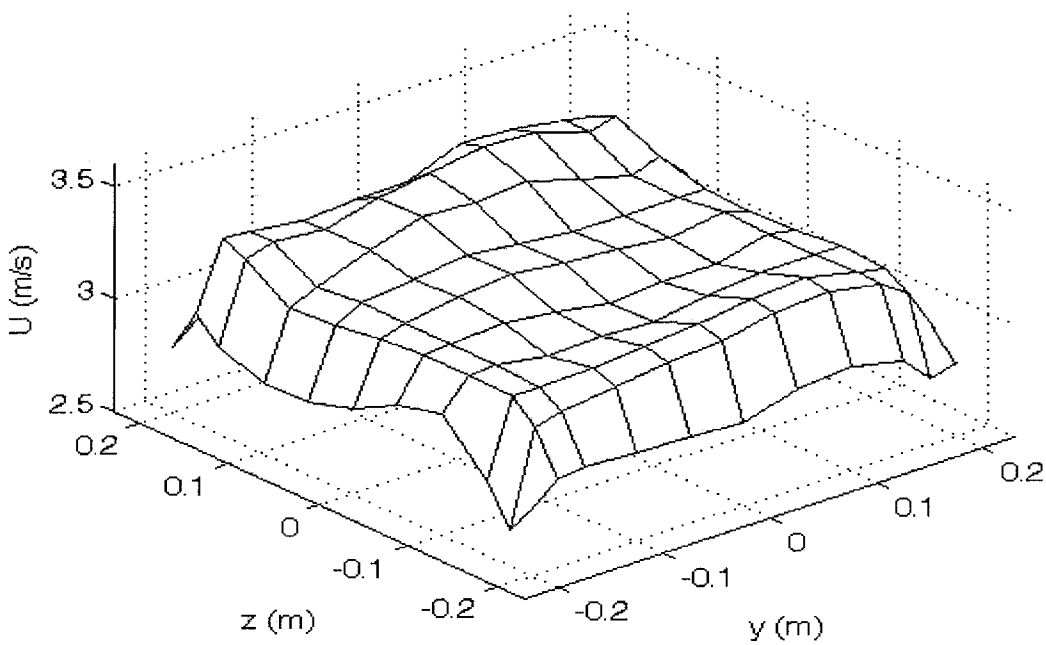

Figure 5.12 (b) The velocity profile at 6.5 D_h downstream and Re of 90,835.

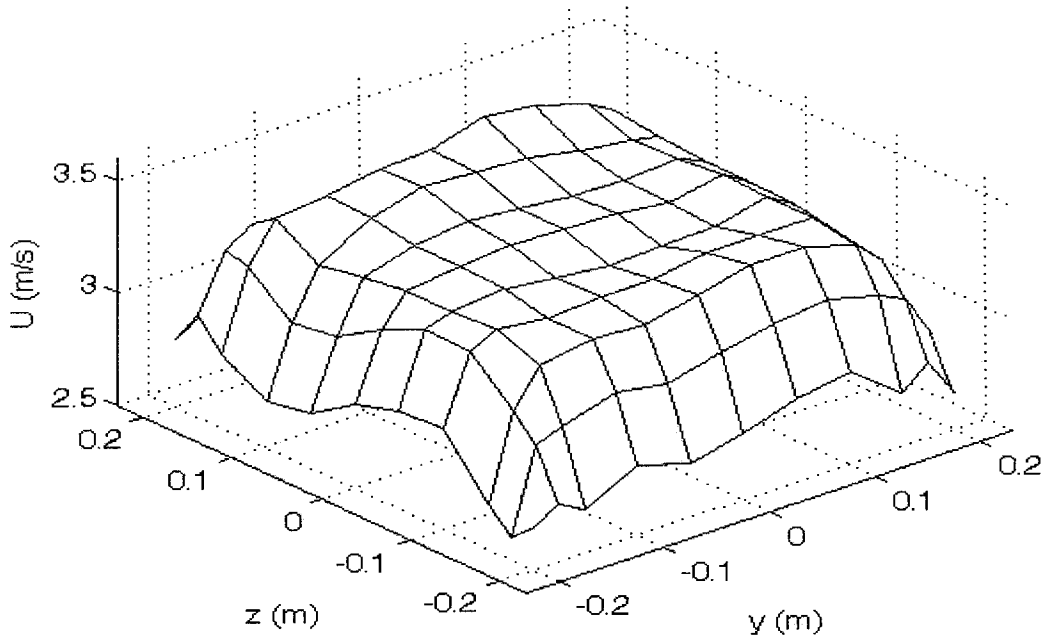

Figure 5.12 (c) The velocity profile at 9.6 D_h downstream and Re of 89,721.

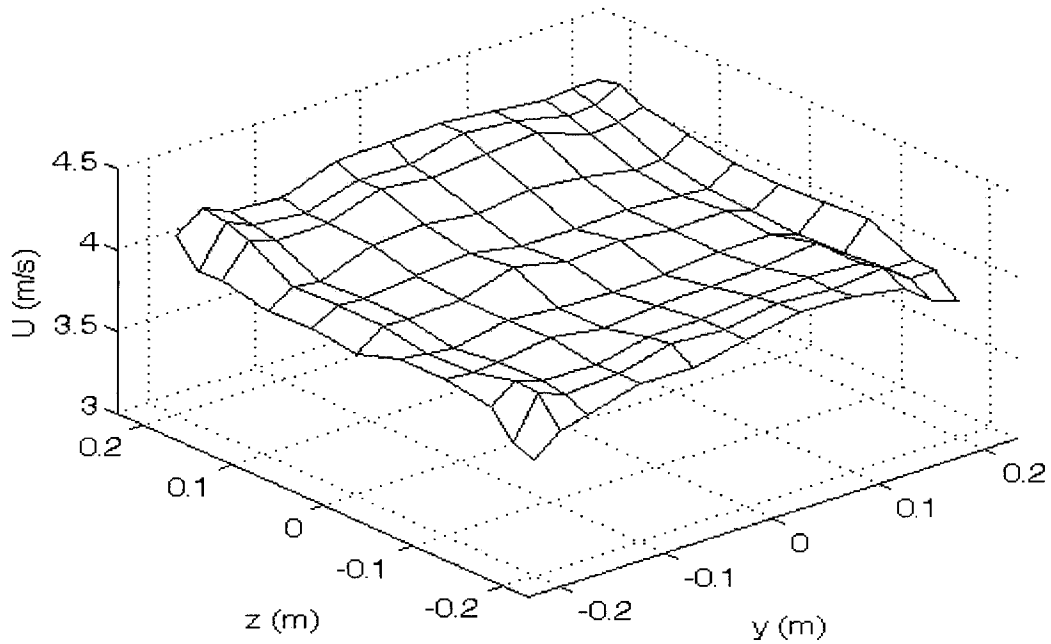

Figure 5.13 (a) The velocity profile at 3.4 D_h downstream and Re of 115,960.

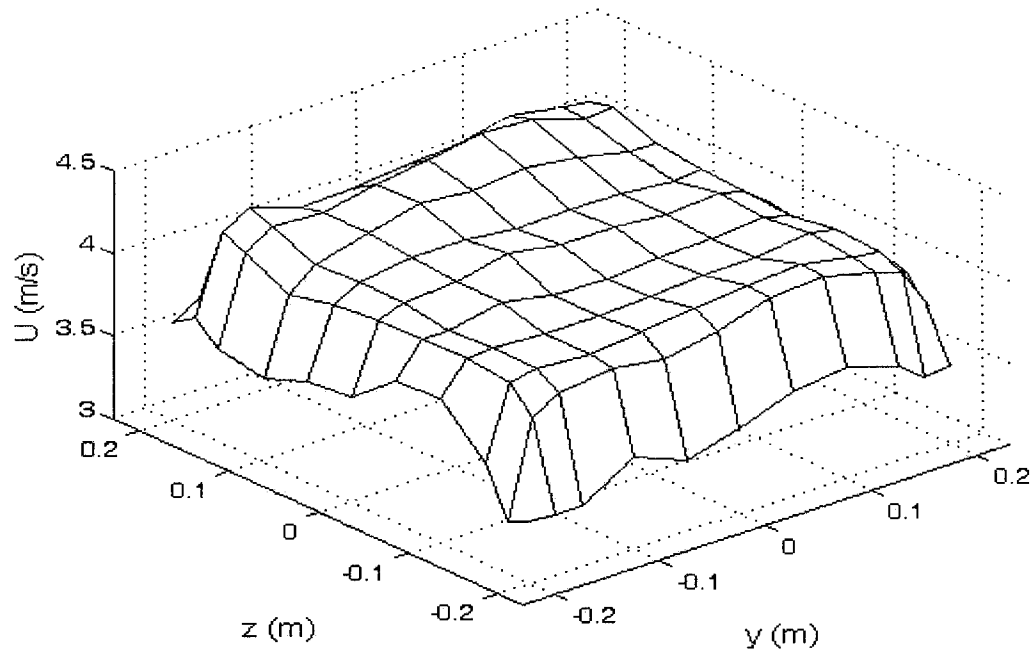

Figure 5.13 (b) The velocity profile at 6.5 D_h downstream and Re of 116,071.

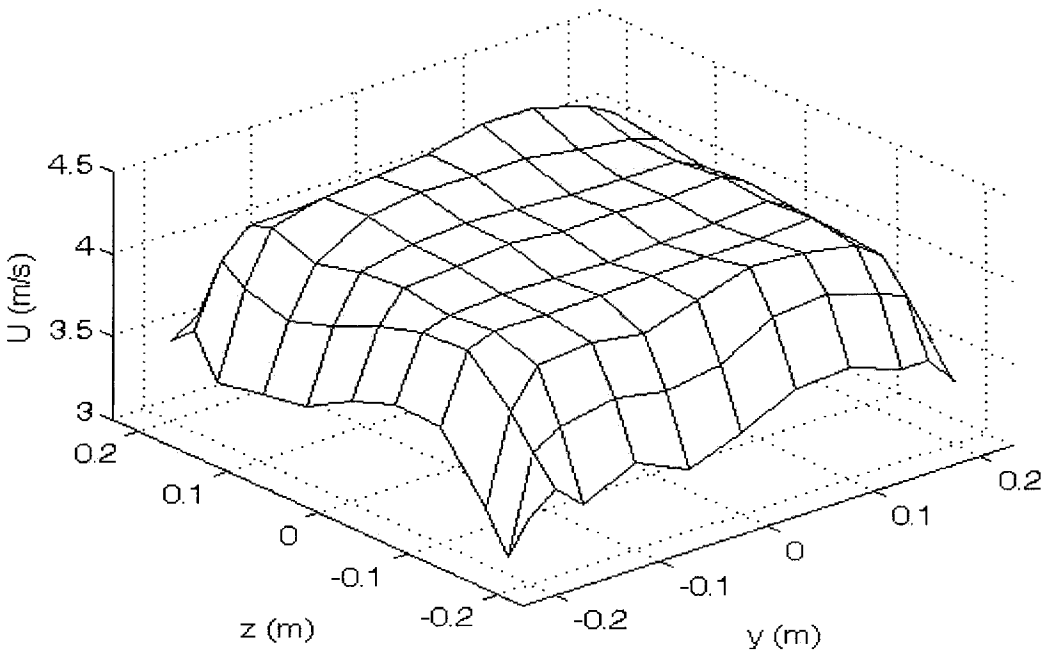

Figure 5.13 (c) The velocity profile at 9.6 D_h downstream and Re of 114,778.

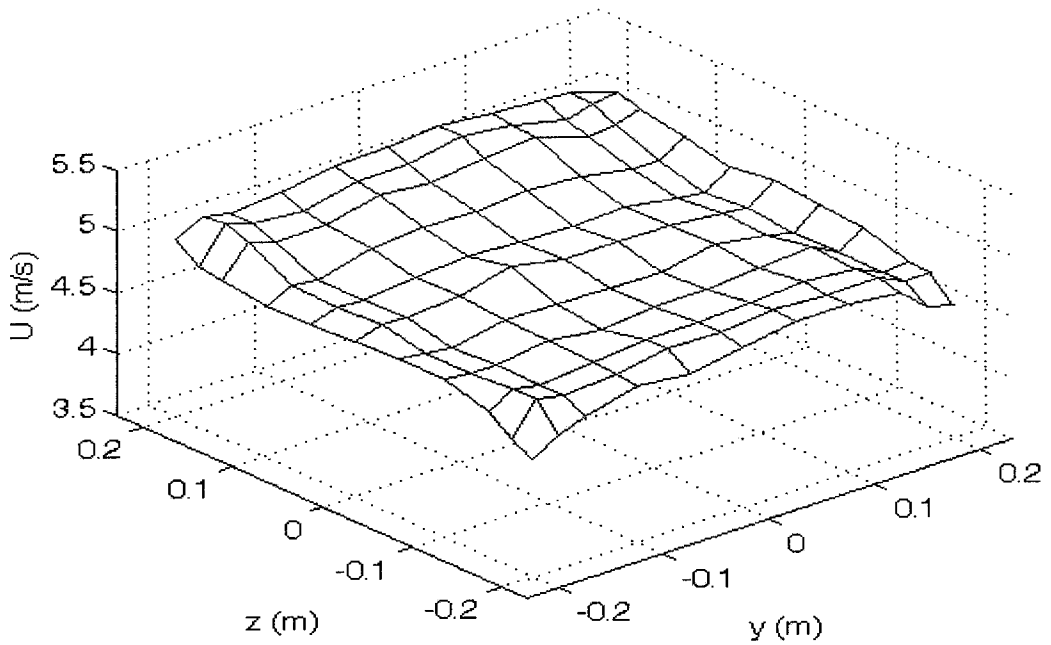

Figure 5.14 (a) The velocity profile at 3.4 D_h downstream and Re of 143,497.

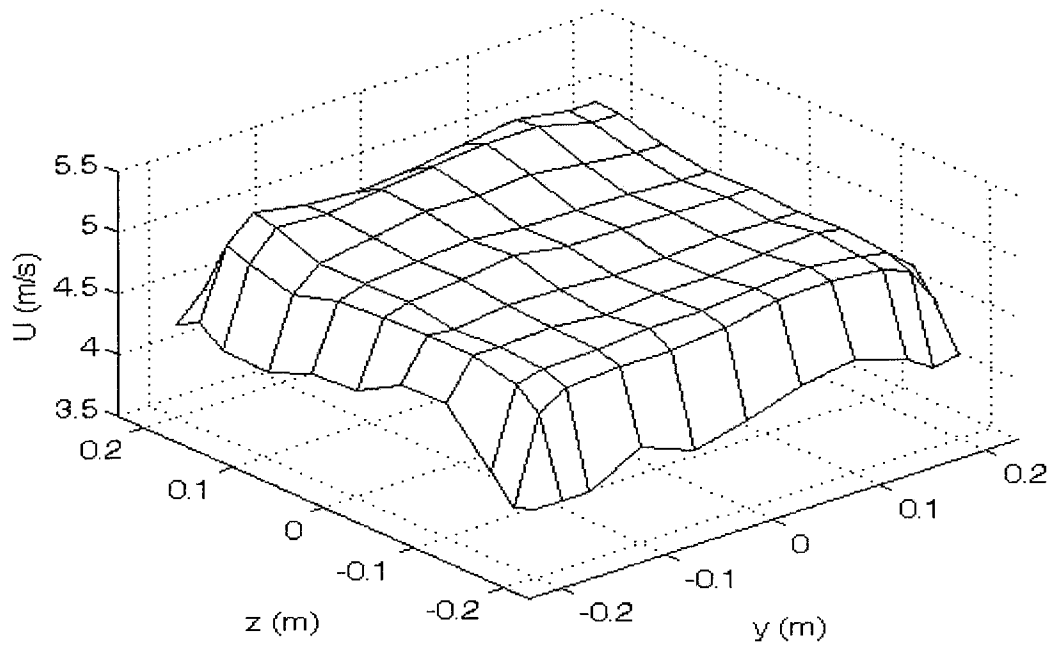

Figure 5.14 (b) The velocity profile at 6.5 D_h downstream and Re of 135,383.

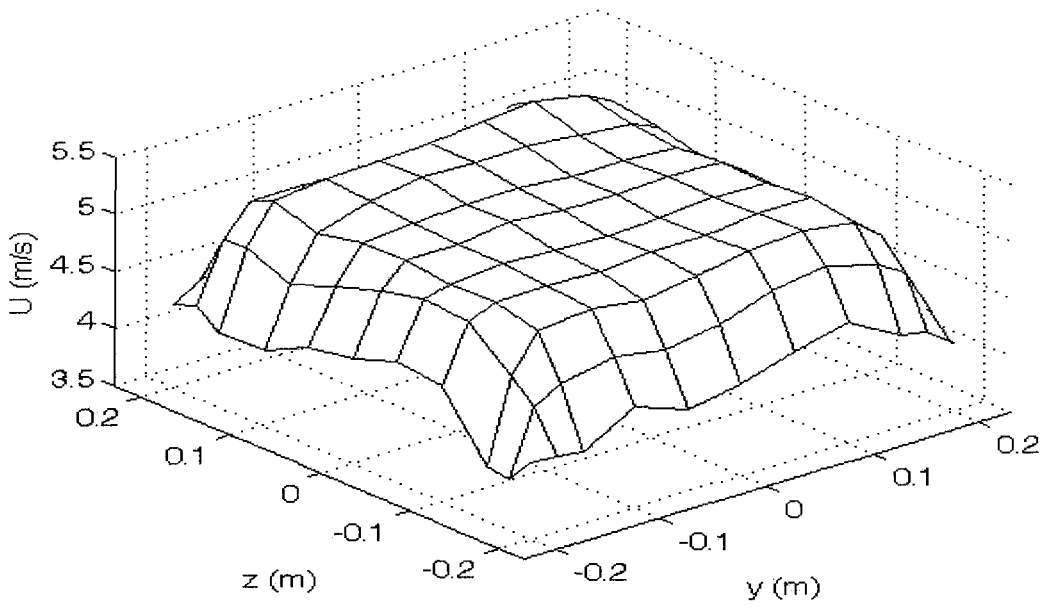

Figure 5.14 (c) The velocity profile at 9.6 D_h downstream and Re of 137,393.

5.2.1.3 Flow development process along *Y*-axis

The flow development process can be expressed by depicting the dimensionless velocity profiles along *Y-axis* at different streamwise locations, as portrayed in Figure 5.15. It depicts that as flow moves downstream, the velocities drop at the near-wall region with a sequence from the outmost points to the inner points. On the other hand, the velocities in the central region slightly increase to keep the total flow rate constant. It appears that the boundary layers grow thicker with flow developing downstream.

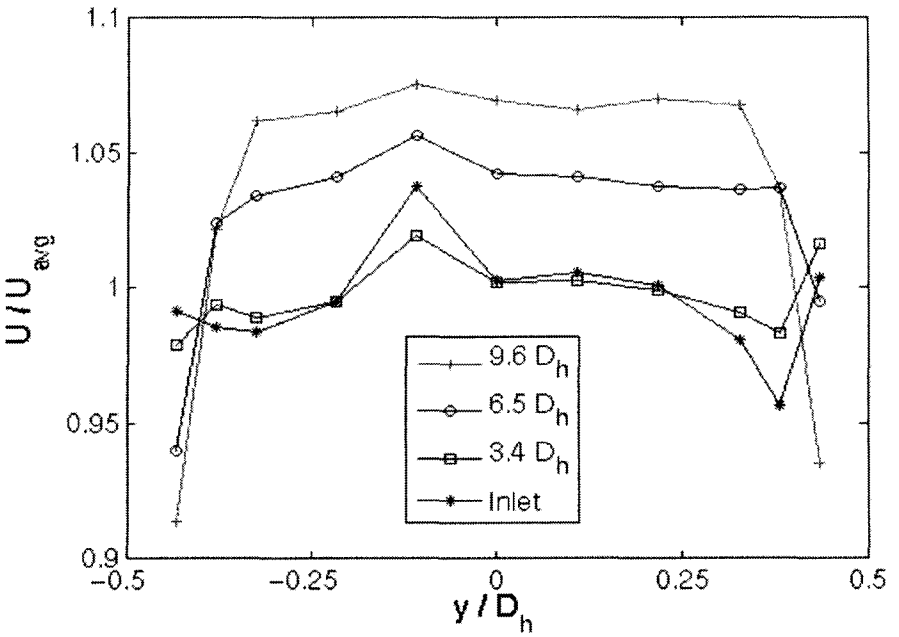

Figure 5.15 The velocity development process along *Y*-axis at Re of 140,000.

5.2.2 Accuracies of the Equal Area and the Log-Tchebycheff methods on airflow rate estimation

Both the Equal Area and the Log-Tchebycheff methods deduce the volumetric flow rate based on finite numbers of point velocities at specific locations. The flow profile varies at different streamwise locations, especially at the near-wall region, where high velocity gradients were observed. The effects of velocity profile and streamwise locations on deducing volumetric flow rates are described below.

Figures 5.16–5.18 portray the locations of traverse points corresponding to measured velocity profiles. The circular markers ("O") depict the point velocities for the Equal Area method and the square markers ("□") portray the point velocities for the Log-Tchebycheff method. The velocities of these points were measured by the hot-wire system based on locations defined by the Equal Area (16 points) and the Log-

Tchebycheff (25 points) methods. Note that some points are hidden by the image of the velocity profile. The mesh-shaped velocity profiles were plotted based on the 11 × 11 traverse measurements and linear interpolations between measurement points. It shows that the measured point velocities based on the Equal Area and the Log-Tchebycheff methods agree well with the plotted velocity profiles.

At 3.4 D_h downstream, the velocity profile is relatively flat and there is no significant velocity difference between the outmost traverse points and the points in the central region. Thus there is no obvious difference for the volumetric flow rates deduced from the two methods. When the flow goes further downstream to 6.5 D_h and 9.6 D_h, due to the development of the boundary layer, the velocities in the near-wall regions decrease sharply.

The Equal Area method divides the duct cross section into 16 subsections, among which 12 subsections are near-wall subsections. Correspondingly, there are 12 outmost points in the near-wall region and 4 points in the central region. These outmost points have a distance of 0.058 m from the wall surface according to Table 4.3. Similarly, there are 16 outmost points in the near-wall region and 9 remaining points in the central region for the Log-Tchebycheff method. The outmost traverse points have a closer distance to the wall surfaces (0.034 m) than those in the Equal Area method and are significantly influenced by high velocity gradients in the near-wall region.

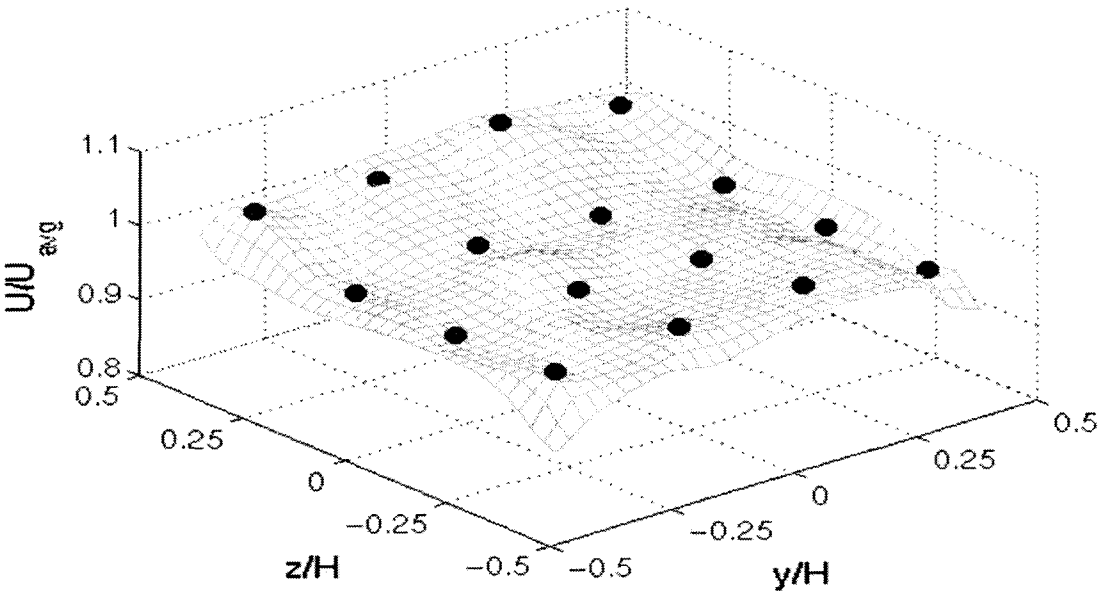

(a) The Equal Area method.

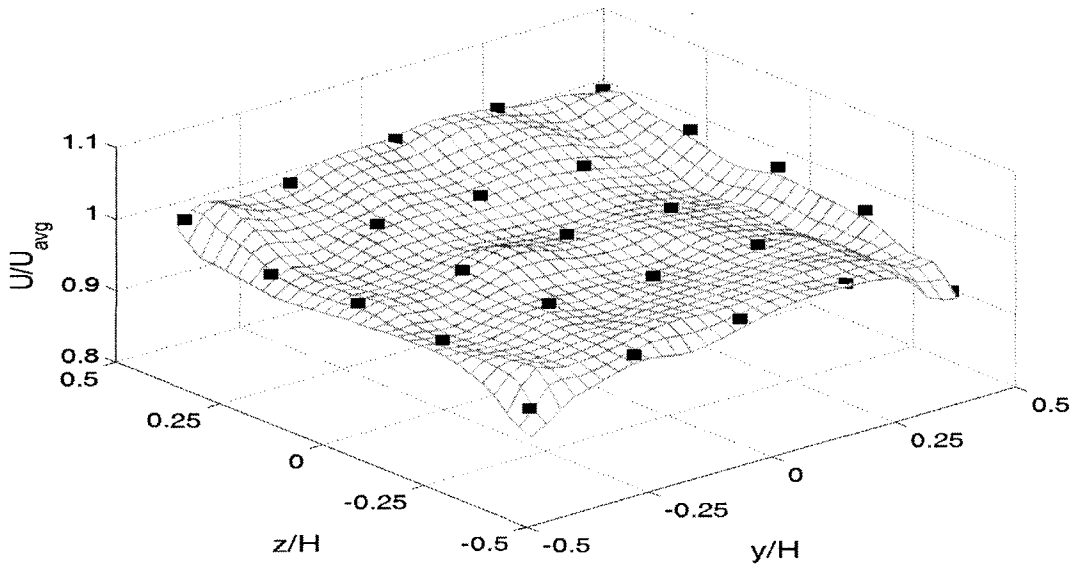

(b) The Log-Tchebycheff method.

Figure 5.16 The traverse locations combining with the velocity profile at 3.4 D_h downstream. (a) The Equal Area method; (b) The Log-Tchebycheff method.

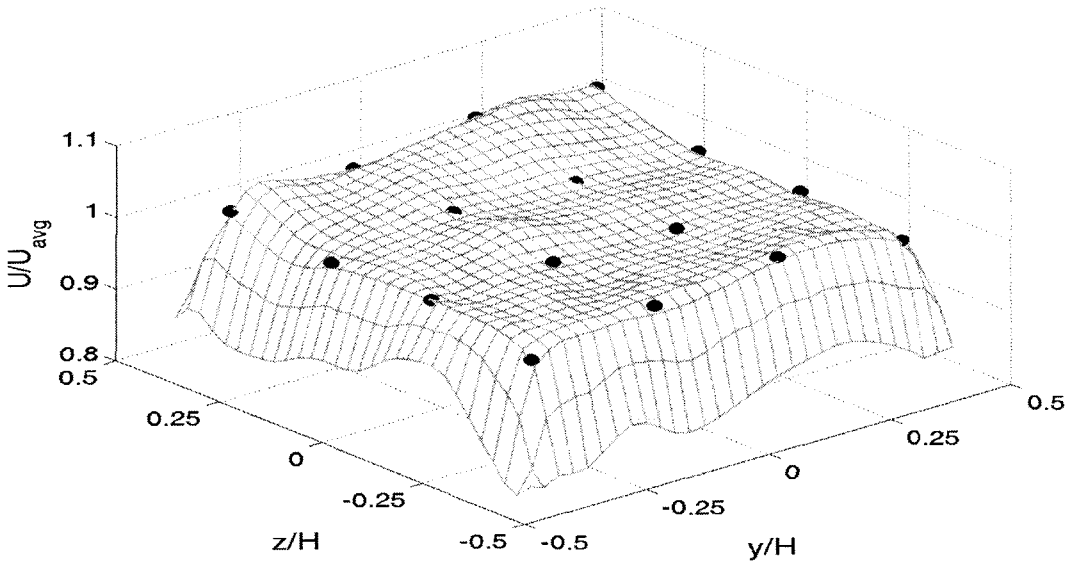

(a) The Equal Area method.

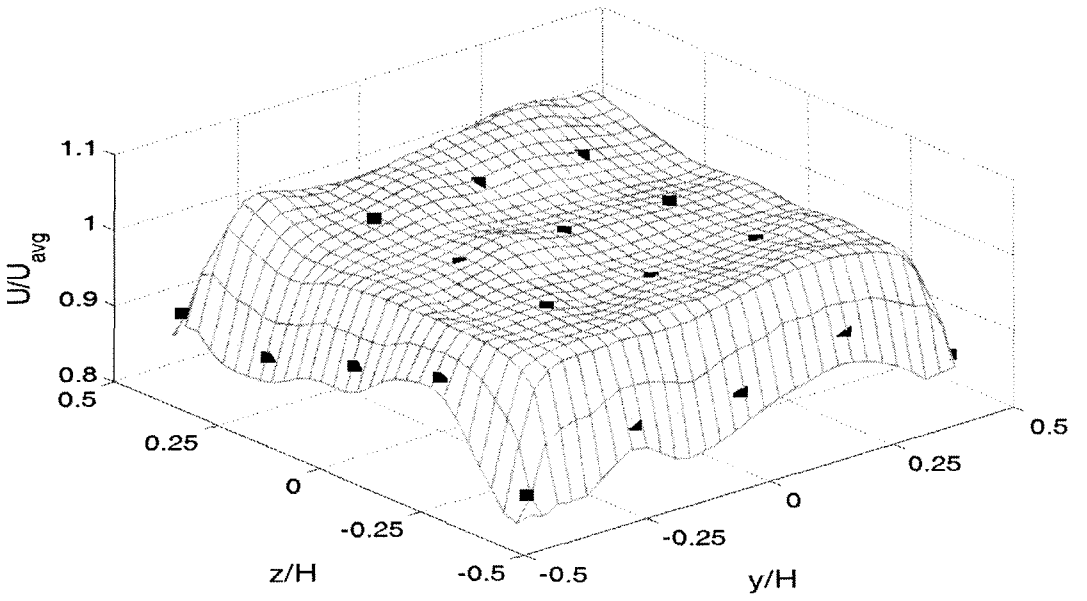

(b) The Log-Tchebycheff method.

Figure 5.17 The traverse locations combining with the velocity profile at 6.5 D_h downstream. (a) The Equal Area method; (b) The Log-Tchebycheff method.

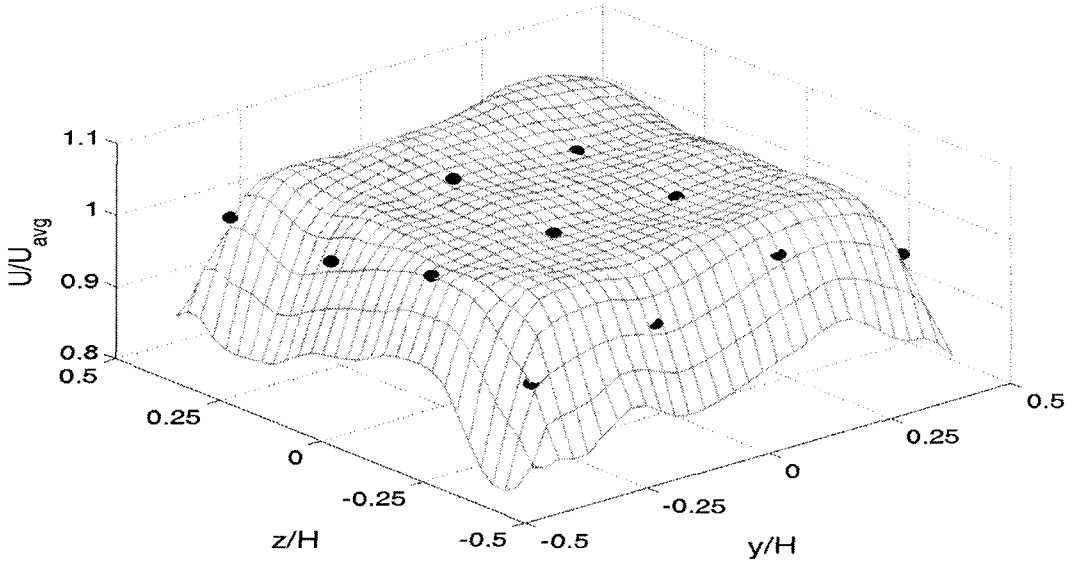

(a) The Equal Area method.

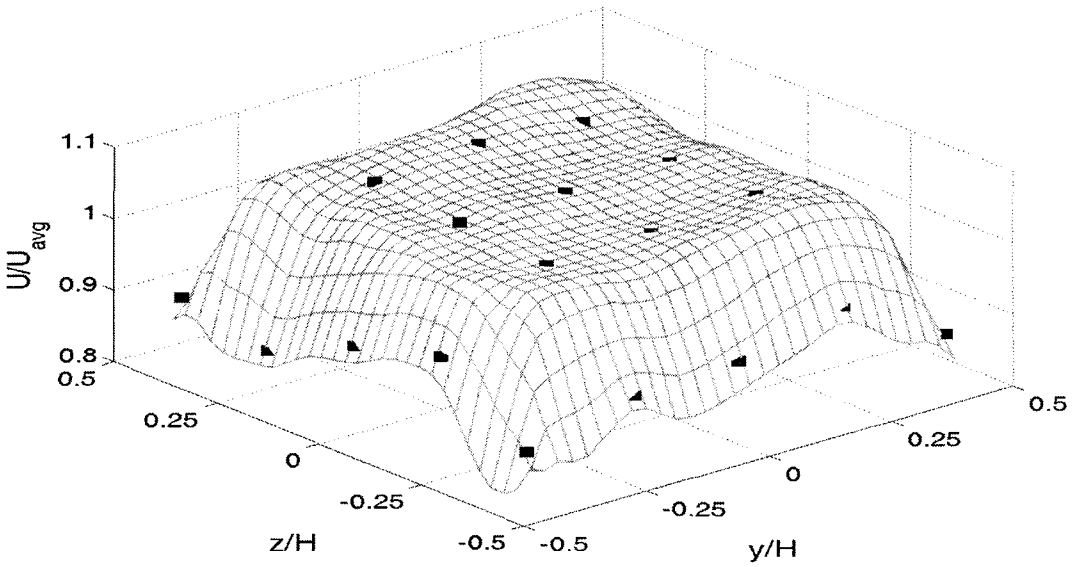

(b) The Log-Tchebycheff method.

Figure 5.18 The traverse locations combining with the velocity profile at 9.6 D_h downstream. (a) The Equal Area method; (b) The Log-Tchebycheff method.

It can be seen that in Figures 5.17 (b) and 5.17 (b) the velocities for the 16 outmost points in the Log-Tchebycheff method are lower than those 9 points in the central region. Thus the average velocity (U_{LT}) based on these 25 points will decrease. On the other hand, since the outmost 9 points for the Equal Area method have a larger distance from duct walls than those in the Log-Tchebycheff method, the velocity differences between the points in the central region and those in the outer region are relative small. Thus the boundary layer effect on the traverse point velocities appears to be insignificant, as shown in Figure 5.17 (a) and 5.17 (a).

Table 5.4 depicts the volumetric flow rates deduced from the Equal Area (Q_{EA}) and the Log-Tchebycheff (Q_{LT}) methods at all measurements. The flow rate acquired from the Venturi meter (Q_{ven}) was considered as the reference flow rate. The relative error was quantified according to Equation (5-2),

$$Error = \frac{Q - Q_{ven}}{Q_{ven}} \times 100\%. \tag{5-2}$$

The uncertainty analysis in Appendix D shows that, the relative uncertainty for the reference flow rate is 0.8%. The relative uncertainties for Q_{EA} and Q_{LT} are 2.1% and 2.4% respectively whereas the uncertainty for the Reynolds number is 1.2%.

Table 5.4 The accuracies of the Equal Area and the Log-Tchebycheff methods in deducing the volumetric flow rate.

Location (D_h)	Re	Q_{ven} (m^3/s)	Equal Area		Log-Tchebycheff	
			Q_{EA} (m^3/s)	Error (%)	Q_{LT} (m^3/s)	Error (%)
3.4	143,497	1.054	1.048	-0.56	1.042	-1.11
	115,960	0.852	0.854	0.27	0.857	0.59
	90,396	0.664	0.668	0.59	0.671	1.05
6.5	135,383	1.042	1.088	4.63	1.035	-0.64
	116,071	0.853	0.881	3.32	0.841	-1.39
	90,835	0.667	0.690	3.55	0.656	-1.65
9.6	137,393	1.038	1.075	3.6	1.022	-1.5
	114,778	0.843	0.867	2.85	0.826	-1.97
	89,721	0.659	0.679	3.0	0.644	-2.27

Figure 5.19 depicts the effect of downstream location on the accuracies of the Equal Area and the Log-Tchebycheff methods in obtaining volumetric flow rates at Reynolds number of 140,000. At 3.4 D_h downstream, there is no obvious difference between the Equal Area and the Log-Tchebycheff methods in deducing volumetric flow rates. This is because at this location, the velocity profile is relatively flat, thus there is no significant velocity difference among all traverse points, as portrayed in Figure 5.16. However, as it is shown in the Figure 5.19 at downstream locations of 6.5 D_h and 9.6 D_h, the volumetric flow rate estimates by the Equal Area method deviates more significantly from the actual flow rate with respect to the estimates made from the Log-Tchebycheff

method. This is due to the fact that as the flow moves further downstream, the velocities of those outmost points in the Log-Tchebycheff method drop significantly while the velocities of those outmost points in the Equal Area method still keep relatively high values, as depicted in Figures 5.17 and 5.18. Therefore, it can be concluded that the Equal Area method overestimates the volumetric flow rate as compared to the Log-Tchebycheff method.

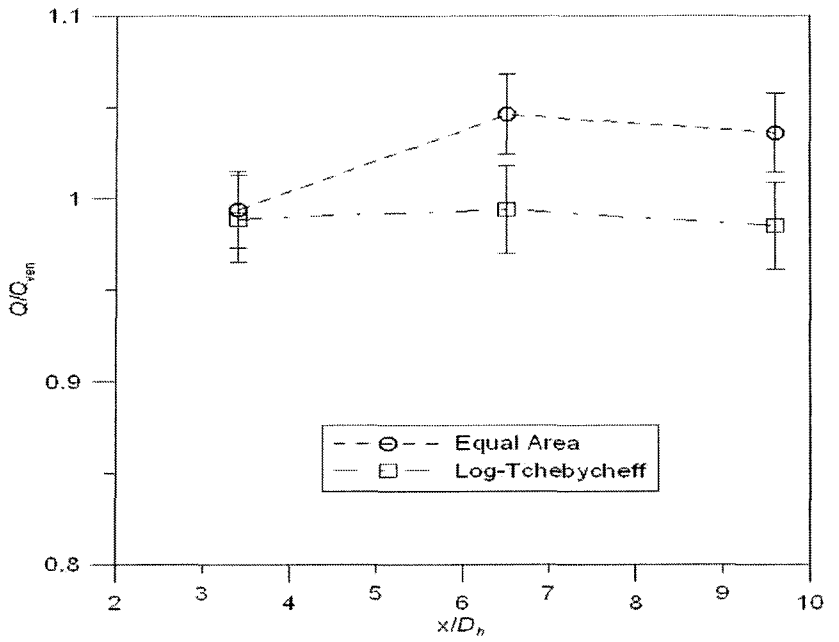

Figure 5.19 The effect of downstream location on the volumetric flow rate estimation at Re of 140,000.

Since in practical applications traverse measurements are required to be carried out at the downstream location between 6 to 10 D_h, the comparison between these two methods in estimating volumetric flow rates were made on the downstream locations of 6.5 D_h and 9.6 D_h. Figure 5.20 portrays the effect of Reynolds number on the accuracies of the Equal Area and the Log-Tchebycheff methods at these two downstream locations.

For both methods at the same downstream location, the estimated flow rates acquire less than 1% variation with different Re values. This indicates that varying Reynolds number does not significantly affect the accuracies of either method in estimating the volumetric flow rate.

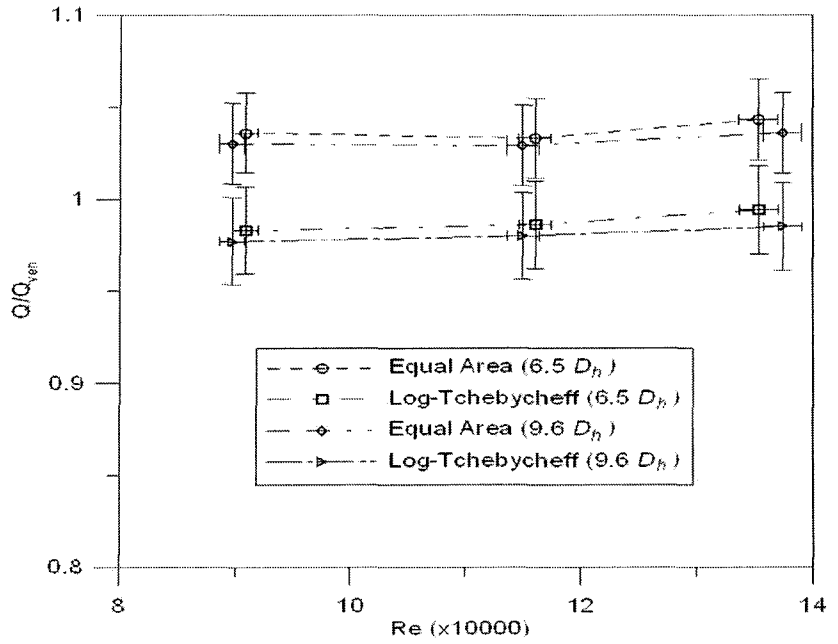

Figure 5.20 The effect of Re on the volumetric flow rate estimation at the downstream location of 6.5 D_h and 9.6 D_h.

In the light of above discussions and tabulated values in Table 5.4 it can be concluded that at the downstream locations of 6.5 D_h and 9.6 D_h, the Equal Area method overestimated the flow rate by 3 ~ 4.6%, whereas the Log-Tchebycheff method underestimated the flow rate by 0.6 ~ 2.3%. These results indicate that the Log-Tchebycheff method estimates the flow rate with better accuracy, which is in agreement with the numerical findings.

5.2.3 Comparison of the hot-wire system and a hand-held anemometer in measuring air velocity

Hand-held instruments are widely used to take velocity traverse measurement in practice since they are inexpensive and easy to handle. The main difference between a hand-held instrument and an automated hot-wire system is the accuracy. In view of this, a TSI hand-held anemometer (Velocimeter® Model 8345) was used to take the point velocity measurement. The velocity values were compared with those measured by the hot-wire system at the same location and flow condition.

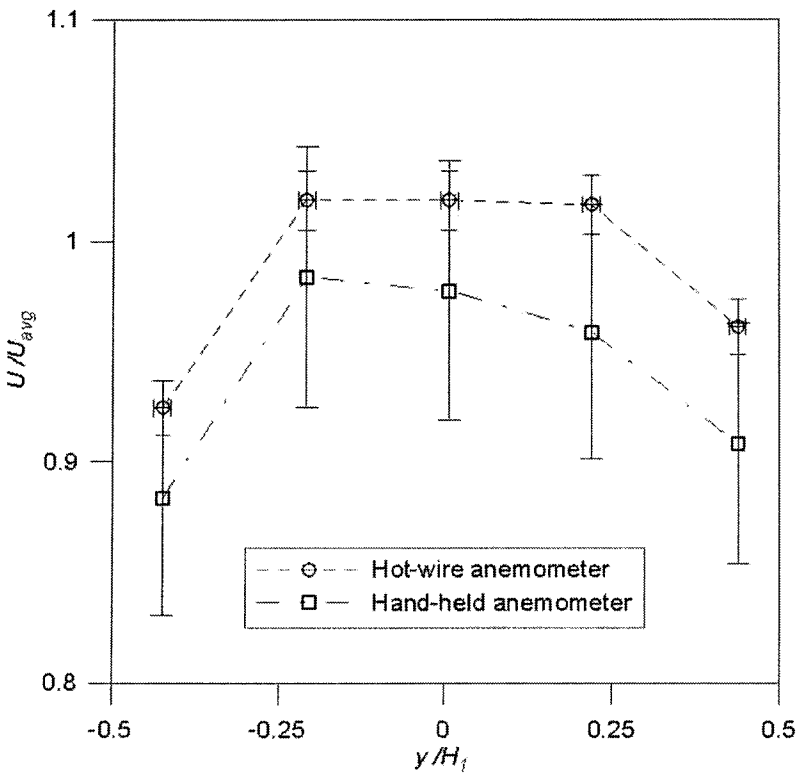

Figure 5.21 Comparison of velocity measurements using hand-held anemometer and hot-wire system at Re of 135,383 and 6.5 D_h downstream.

Figure 5.21 depicts the dimensionless point velocities measured at Re of 135,383, 6.5 D_h downstream. The measurement locations were defined according to the central row of the Log-Tchebycheff method, i.e. along the Y-axis. The uncertainty of point velocity for the hot-wire system was 1.3% without accounting for the spatial uncertainty. The uncertainty for the hand-held anemometer was calculated to be 6.0% including 4.9% spatial uncertainty, as detailed in Appendix D. The hand-held anemometer was shown to underestimate the velocities, probably due to the misalignment of probe. However, they are within the uncertainty limits. Compared to the hot-wire measurement system, the hand-held anemometer has a larger measurement uncertainty due to the instrument accuracy and positioning error. This measurement uncertainty is greater than the difference of the Equal Area and the Log-Tchebycheff methods in estimating the flow rate. That is why in practice technicians cannot tell which method is superior than another.

5.3 Comparison between simulation and experimental results

In this section, the simulation and experimental results, including the velocity profiles and the accuracies of the Equal Area and the Log-Tchebycheff methods in deducing volumetric flow rates, are compared. Note that in the simulation, the inlet was treated to have a uniform velocity profile. In the experiment the inlet was measured to have a close-to-uniform velocity profile with a ratio of the maximum to the minimum velocity of 10 ~ 11.8%.

5.3.1 Comparison of the velocity profile along *Y*-axis

Figure 5.22 (a) portrays the dimensionless inlet velocity profile along *Y*-axis of the cross section at Re of 90,000 (90,336 for the experiment). The velocity profile measured from the experiment varies around the horizontal line, which represents the uniform velocity profile at the inlet in the simulation. Figure 5.22 (b) depicts the comparison of the velocity profile at 9.6 D_h downstream. It can be seen that the velocity profile along *Y*-axis is quite similar to the simulated profile. The experimental-measured velocity profile also agrees with the simulation that the velocities of the two outmost measurement points coincide with the rounded shape of the simulated velocity profile.

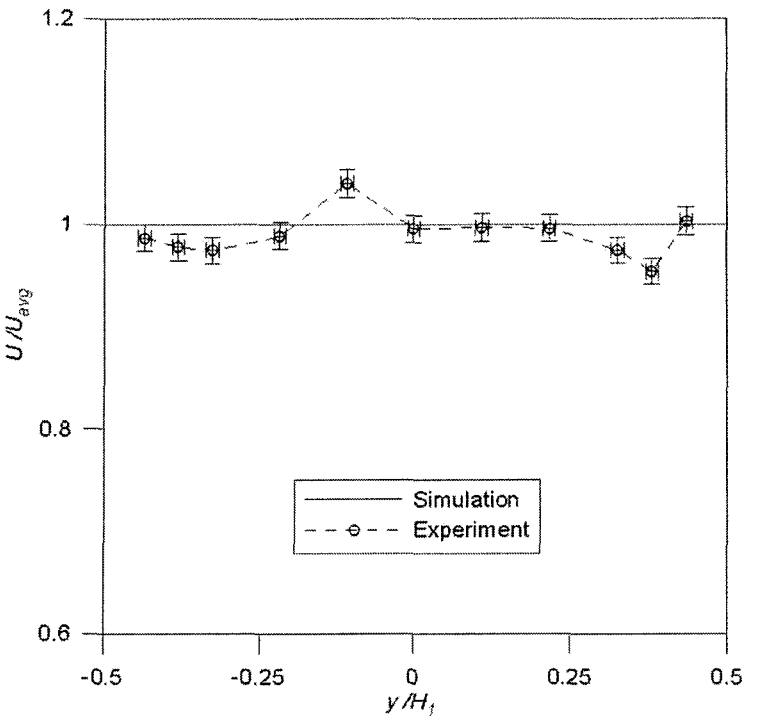

Figure 5.22 (a) Comparison of velocity profiles along *Y*-axis at the inlet and Re of 90,000 (Re = 90,336 for the experiment).

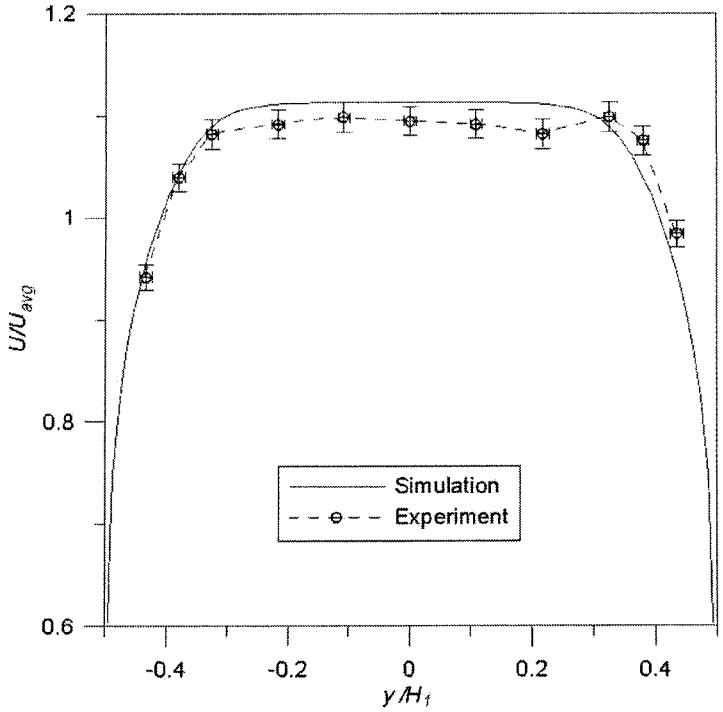

Figure 5.22 (b) Comparison of velocity profiles along *Y-axis* at 9.6 D_h downstream and Re of 90,000 (Re = 89,721 for the experiment).

5.3.2 Comparison of accuracies of the Equal Area and the Log-Tchebycheff methods

Figure 5.23 represents both the numerical and experimental results on the estimated flow rates from the Equal Area and the Log-Tchebycheff methods. The simulation expanded the investigation on the Reynolds number range of 10,000 ~ 500,000 while the experiment carried out the study at a relative narrower Reynolds number range of 90,000 ~ 140,000 due to the limitation of facility.

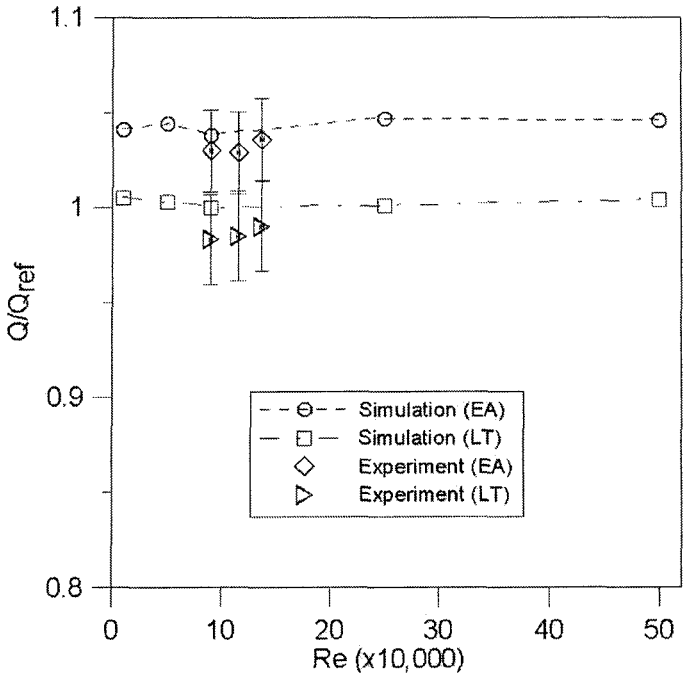

Figure 5.23 Comparison of the estimated flow rates from the Equal Area and the Log-Tchebycheff methods versus Re at 9.6 D_h downstream.

We can see that there is a good agreement between the numerical and experimental studies on the estimated volumetric flow rates from the Equal Area and the Log-Tchebycheff methods. The estimated flow rates in the experimental study are slightly lower than that in the numerical study, however within the measurement uncertainty range. In comparison to the two techniques, the figure shows that the Log-Tchebycheff method had a better accuracy whereas the Equal Area method overestimated the flow rate about 4%.

Figure 5.24 depicts both the numerical and experimental results on the estimated volumetric flow rates from the Equal Area and the Log-Tchebycheff methods with respect to the downstream location at Re of 90,000. For the experiment, the estimated flow rates at 3.4 D_h are nearly identical for the two methods whereas there is 3%

difference in the simulation. With the flow moving downstream, a 3 ~ 4% difference of flow rates between the two methods can be observed in both the numerical and experimental results. There is no significant difference between the 6.5 D_h and 9.6 D_h downstream on the accuracies of the two traverse methods.

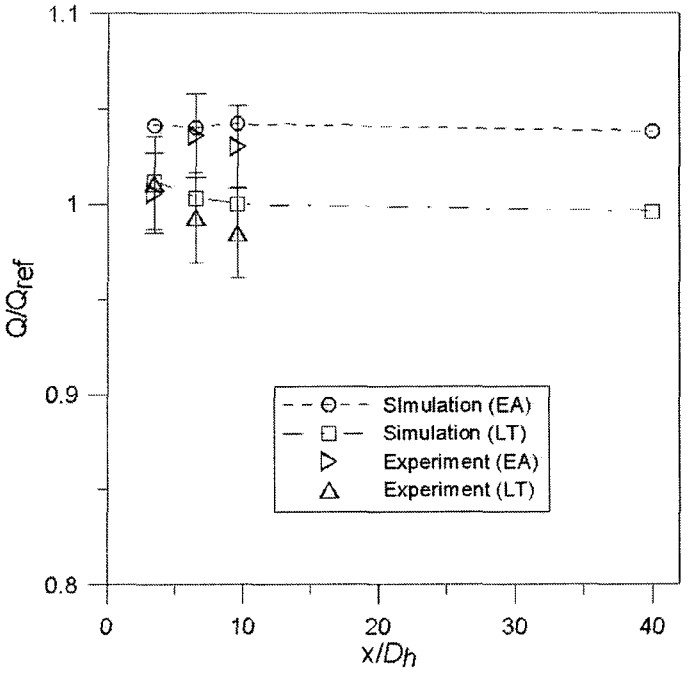

Figure 5.24 Comparison of the estimated flow rates from the Equal Area and the Log-Tchebycheff methods versus downstream location at Re of 90,000.

CHAPTER 6 CONCLUSIONS AND RECOMMENDATIONS

The estimations of the volumetric flow rate in a square duct using the Equal Area and the Log-Tchebycheff methods were studied numerically and experimentally over a range of flow conditions. The numerical investigations were performed using the commercial CFD code FLUENT (Version 6.2, 2003). The airflow in a 0.46 square duct with a straight length of 40 D_h was simulated with the RNG k-ε model in the turbulent flow regime with the Reynolds number range of 10,000 ~ 500,000. The accuracies of the Equal Area and the Log-Tchebycheff methods in estimating the volumetric flow rate were evaluated at different downstream locations. On the other hand, the experimental study was carried out in a blower-duct test bench in the Reynolds number range of 90,000 to 140,000. A hot-wire anemometer system was used to take velocity traverse measurements. The estimated flow rates using the Equal Area and the Log-Tchebycheff methods were compared with the reference flow rate measured by a Venturi meter. With the combination of the numerical and experimental investigations, the accuracies of the Equal Area and the Log-Tchebycheff methods were evaluated and the following conclusions and recommendations were drawn.

6.1 Conclusions

The following conclusions can be drawn from the numerical simulations:

- The simulated mean flow field agreed well with previously published investigations by comparing the dimensionless center line velocity (U_C / U_b) and the velocity distribution along Y-axis.
- In simulating the square duct flow, the RNG k-ε model was found to have better accuracies than the Standard k-ε model as indicated by the dimensionless center line velocity (U_C / U_b).
- At 6.5 D_h or further downstream, the Equal Area method overestimated the flow rate by 3.5 ~ 4.7%, while the Log-Tchebycheff method predicted the flow rate with an accuracy of –0.4% ~ 0.8%. The simulated results show that the Log-Tchebycheff method has better accuracies than the Equal Area method in estimating volumetric flow rates.
- The accuracies of the volumetric flow rates estimated by the Equal Area and the Log-Tchebycheff methods are insensitive to the Reynolds number within the investigated flow regime.

The following conclusions can be drawn from the experimental investigations:

- At the measurement downstream location of 3.4 D_h, there is no obvious difference of the estimated flow rates using the Equal Area and the Log-Tchebycheff methods. When the measurement downstream location is larger than 6.5 D_h, there is no significant variation of the accuracies of the volumetric flow rates for both methods.
- At the traverse planes of 6.5 D_h and 9.6 D_h, the Equal Area method overestimated the flow rate by 3 ~ 4.6 % whereas the Log-Tchebycheff method underestimated the flow rate by 0.6 ~ 2.3 %. The Log-Tchebycheff

method has better accuracies than the Equal Area method in estimating volumetric flow rates.

- Compared to the hot-wire measurement system used in this study, the hand-held anemometer has a larger measurement uncertainty due to the instrument accuracy and positioning error. This measurement uncertainty is greater than the difference of the Equal Area and the Log-Tchebycheff methods in estimating the flow rate. That is why in practice technicians can not tell which one of them is more accurate.

6.2 Recommendations

The observations from the current study might help carrying forward further study in this subject area. The author strongly recommends further study to be extended in the following directions:

- Expand the experimental study over a wider range of Reynolds numbers.
- Replicate the inlet flow condition behind different duct fittings, such as elbow, dampers, etc.
- Build the suitable flow conditioner to produce fully or nearly fully developed flow with adequate duct length.

REFERENCES

AABC, 2002. National Standard for Total System Balance, Associate Air Balancing Council, Washington, D. C., USA.

Abernethy, Y. B., Benedict, R. P. and Dowdell, R. B., 1985. ASME Measurement Uncertainty, *Journal of Fluids Engineering, Transaction of ASME*, Vol. 107, pp. 161-164.

ASHRAE 111, 1988, Practices for Measurement, Testing, Adjusting, and Balancing of Building Heating, Ventilating, Air-Conditioning, and Refrigeration Systems, American Society of Heating, Refrigerating, and Air Conditioning Engineers, Atlanta, GA, USA.

ASTM D3464, 1996 (re-approved 2001). Standard Test Method for Average Velocity in a Duct Using a Thermal Anemometer, American Standard for Testing and Materials, West Conshohocken, PA, USA.

ASME, 1971, Fluid Meters: Their Theory and Application, American Society of Mechanical Engineers, New York, USA.

Barton, J. M., Rubinstein, R. and Kirtley, K. R., 1991. Non-linear Reynolds Stress Model for Turbulent Shear Stress, *AIAA (American Institute of Aeronautics and Astronautics)* paper 91-0609.

Baumgartner, J. E., 2001. To Use Log-Tchebycheff or not to Use Log-Tchebycheff, Is That the Question, *TAB Journal (Test and Air Balance)*, Associated Air Balance Council, Summer 2001, pp. 2-5.

Bradshaw, P. and Pankhurst, R. C., 1964. The Design of Low-speed Wind Tunnels, *Progress in Aeronautical Sciences*, Vol. 6, pp. 1-69.

BSI 1042, 1943. Code for Flow Measurement, British Standards Institution, London, England.

Coleman, H. W. and Steele, W. G., 1999. *Experimentation and Uncertainty Analysis for Engineers*, 2nd Edition, John Wiley & Sons, Inc., USA.

Damodaran, V., Zhang, C. and Rankin, G. W., 1995. Comparison of k-ε Turbulence Models for Pipe Flows, *Mathematic Modeling and Scientific Computing*, Vol. 5, No. 1, pp. 57-72.

Demuren, A. O. and Rodi, W., 1984. Calculation of Turbulence-driven Secondary Motion in Non-circular Ducts, *Journal of Fluid Mechanics*, Vol. 140, pp. 189-222.

Fluent Inc., 2003. *FLUENT 6.2 User Guide.*

Fluent Inc., 2004. *GAMBIT 2.2 User Guide.*

Gessner, F. B. and Emery, A. F., 1981. The Numerical Prediction of Developing Turbulent Flow in Rectangular Ducts, *Journal of Fluids Engineering, Transaction of ASME*, Vol. 103, pp. 445-455.

Gessner, F. B. and Jones, J. B., 1965. On some Aspects of Fully-Developed Turbulent Flow in Rectangular Channels, *Journal of Fluid Mechanics*, Vol. 23, pp. 689-713.

Harris, R. D., 2005. Technical Note 001, Water Level Accuracy and correcting for Errors due to Gravitational Acceleration and Liquid Density, In-Situ Inc.

ISO 3966 (E), 1977. Measurement of Fluid Flow in Closed Conduits-Velocity Area Method Using Pitot Static Tubes, International Organizations for Standardization.

ISO 5167-1, 2003. Measurement of Fluid Flow by Means of Pressure Differential Devices, Part 1: Orifice Plates, Nozzles, and Venturi Tubes Inserted in Circular Cross-section Conduits running Full, International Organization for Standardization.

Kim, W. J. and Patel, V. C., 1993. An experimental Study of Boundary-layer Flow in a Curved Rectangular Duct, *ASME Fluids Engineering Division Meeting*, FED-Vol. 146, pp. 13-28, Washington D. C., USA.

Kinghorn, F. C., McHugh, A. and Duncan, W., 1973. An experimental Comparison of Two Velocity Area Numerical Integration Techniques, *Water Power*, Vol. 25, pp. 330-335.

Klaassen, C. J. and House, J. M., 2001. Equal Area vs. Log-Tchebycheff, *HPAC (Heating, Piping, Air Conditioning Engineering)*, Vol. 73, pp. 31-35.

Kuehn, T. H., Ramsey, J. W. and Threlkeld, J. L., 1998. *Thermal Environmental Engineering*, 3rd Edition, Simon & Schuster /A Viacom Company, NJ, USA.

Lambda Square Inc., 2005. Model 2300 Insert Fibreglass Venturi-Typical Specification, New York.

Launder, B. E. and Spalding, D. B., 1972. *Lectures in Mathematical Models of Turbulence*, Academic Press, London, England.

Launder B. E. and Spalding, D. B., 1974. The Numerical Computation of Turbulent Flow, *Computer Methods in Applied Mechanics and Engineering*, Vol. 3, pp. 269-289.

Laws, E. and Livesey, J., 1978. Flow through Screens, *Annual Review of Fluid Mechanics*, Vol. 10, pp. 247-266.

Lindgren, B. and Johansson, A. V., 2002. Design and Evaluation of a Low-speed Wind Tunnel with Expanding Corners, Technical Report from Royal Institute of Technology, Stockholm, Sweden.

Macferran, E., 1999(a). Equal Area vs. Log-Tchebycheff, *HPAC (Heating, Piping, Air Conditioning Engineering)*, Vol. 71, pp. 26-31.

Macferran, E., 1999(b). One Person's Opinion: The case for Log-Tchebycheff, *Engineered Systems*, Vol. 16, pp. 54-56.

Macquiston, F. C. and Parber, J. D., 1994. *Heating, Ventilating, and Air Conditioning Analysis and Design*, 4th Edition, John Wiley and Sons, Inc., USA.

Munson, B. R., Young, D. F., Okiishi, T. H., 2002. *Fundamental of Fluid Mechanics*, 4th Edition, John Wiley & Sons, Inc., USA.

Naimi, M. and Gessner, F. B., 1994. A Calculation Method for Developing Turbulent Flow in Rectangular Ducts of Arbitrary Aspect Ratio, *Boundary Layer and Free Shear Flows*, ASME, FED-Vol. 184, pp. 63-73.

Norfleet, S. K., 1998. An Evaluation of Wall Effects on Stack Flow Velocities and Related Overestimation Bias in EPA's Stack Flow Reference Methods, *EPRI CEM Users Group Meeting*, New Orleans, Louisiana, USA.

Ower, E. and Pankhurst, R. C., 1977. *The Measurement of Airflow*, 4th Edition, Pergamon Press, USA.

Reynolds, O., 1990. On the Dynamical Theory of Incompressible Viscous Fluids and the Determination of the Criterion, *Collected Work on Mechanical and Physical Subjects 1881-1900*, Vol. 2, Cambridge University Press.

Richardson, G., 2001. Traversing for Accuracy in a Rectangular Duct, *TAB Journal*, Associated Air Balance Council, Summer 2001, pp. 20-27.

Rokni, M., Olsson C. and Sunden, B., 1998. Numerical and Experimental Investigation of Turbulent Flow in a Rectangular Duct, *International Journal for Numerical Methods in Fluids*, Vol. 28, pp. 225-242.

Saxon, P. R, 2001. Equal Area vs. Log-Tchebycheff, Letters, *HPAC (Heating, Piping, Air Conditioning Engineering)*, http://www.hpac.com/member/archive/0003open.htm.

Scheiman, J. and Brooks, J. D., 1981. Comparison of Experimental and Theoretical Turbulence Reduction from Screens, Honeycomb and Honeycomb-screen Combinations. *JAS*, Vol. 18, pp. 638-643.

SMACNA, 1983. HVAC System Adjusting and Balancing, 1st Edition, Sheet Metal and Air Conditioning Contractors National Association, Inc., Virginia, USA.

Speziale, C. G., 1987. On Non-linear *k-l* and *k-ε* Models of Turbulence, *Journal of Fluid Mechanics*, Vol. 178, pp. 459-475.

TSI, 2000. IFA 300 Constant Temperature Anemometer Systems, Fluid Mechanics Instrument Division, TSI Incorporated. MN, USA.

TSI, 2002(a), Innovation in Thermal Anemometry, Fluid Mechanics Instrument Division, TSI Incorporate, MN, USA.

TSI, 2002(b). Model 8345 VelociCalc Portable Air Velocity Meter, Fluid Mechanics Instrument Division, TSI Incorporated, MN, USA.

TSI, 2003. Model 1129 Automated Air Velocity Calibrator, Fluid Mechanics Instrument Division, TSI Incorporated, MN, USA.

Weather Underground, 2005. http://www.wunderground.comglobal/statins/71538, the Weather Underground Inc.

Wilcox, D.C., 1994. *Turbulence Modeling for CFD*, 2nd Edition, DCW Industries, USA.

Winternitz, F. A. L. and Fischl, C. F., 1957. A simplified Integration Technique for Pipe-flow Measurement, *Water Power*, Vol. 9, pp. 225-234.

Yakhot, V. and Orszag, S. A., 1986. Renormalization Group Analysis of Turbulence: 1. Basic Theory, *Journal of Scientific Computing*, Vol. 1, pp. 3-51.

Yavuzkurt, S, 1984. A guide to Uncertainty Analysis of Hot-wire Data. *Journal of Fluids Engineering*, Vol 106, pp. 181-186.

Appendix A The Standard *k-ε* and RNG *k-ε* models

As described in Section 3.1, turbulent flow introduces six additional terms of Reynolds stress tensor after the decomposition of turbulent fluctuating variables, they are $\overline{uv}$, $\overline{uw}$, $\overline{vw}$ and $\overline{u^2}, \overline{v^2}, \overline{w^2}$. To resolve the problem, additional relationship between the mean flow variables and turbulent components have to be found. Among a variety of methods to do this, the two equation *k-ε* models, including the Standard k-ε model and the RNG *k-ε* model, are thoroughly used with reasonably accuracy.

In the *k-ε* model, the Reynolds stress terms, $-\rho\overline{u_i u_j}$, are replaced by using Boussinesq eddy viscosity definition (Launder and Spalding, 1974),

$$-\rho\overline{u_i^2} = 2\mu_t \frac{\partial U_i}{\partial x_i} - \frac{2}{3}\rho k \ , \tag{A-1}$$

$$-\rho\overline{u_i u_j} = \mu_t \left(\frac{\partial U_i}{\partial x_j} + \frac{\partial U_j}{\partial x_i}\right) \ , \tag{A-2}$$

where k is the turbulent kinetic energy, μ_τ is the turbulence eddy-viscosity expressed as,

$$\mu_\tau = \rho C_\mu \frac{k}{\varepsilon^2}, \tag{A-3}$$

where ε is the turbulent dissipation rate, C_μ is the eddy-viscosity coefficient.

The application of Boussinesq hypothesis requires two additional equations for k and ε to close the problem. In the Standard *k-ε* model, the transport equations for the turbulent kinetic energy, k, and its rate of dissipation, ε, are obtained using the general discretization equations displayed as follows (FLUENT Version 6.2, 2003),

$$\frac{\partial}{\partial}(\rho k u_i) = \frac{\partial}{\partial x_j}\left[\left(\mu + \frac{\mu_t}{\sigma_k}\right)\frac{\partial \varepsilon}{\partial x_j}\right] + G_k + G_b - \rho\varepsilon - Y_M + S_k \,, \tag{A-4}$$

$$\frac{\partial}{\partial x_i}(\rho\varepsilon U_i) = \frac{\partial}{\partial x_j}\left[\left(\mu + \frac{\mu_t}{\sigma_\varepsilon}\right)\frac{\partial \varepsilon}{\partial x_j}\right] + C_{1\varepsilon}\frac{\varepsilon}{\kappa}(G_k + C_{3\varepsilon}G_b) - C_{2\varepsilon}\rho\frac{\varepsilon^2}{k} + S_\varepsilon. \tag{A-5}$$

For both Equations, the left hand side is convection term and the first term of right hand side is diffusion term. Among other terms, G_k represents the generation of turbulent kinetic energy due to the mean velocity gradients,

$$G_k = -\rho\overline{u_i u_j}\frac{\partial U_j}{\partial x_j}, \tag{A-6}$$

The coefficient G_b is the generation of turbulent kinetic energy due to buoyancy. It is related to temperature gradient. Since the flow is assumed to be isothermal flow so there is no temperature gradient, so G_b was ignored in this study. S_k and S_ε are user-defined source terms. The coefficient Y_M represents the dilatation dissipation term in consideration of compressibility at high velocity,

$$Y_M = 2\rho\varepsilon\frac{k}{M^2} \,, \tag{A-7}$$

where M is flow Mach number.

The RNG k-ε model is derived from the instantaneous Navier-Stokes equations, using a mathematical technique called "renormalization group" (RNG) methods. It has a similar form as the Standard k-ε model,

$$\frac{\partial}{\partial x_i}(\rho k u_i) = \frac{\partial}{\partial x_j}\left[\alpha_k \mu_{eff}\frac{\partial k}{\partial x_j}\right] + G_k + G_b - \rho\varepsilon - Y_M + S_k \,, \tag{A-8}$$

$$\frac{\partial}{\partial x_i}(\rho \varepsilon U_i) = \frac{\partial}{\partial x_j}\left[\alpha_k \mu_{eff} \frac{\partial \varepsilon}{\partial x_j}\right] + C_{1\varepsilon} \frac{\varepsilon}{\kappa}(G_k + C_{3\varepsilon} G_b) - C_{2\varepsilon}^* \rho \frac{\varepsilon^2}{k} + S_\varepsilon, \quad \text{(A-9)}$$

where α_k and α_ε are coefficients called the inverse effective Prandtl numbers. It is considered to be,

$$\alpha_k = \alpha_\varepsilon \approx 1.393. \quad \text{(A-10)}$$

The main difference between the RNG and Standard k-ε models lies in an additional term in the coefficient $C_{2\varepsilon}^*$ equation given by,

$$C_{2\varepsilon}^* \equiv C_{2\varepsilon} + \frac{C_\mu \rho \eta^3 (1 - \eta/\eta_0)}{1 + \gamma \eta^3}, \quad \text{(A-11)}$$

where $\eta \equiv S_k / \varepsilon$, $\eta_0 = 4.38, \gamma = 0.012$.

In a region where $\eta < \eta_0$, $C_{2\varepsilon}^*$ becomes larger than $C_{2\varepsilon}$, in the square duct flow, the RNG *k-ε* model yields a lower turbulent viscosity than the Standard *k-ε* model. Thus the RNG model is more response to the effects of rapid strain and streamline curvature than the Standard *k-ε* model, which explains the superior performance of the RNG model in this study.

The model constants, $C_{1\varepsilon}$, $C_{2\varepsilon}$ and C_μ are derived analytical by the RNG theory with the default values used in this study (FLUENT, 2003),

$$C_{1\varepsilon} = 1.42,\ C_{2\varepsilon} = 1.68,\ C_\mu = 0.0845. \quad \text{(A-12)}$$

Appendix B Hot-wire Calibration Procedure

The calibration process should be carried out to establish a current velocity-voltage correlation due to its sensitivity to the outside environment. In this study, the calibration was taken at the beginning of each measurement process. The detailed calibration procedures are as below.

1. Connection

   The computer, calibrator, thermocouple, pressure transducer, A/D board were connected according to TSI calibration manual (2003) and setup in a portable cart. The power of the computer, pressure transducer, and anemometer were connected to the power jack. An air filter and a pressure regulator were fixed at the terminal of compressed air supply. The compressed air was supplied to the calibrator through a plug-in air connector.

   Adjust the regulator valve to maintain the reading of the pressure gage above 207 kPa (30 psi). As mentioned in TSI manual (2003), in order to work under a stable condition, the pressure transducer is required to warm up for 45 minutes before calibration. In the actual operation, all the calibration facilities were turned on one hour before the formal calibration.

2. Place the Calibrator arms in the vertical position and the probe support into the clamp ring on the calibrator and tighten it using the securing knob.

3. Go to the interface of THERMALPRO software, select *Calibration* on the main menu, then select *Probe Data*. The *Probe Data* screen appears (Figure B.2).

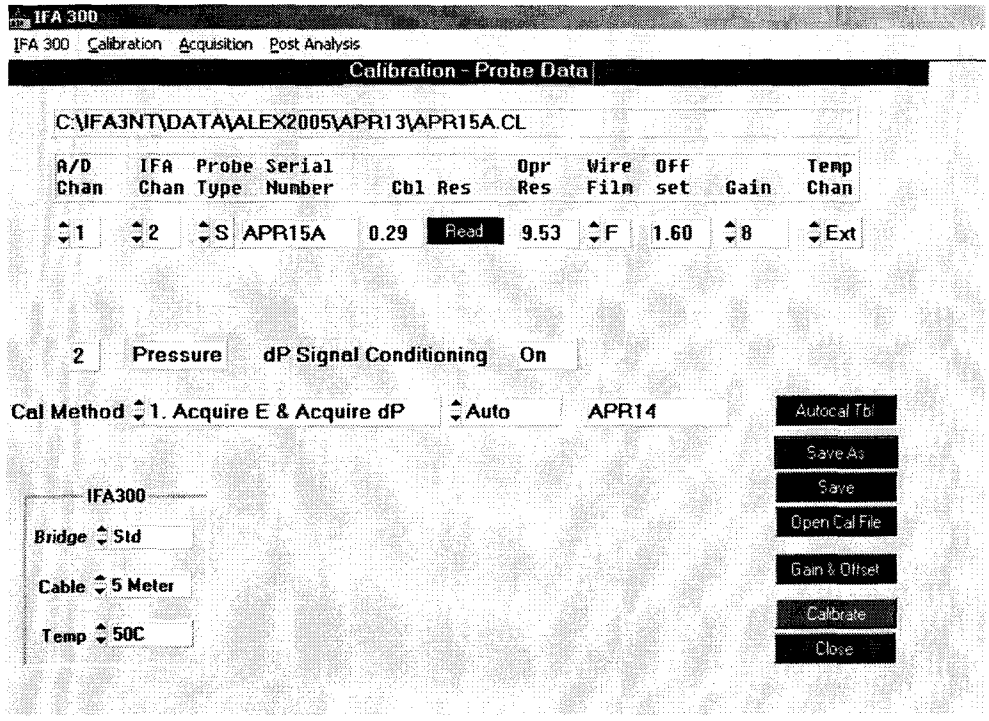

Figure B.1 *Probe Data* screen.

4. Click on *Open Cal File* button. Select an applicable calibration file from the list of provided probe data files and press *OK*.
5. In the *Probe Data* screen, setup the *A/D channel* to 1 and *IFA channel* to 2 that were used in current study. The *Offset* and *Gain* are input with proper value to span the voltage signal with the whole range of the A/D converter, i.e. –5 ~ 5 V.
6. Place a shorting probe into the probe support to shorten the calibration circuit. In the *Probe Data* screen, click on the *Read /Cable Resistance* button to measure the cable resistance. This measures the cable resistance and writes it to the probe file. The typical value for the present setup is around 0.3 Ohms.

7. Click on *Autocal Tbl* button and select an applicable auto-calibration table with the expected velocity range.

8. Select *Save As* to save the current calibration file with a new name, e.g. *APR15A.CL* as in Figure B.1.

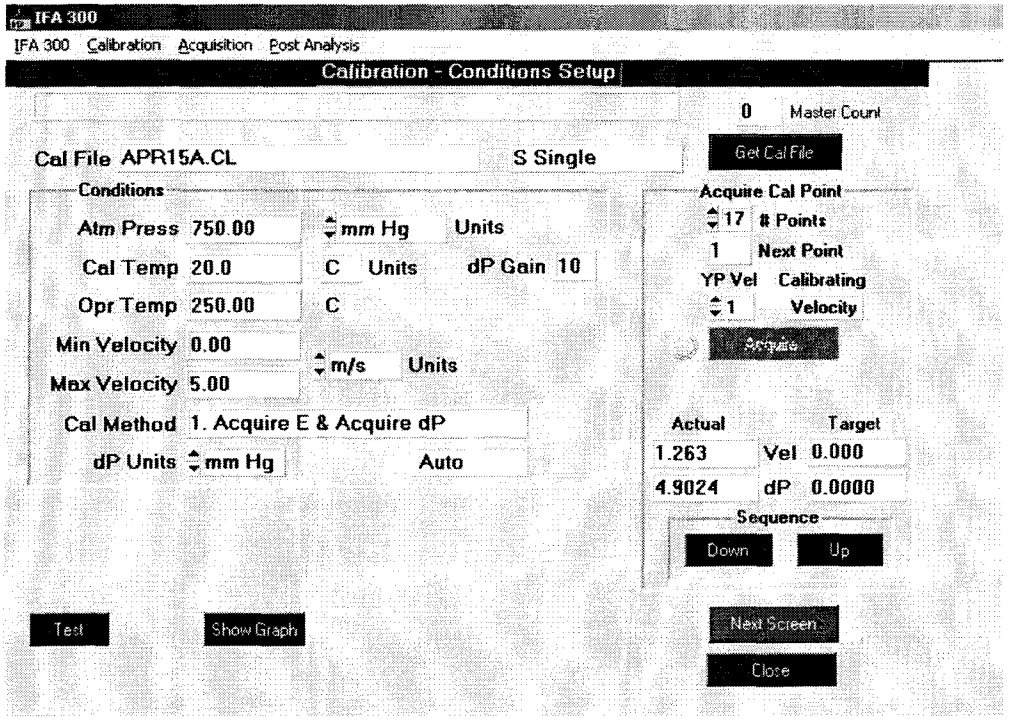

Figure B.2 *Calibration /Condition Setup* screen.

9. Place the probe into the probe support. Locate the probe support in the clamp ring so that the sensor is directly above the calibrator nozzle with a distance about 10 mm.

10. Select *Calibrate* from the *Probe Data* screen. This powers on the sensor, and the *Conditions Setup* screen appears (Figure B.2).

11. The calibration program automatically steps through all the calibration points. During the calibration process, the program displays values of current velocity and Δp (differential pressure) as well as the next velocity and Δp values that will be set.

12. When the calibration data set is complete, select *Next Screen.* The *Calibration /Data Table* appears. This table lists the bridge voltage, differential Pressure, actual velocity, and temperature at each calibration point. Click on *Curves*, the curve fit for the calibration is calculated, plotted, and displayed. The polynomial coefficients are also shown in the upper right corner of the screen, as shown in Figure B.3.

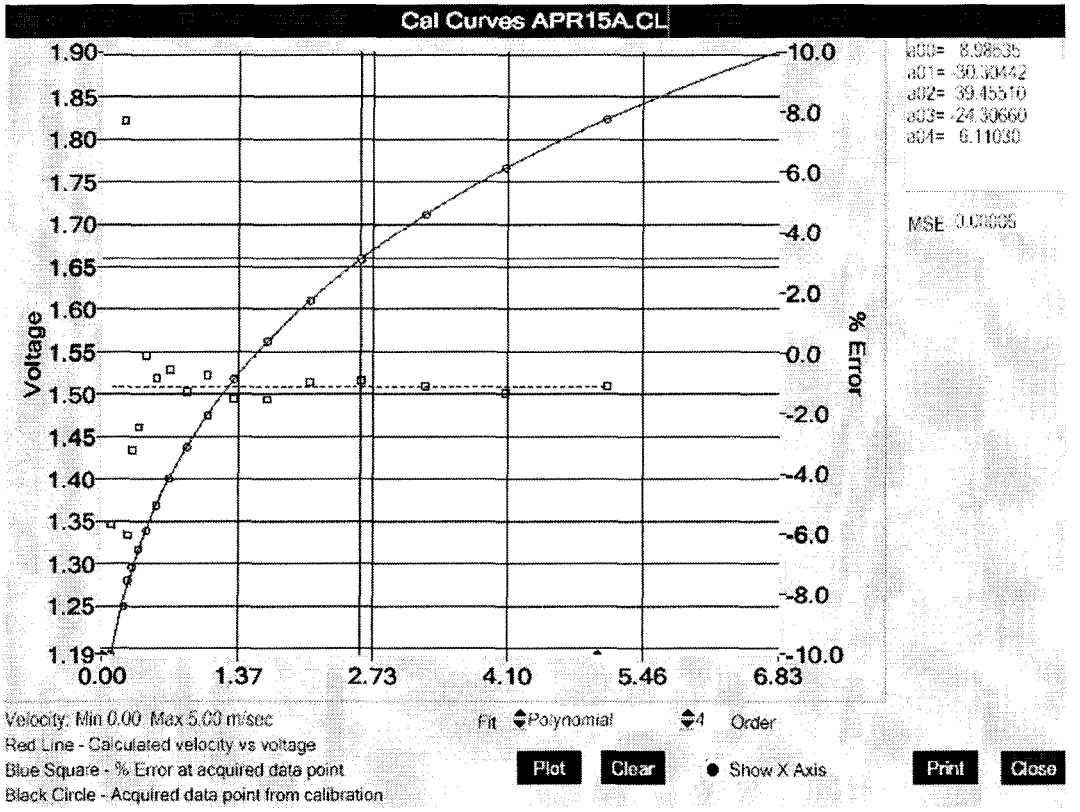

Figure B.3 Calibration curve shown on screen.

The calibration is now complete and the calibration file can be used to take the velocity measurement.

Appendix C Hot-wire Measurement Procedure

The detailed velocity traversing measurement process with the TSI hot-wire anemometer instrumentation is described as below.

1. Calibrate the probe following the calibration procedure in Appendix B.
2. Move the cart beside the duct exit, connect the automatic traversing mechanism with the computer and power jack.
3. Setup the traversing mechanism 0.5 m (~1 D_h) from the exit of the square duct as shown in Figure 4.5. The traversing mechanism is put in such a way that the probe support can traverse the whole cross section of the test duct. The probe support is adjusted to normal to the measuring plane.
4. Use the adjusting switch on the traversing mechanism to locate the relative origin of the probe with the distance of 0.03 m to both left and top duct inner walls.
5. Based on the relative origin, compile the traversing file with EXCEL where the locations and sequence of measuring points are defined.
6. Open *IFA 300/Traverse Control* from the main menu of the THERMALPRO software, first click S*et relative home* to define the current position of the probe as relative origin, then click *open* to activate the compiled traversing file; see Figure C.1. The measurements are taken automatically based on the defined locations.

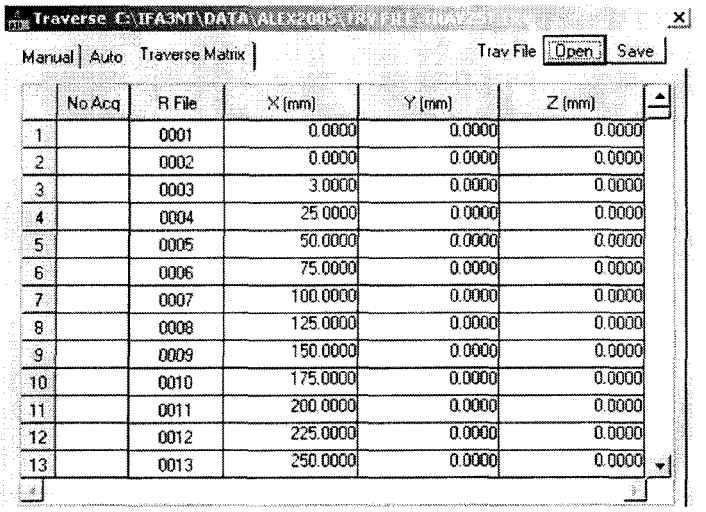

	No Acq	R File	X (mm)	Y (mm)	Z (mm)
1		0001	0.0000	0.0000	0.0000
2		0002	0.0000	0.0000	0.0000
3		0003	3.0000	0.0000	0.0000
4		0004	25.0000	0.0000	0.0000
5		0005	50.0000	0.0000	0.0000
6		0006	75.0000	0.0000	0.0000
7		0007	100.0000	0.0000	0.0000
8		0008	125.0000	0.0000	0.0000
9		0009	150.0000	0.0000	0.0000
10		0010	175.0000	0.0000	0.0000
11		0011	200.0000	0.0000	0.0000
12		0012	225.0000	0.0000	0.0000
13		0013	250.0000	0.0000	0.0000

Figure C.1 Pre-compiled traversing file.

7. Start the blower and keep it running for 15 minutes to stable the flow before taking measurement.
8. Go to *Acquisition /probe data* interface, the *Probe Table* screen is shown as Figure C.2. Click *Get file* and give a new name to record the experimental data, e.g. *APR15.R0001* in current example.

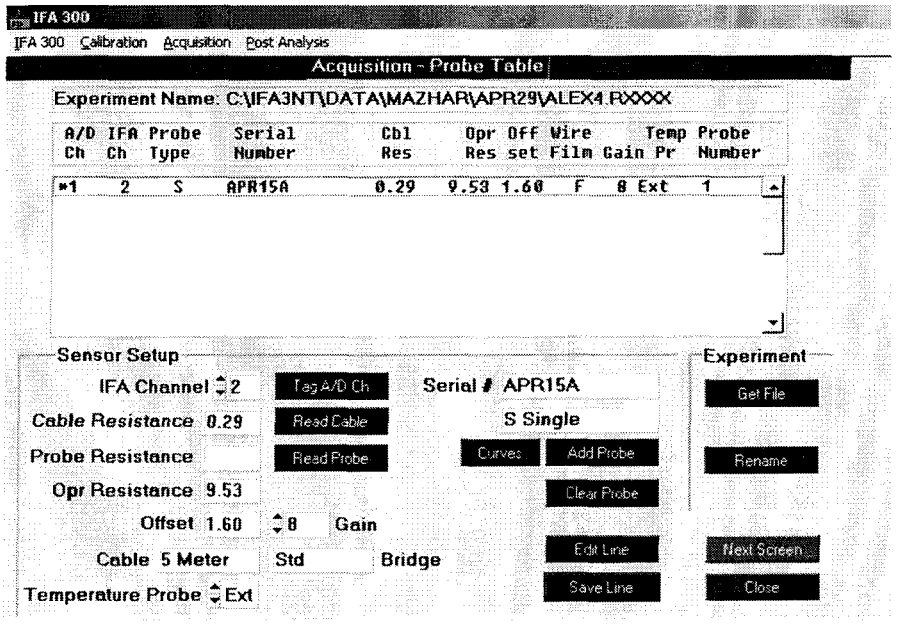

Figure C.2 *Acquisition /Probe Table* screen.

9. Click *Add Probe* and input the current calibration file (e.g. *APR15A.CL*). Then click next, a new screen, *Acquisition /Condition Setup* screen, appears as Figure C.3,

10. Setup the turbulence parameters, such as sampling rate, time, etc.

11. Click *Acquire* to take measurement, the measurement is carried out with automatically traversing the measuring points.

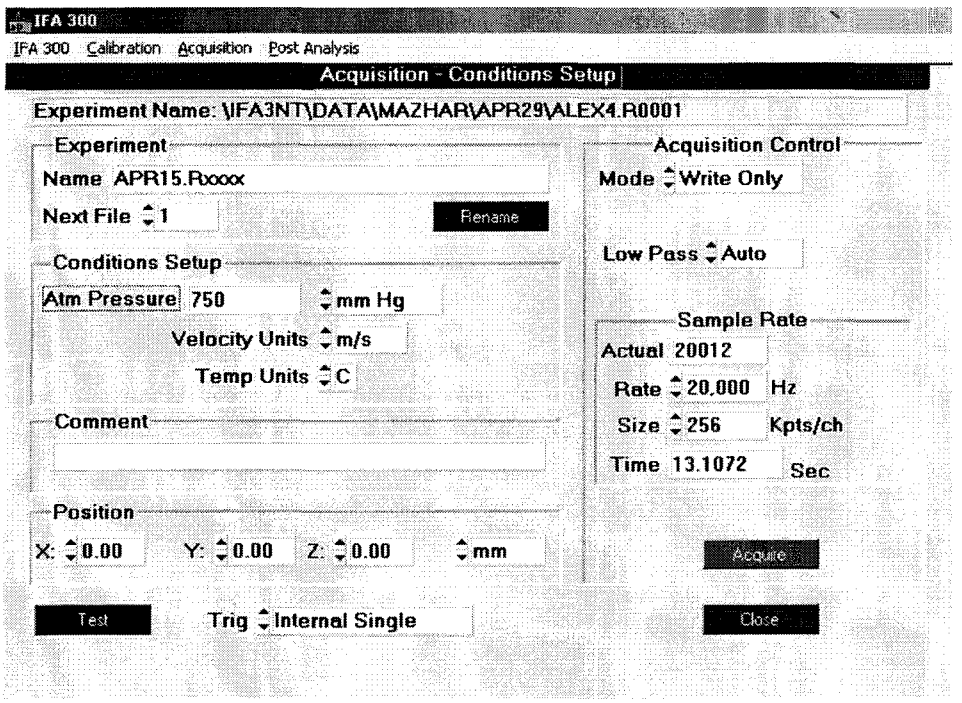

Figure C.3 *Acquisition /Condition Setup* screen.

12. When a message, " Reach end of the traversing file", is popped-up, the measurement process is complete. The blower can be shut off.

13. Click *Post-process* to analyze the collected data, the program will process raw data to get statistical values such as mean velocity, turbulence intensity, skewness, etc.

Appendix D Uncertainty Analysis

The experimental study involves independent variables, whose values are directly measured using instruments, and dependent variables, whose values are calculated from independent variables via a series of parametric relationships. The uncertainties of independent variables come from instruments and measurement processes. The uncertainties of dependent variables involve the uncertainty propagations from independent variables to dependent variables. In this study, the uncertainties were dealt mainly following the procedure of Coleman and Steele (1999), and other notable works.

The ultimate dependent variables are: the reference flow rate acquired from the Venturi meter, Q_{ven}, the flow rates estimated from the Equal Area method, Q_{EA}, and that estimated from the Log-Tchebycheff method, Q_{LT}. The corresponding uncertainties were calculated to be 0.8%, 2.1% and 2.4% respectively. The details of the uncertainty analysis are outlined as below.

In this appendix, first the procedure for carrying out uncertainties was introduced. Second, the uncertainties for independent variables were calculated. Third, the uncertainties for the thermal-physical properties were determined. Fourth, the uncertainties propagations from independent variables to dependent variables were analyzed. Fifth, the uncertainties of the hot-wire measurement and the propagated uncertainties to the volumetric flow rate using the Equal Area and the Log-Tchebycheff methods were determined. Finally, the uncertainty of the velocity using the hand-held anemometer were calculated.

D.1 Procedures for uncertainty analysis

There are two kinds of parameters to be identified in current study. One is independent variables and another one is the dependent variables. The independent variables are the basic parameters whose values can be directly measured using instruments. In this study they are the dimensions of the square ducts (H_1, H_2), the flow velocity (U), the length of the indication fluid in the inclined manometer (ℓ), etc. On the other hand, the dependent variables are functions of the independent variables or thermal-physical properties. They include, the area of square duct (A_{SD}), the differential pressure and the reference flow rate across the Venturi meter (Δp_{ven}, Q_{ven}), the spatial-averaged velocity and the volumetric flow rate deduced from the Equal Area (U_{EA}, Q_{EA}) and the Log-Tchebycheff (U_{LT}, Q_{LT}) methods, etc. These dependent variables were not directly measured by any instrument, but calculated from the measured independent variables following specific functional relationships.

The independent variables were directly measured from single sample measurements. The bias (B) and precision (P) errors were calculated by using the root-sum-square (RSS) method as follows,

$$B = \pm\sqrt{B_1^2 + B_2^2 + B_3^2 + \ldots + B_n^2}\,, \tag{D-1}$$

$$P = \pm\sqrt{P_1^2 + P_2^2 + P_3^2 + \ldots + P_n^2}\,, \tag{D-2}$$

where n is the total number of error sources. The combined bias and precision errors were calculated as,

$$\Delta = \pm\sqrt{B^2 + P^2}\,. \tag{D-3}$$

For the independent variables, the bias errors (B) were taken to be the same as a single measurement whereas the precision errors (P) at 95% confidence interval were statistical results of multiple measurements using the standard deviation of the sample mean ($S_{\overline{F}}$) and t-distribution value as $P_{\overline{F}} = t_{N-1,95\%} S_{\overline{F}}$.

For the dependent variables that were calculated from measured independent variables, their uncertainties were estimated by following the RSS method based on their functional relationships. Generally, the dependent parameter, F, is a function of independent variables, F_1, F_2, ...F_n, as shown below,

$$F = f(F_1, F_2, F_3 ..... F_n). \tag{D-4}$$

The absolute uncertainty can be estimated as,

$$\Delta F = \sqrt{\left(\frac{\partial F}{\partial F_1}\Delta F_1\right)^2 + \left(\frac{\partial F}{\partial F_2}\Delta F_2\right)^2 + \left(\frac{\partial F}{\partial F_3}\Delta F_3\right)^2 + ... + \left(\frac{\partial F}{\partial F_n}\Delta F_n\right)^2}. \tag{D-5}$$

Correspondingly, the relative uncertainty,

$$\frac{\Delta F}{F} = \frac{\sqrt{\left(\frac{\partial F}{\partial F_1}\Delta F_1\right)^2 + \left(\frac{\partial F}{\partial F_2}\Delta F_2\right)^2 + \left(\frac{\partial F}{\partial F_3}\Delta F_3\right)^2 + ... + \left(\frac{\partial F}{\partial F_n}\Delta F_n\right)^2}}{f(F_1, F_2, F_3, ... F_n)}. \tag{D-6}$$

where the partial derivatives $\left(\frac{\partial F}{\partial F_1}, \frac{\partial F}{\partial F_2}, \frac{\partial F}{\partial F_3}, ... \frac{\partial F}{\partial F_n}\right)$ are derived from the functional relationship as Equation (D-4).

D.2 Instrumental and measurement uncertainties for independent parameters

All the instruments and individual measurements have errors with them. The bias error is the systematic error of instruments and measurement process, such as instruments

accuracy, resolution, etc. The precision error is a random error and can be diminished by repeating a single measurement several times. The mean of these measured values ($\overline{F}$) was taken as the value of the variable and the standard deviation ($S_{\overline{F}}$) of the sample mean, multiplied by a coefficient, t_d, a function of the 95% confidence level with *N-1* degree of freedom (Coleman and Steele, 1999), was considered as the precision limit.

D.2.1 Uncertainty of the dimensions of the duct

The dimensions of the square ducts were measured using a vernier. The vernier has an instrumental error (accuracy) of $B_{accuracy}$ = 0.00004 m and an instrumental bias limit (resolution) of $B_{resolution}$ = 0.00002 m. According to Equation (D-1), the total bias error using this vernier was estimated as,

$$B_{vernier} = \sqrt{B_{accuracy}^{\ 2} + B_{resolution}^{\ 2}} = 4.472 \times 10^{-5}\ m. \qquad \text{(D-7)}$$

The precision errors for the duct dimensions were based on the measurement at different cross sections each with 3 repeated measurements. Since the duct is not exactly square, all sections were aligned such that the longer sides (H_1) were parallel to the horizontal direction. Thus the longer and shorter (H_2) sides of the duct sections were measured and calculated separately. Due to the limitation of the instrument, only the end cross sections can be measured by the vernier. There are four short sections of square ducts utilized in this study, thus there were totally 24 readings. The sample mean ($\overline{H_1}$) was calculated as,

$$\overline{H_1} = \frac{1}{N}\sum_{i=1}^{N}(H_1)_i = \frac{1}{24}\sum_{i=1}^{24}(H_1)_i = 0.46222\,m. \qquad \text{(D-8)}$$

The standard deviation (S_{H_1}) of the sample was calculated as,

$$S_{H_1} = \sqrt{\frac{1}{N-1}\sum_{i=1}^{N}\left((H_1)_i - \overline{H_1}\right)} = \sqrt{\frac{1}{23}\sum_{i=1}^{24}\left((H_1)_i - \overline{H_1}\right)} = 0.00253\,m. \quad \text{(D-9)}$$

where N is the number of repeated measurements.

The standard deviation of the sample mean ($S_{\overline{H_1}}$) was deduced using the following relation,

$$S_{\overline{H_1}} = \frac{S_{H_1}}{\sqrt{N}} = 0.00052\,m. \quad \text{(D-10)}$$

For (N-1) = 23 degrees of freedom, the t-distribution value at 95% confidence level is 2.069 (Coleman and Steele, 1999). Thus the mean precision limit, $P_{\overline{H_1}}$, was estimated as,

$$P_{\overline{H_1}} = t_{N-1,95\%}\, S_{\overline{H_1}} = 0.0011\,m. \quad \text{(D-11)}$$

Thus the overall uncertainties in the measurement of H_1 were calculated as,

The absolute uncertainty:

$$\Delta H_1 = \pm\sqrt{(B_{vernier})^2 + (P_{\overline{H_1}})^2} = 0.00107\,m. \quad \text{(D-12)}$$

The relative uncertainty:

$$\frac{\Delta\overline{H_1}}{\overline{H_1}} = \frac{0.00107}{0.46222} = 0.23\%. \quad \text{(D-13)}$$

Following the same procedure, the $\overline{H_2}$ and its uncertainty was calculated as,

$$\overline{H_2} = 0.45799\,m. \quad \text{(D-14)}$$

$$\Delta H_2 = 0.00122m \quad \text{(D-15)}$$

$$\frac{\Delta H_2}{H_2} = 0.27\%. \qquad \text{(D-16)}$$

D.2.2 Uncertainty of fluid column along the inclined manometer

The volumetric airflow rate was measured by a Venturi flow meter, where an inclined manometer was used to measure the differential pressure (Δp) across the Venturi meter. The Δp was indicated in the form of fluid length (ℓ) by an attached scale (resolution: 0.001 m; accuracy: 0.002 m). The total bias error was calculated as,

$$B_\ell = \sqrt{0.002^2 + 0.001^2} = 0.0022 m. \qquad \text{(D-17)}$$

A readability error of 0.001 m was considered as a precision error. A 0.001 m fluctuation was also considered as the precision error. Thus the total precision error were estimated as,

$$P_\ell = 0\sqrt{0.001^2 + 0.001^2} = 0.0014 m. \qquad \text{(D-18)}$$

The overall uncertainties in measuring ℓ were obtained as,

The absolute uncertainty:

$$\Delta\ell = \pm\sqrt{(B_\ell)^2 + (P_\ell)^2} = \pm 0.0026 m. \qquad \text{(D-19)}$$

The relative uncertainty:

$$\frac{\Delta\ell}{\ell} = \pm\sqrt{(\frac{B_\ell}{\ell})^2 + (\frac{P_\ell}{\ell})^2} = \pm 0.5\%. \qquad \text{(D-20)}$$

D.3 Uncertainties in the evaluation of thermo-physical properties of airflow

The thermo-physical properties, can be accounted as bias error limit, though they may have some precision error. Generally, the thermal-physical properties of air are

influenced by the temperature and atmospheric pressure. Since during each run of experiments the variation of p_{atm} was very small (e.g. 3 mmHg or 0.4 kPa) and within the estimated uncertainty, the effect of the variation of the atmospheric pressure to the thermal-physical properties was neglected in this study. The thermal physical properties were evaluated at the mean of the maximum ($T_{a,\,max}$) and minimum ($T_{a,\,min}$) temperatures, i.e.,

$$T_a = T_{a,mean} = \frac{1}{2}(T_{a,max} + T_{a,min}). \tag{D-21}$$

$$Property = Property@T_a. \tag{D-22}$$

The uncertainty of a typical thermal-physical property was evaluated as the half difference of the properties which were at the maximum ($T_{a,\,max}$) and the minimum ($T_{a,\,min}$) temperatures, as shown below,

$$\Delta Property = \pm\frac{1}{2}\left|Property@T_{a,max} - Property@T_{a,min}\right|. \tag{D-23}$$

Thus, the relative property uncertainty is,

$$\frac{\Delta Property}{Property} = \pm\frac{\left|Property@T_{a,max} - Property@T_{a,min}\right|}{2\,Property@T_{a,mean}}. \tag{D-24}$$

D.3.1 Uncertainty of the air density

In this study each run of experiments took a few hours. During the experimental process, the temperature was recorded automatically by the hot-wire system for each velocity measurement. A Mercury barometer was used to indicate the atmospheric pressure in the laboratory. Considering the room temperature (T_r), the density of mercury (ρ_{Hg}) was calculated as,

$$\rho_{Hg} = 13556.786(1 - 0.0001818(T_r - 15.5556)), \quad \text{(D-25)}$$

The atmospheric pressure was calculated as,

$$p_{atm} = \rho_{Hg} \times g \times h_{Hg}, \quad \text{(D-26)}$$

where h_{Hg} is the height of the mercury column in the barometer and g is the gravitational acceleration, which was estimated according to Harris (2005),

$$\begin{aligned} g &= 9.78(1 + 0.0053 \sin^2 \varphi - 0.0000069 \sin^2 2\varphi) - 0.003086 H_{sea} \\ &= 9.8027 \, m^2 / s. \end{aligned} \quad \text{(D-27)}$$

where φ is the latitude and H_{sea} is the altitude above the sea level. For the city Windsor, φ = 42.3° and H_{sea} = 0.19 km (Weather Underground, 2005).

The density of airflow was calculated as,

$$\rho = \frac{p_{atm}}{R(T_a + 273.15)}, \quad \text{(D-28)}$$

where T_a is the temperature of airflow through the test duct, R is the gas constant of air with the value of 287.1 J/kg·K (Kuehn et al., 1998).

Since most experiments were run at the airflow temperature of 25-30°C and the barometric pressure around 750 mmHg, the room temperature (T_r) was found to be about 2°C lower than that of the airflow, probably due to heat transfer from the blower and friction between airflow and blower and duct walls. To simplify the process of the uncertainty analysis, $T_{a,\,max}$, $T_{a,\,min}$, and T_r were defined to be 30°C, 25°C and 25°C respectively. The atmospheric pressure and air densities were calculated according to Equation (D-25)-(D-28), as shown below,

$\rho_{Hg} = 13537.7\ kg/m^3$.

$p_{atm} = 99.53\ kPa$.

$\rho\ @25°C = 1.162\ kg/m^3$;

$\rho\ @30°C = 1.157\ kg/m^3$;

$\rho @27.5°C = 1.160\ kg/m^3$.

The relative uncertainty of air density was calculated according to Equation (D-6),

$$\frac{\Delta\rho}{\rho} = \pm\frac{|1.157 - 1.162|}{2\times 1.160} = \pm 0.22\%. \quad \text{(D-29)}$$

D.3.2 Uncertainty of the air dynamic viscosity

The minimum, maximum and mean values of air viscosity were taken from the property table (Munson et al., 2002) as follows,

$\mu\ @25°C = 1.85\times10^{-5}\ N.s/m^2$;

$\mu\ @30°C = 1.86\times10^{-5}\ N\cdot s/m^2$;

$\mu @27.5°C = 1.855\times10^{-5}\ N\cdot s/m^2$;

Thus, the relative uncertainty,

$$\frac{\Delta\mu}{\mu} = \frac{\left|1.85\times10^{-5} - 1.86\times10^{-5}\right|}{2\times 1.855\times10^{-5}} = \pm 0.27\%. \quad \text{(D-30)}$$

D.4 Propagation of uncertainties from independent to dependent variables

The uncertainties of the dependent variables were calculated according to the relationship with independent variables. The uncertainties associated with these dependent variables were estimated in the following subsections.

D.4.1 Uncertainty of the area of the square duct

The area of the square duct was calculated as,

$$A_{SD} = H_1 \times H_2 . \tag{D-31}$$

The calculated mean area of the duct was,

$$\overline{A_{SD}} = \overline{H_1} \times \overline{H_2} = 0.46222 \times 0.45799 = 0.2117\, m^2 . \tag{D-32}$$

According to Equation (D-5), the associated uncertainties was estimated as,

$$\begin{aligned} \Delta\left(\overline{A_{SD}}\right) &= \pm\sqrt{\left(\frac{\partial \overline{A_{SD}}}{\partial \overline{H_1}}(\Delta H_1)\right)^2 + \left(\frac{\partial \overline{A_{SD}}}{\partial \overline{H_2}}(\Delta H_2)\right)^2} \\ &= \pm\sqrt{(\overline{H_2} \times \Delta H_1)^2 + (\overline{H_1} \times \Delta H_2)^2} \\ &= \pm\sqrt{(0.45799 \times 0.00107)^2 + (0.46222 \times 0.00122)^2} \\ &= \pm 0.0011\, m^2 . \end{aligned} \tag{D-33}$$

the relative uncertainty,

$$\frac{\Delta\left(\overline{A_{SD}}\right)}{\overline{A_{SCD}}} = \pm\frac{0.0011}{0.2117} = \pm 0.52\% . \tag{D-34}$$

D.4.2 Uncertainty of Δp across the Venturi meter

The differential pressure across the Venturi meter was estimated as,

$$\Delta p = \rho_{fluid} \times g \times \ell \times r_{inclination}, \tag{D-35}$$

where ρ_{fluid} is the density of the fluid in the inclined manometer, its value is 827 kg/m^3; ℓ is the length of the fluid along the indication scale, $r_{inclination}$ is the inclination ratio of the fluid column, i.e. the ratio of the height to the length of the fluid column.

The relative uncertainty was calculated as,

$$\frac{\Delta(\Delta p)}{\overline{\Delta p}} = \sqrt{\left(\frac{\partial(\Delta p)}{\partial \ell}\right)^2} \Bigg/ \overline{\Delta p} = \frac{\Delta \ell}{\overline{\ell}} = \pm 0.5\% . \tag{D-36}$$

D.4.3 Uncertainty of the density correction factor C_ρ

The uncertainty of C_ρ was calculated based on the average air temperature of 30°C. According to Equation (D-5), (4-6) and (D-29), the uncertainty of C_ρ was estimated to be,

$$\begin{aligned}\frac{\Delta C_\rho}{C_\rho} &= \frac{\partial\left(\sqrt{\frac{\rho_{STP}}{\rho}}\right)}{\partial \rho} \Bigg/ \sqrt{\frac{\rho_{STP}}{\rho}} = -\frac{1}{2}\left(\frac{\Delta \rho}{\rho}\right) \\ &= -\frac{1}{2} \times (\pm 0.22\%) \\ &= \pm 0.11\% .\end{aligned} \tag{D-37}$$

D.4.4 Uncertainty of the reference flow rate using Venturi meter

The uncertainty of the reference volumetric flow rate using the Venturi flow meter and inclined manometer comes from two main sources: the error from the Venturi meter and the error propagated from the differential pressure (Δp) measured by the inclined manometer. The currently used Venturi meter was calibrated by the supplier with an accuracy of 0.75% of reading ($\frac{\Delta Q_{ven,cal}}{Q_{ven}}$). The error from Δp was calculated as follows.

The actual flow rate can be estimated in the form of the following expression according to Equation (4-3) and (4-5),

$$Q_{ven} = 0.03779 C_\rho \sqrt{\Delta p} . \tag{D-38}$$

According to Equation (D-5), the uncertainty of reference flow rate due to the indication of pressure difference ($Q_{ven,\Delta p}$) was calculated to be,

$$\begin{aligned}\frac{\Delta Q_{ven,\Delta p}}{Q_{ven}} &= \pm\frac{\sqrt{\left(\frac{\partial Q_{ven}}{\partial C_\rho}\Delta C_\rho\right)^2+\left(\frac{\partial Q_{ven}}{\partial(\Delta p)}\Delta(\Delta p)\right)^2}}{Q_{ven}} \\ &= \pm\sqrt{\left(\frac{\Delta C_\rho}{C_\rho}\right)^2+\left(\frac{\Delta(\Delta p)}{2(\Delta p)}\right)^2} \\ &= \pm\sqrt{(0.11\%)^2+(0.25\%)^2} \\ &= \pm 0.27\%.\end{aligned} \tag{D-39}$$

Thus the total uncertainty of the reference flow rate is,

$$\begin{aligned}\frac{\Delta Q_{ven}}{Q_{ven}} &= \pm\sqrt{\left(\frac{\Delta Q_{ven,cal}}{Q_{ven}}\right)^2+\left(\frac{\Delta Q_{ven,\Delta p}}{Q_{ven}}\right)^2} \\ &= \pm\sqrt{(0.75\%)^2+(0.27\%)^2} \\ &= \pm 0.8\%.\end{aligned} \tag{D-40}$$

D.4.5 Uncertainty of the average velocity in the square duct

The average velocity (U_{avg}) in the square duct can be estimated based on the reference flow rate measured by the Venturi meter and the area of the square duct; as shown below,

$$U_{avg} = \frac{Q_{ven}}{A_{SD}}. \tag{D-41}$$

According to Equation (D-6), the relative uncertainty was estimated as,

$$\frac{\Delta U_{avg}}{U_{avg}} = \sqrt{\left(\frac{\partial U_{avg}}{\partial Q_{ven}}\Delta Q_{ven}\right)^2 + \left(\frac{\partial U_{avg}}{\partial A_{SD}}\Delta A_{SD}\right)^2} \Bigg/ \frac{Q_{ven}}{A_{SD}}$$

$$= \sqrt{\left(\frac{\Delta Q_{ven}}{Q_{ven}}\right)^2 + \left(\frac{\Delta A_{SD}}{A_{SD}}\right)^2} \qquad \text{(D-42)}$$

$$= \sqrt{0.008^2 + 0.0052^2}$$

$$= 0.95\%.$$

D.4.6 Uncertainty of the hydraulic diameter

The hydraulic diameter can be calculated as,

$$D_h = \frac{2H_1H_2}{H_1 + H_2} = \frac{2}{\frac{1}{H_1} + \frac{1}{H_2}}. \qquad \text{(D-43)}$$

According to Equation (D-6)

$$\frac{\Delta D_h}{D_h} = \pm\frac{2\sqrt{\Delta H_1{}^2 + \Delta H_2{}^2}}{H_1 + H_2} = 0.35\%. \qquad \text{(D-44)}$$

D.4.7 Uncertainty of the Reynolds number

The Reynolds number in the square duct was calculated as,

$$Re = \frac{\rho U_{avg} D_h}{\mu_a}. \qquad \text{(D-45)}$$

According to Equation (D-6), the relative uncertainty of Re was calculated as,

$$\frac{\Delta Re}{Re} = \pm\sqrt{\left(\frac{\partial Re}{\partial \rho}\Delta\rho\right)^2 + \left(\frac{\partial Re}{\partial U_{avg}}\Delta U_{avg}\right)^2 + \left(\frac{\partial Re}{\partial D_h}\Delta D_h\right)^2 + \left(\frac{\partial Re}{\partial \mu}\Delta\mu\right)^2} \Bigg/ \frac{\rho\, U_{avg} D_h}{\mu}$$

$$= \pm\sqrt{\left(\frac{\Delta\rho}{\rho}\right)^2 + \left(\frac{\Delta U_{avg}}{U_{avg}}\right)^2 + \left(\frac{\Delta D_h}{D_h}\right)^2 + \left(\frac{\Delta\mu}{\mu}\right)^2} \qquad \text{(D-46)}$$

$$= \pm\sqrt{0.0022^2 + 0.0095^2 + 0.0035^2 + 0.0027^2}$$

$$= \pm 1.22\%.$$

D.5 Hot-wire measurement uncertainty

The uncertainty of the instantaneous velocities using the hot-wire measurement comes mainly from the process of calibrating the hot-wire sensor and acquiring the instantaneous velocity data. Furthermore, the uncertainties of the volumetric flow rate using the Equal Area and the Log-Tchebycheff method are also from the error of the square duct cross-sectional area. Details of each source of uncertainty were considered in the following sections.

D.5.1 Calibration uncertainty

The calibration uncertainty results mainly from three sources: namely, the uncertainty in the reference velocity U_R, which is obtained from the nozzle, the uncertainty in voltage reading, E_R, which corresponds to U_R, and the uncertainty from curve-fitting pairs of U_R and E_R values to the correlation of U~E. Note the U_R~E_R are discrete points at which the calibration is carried out whereas U~E presents a continuous correlation between the air velocity (U)and anemometer voltage (E).

According to TSI (2002(a)), the uncertainty for U_R, ΔU_R, is 0.5% of target velocity, the uncertainty of E_R is negligible. Following the work of Yavuzkurt (1984), the curve fitting uncertainty is found to be,

$$(\Delta U_{eff})_{cf} = \zeta U_{eff}, \tag{D-47}$$

where U_{eff} is the effective velocity calculated from the calibration equation, the coefficient ζ can be calculated from a typical curve fitted data as,

$$\zeta = \sqrt{\frac{1}{N}\sum_{i=1}^{N}\left(\frac{U_{eff,i} - U_R}{U_{eff,i}}\right)^2} = 0.012. \tag{D-48}$$

Thus the calibration uncertainty was calculated to be,

$$\left(\frac{\Delta U}{U}\right)_{cal} = \sqrt{\left(\frac{\Delta U_R}{U_R}\right)^2 + \zeta^2} = 1.3\%. \tag{D-49}$$

D.5.2 Incoming velocity uncertainty

Since the incoming flow has some fluctuations, in order to estimate this uncertainty, 20 times repeated measurements at a typical measurement location were carried out by the hot-wire system with all conditions remaining the same. The standard deviations of the time-mean velocities were computed. The incoming velocity uncertainty for U was estimated as 2 times of the standard deviation and resulted in,

$$\left(\frac{\Delta U}{U}\right)_{incoming} = \pm 0.43\%. \tag{D-50}$$

D.5.3 Total uncertainty in the time-mean velocity

The total uncertainty in U was acquired by combining Equation (D-49) – (D-50) as expressed below,

$$\frac{\Delta U}{U} = \pm\sqrt{\left(\frac{\Delta U}{U}\right)_{cal}^2 + \left(\frac{\Delta U}{U}\right)_{incoming}^2}$$
$$= \pm\sqrt{0.013^2 + 0.0043^2} \qquad \text{(D-51)}$$
$$= \pm 1.32\%.$$

D.5.4 Uncertainty of the volumetric flow rate using the Equal Area and the Log-Tchebycheff methods.

The volumetric flow rate using the Equal Area (Q_{EA}) or the Log-Tchebycheff methods (Q_{LT}) can be calculated as,

$$Q_{EA} = U_{EA} A_{SD}, \qquad \text{(D-52)}$$

$$Q_{LT} = U_{LT} A_{SD}, \qquad \text{(D-53)}$$

where U_{EA} and U_{LT} are the spatial average velocities of the cross section using the Equal Area and the Log-Tchebycheff methods respectively. Their uncertainty was estimated as follows.

D.5.4.1 The uncertainty of the traverse location

The relative origin of the automatic traversing mechanism was setup at the upper-left corner with 0.03 mm normal distance to duct walls. Two holes were drilled on both the top and left walls to specify the probe location. However, the misalignment between the traversing mechanism and the duct may result in inaccurate locations for traverse points when the probe moves to right and bottom sides. In some situation, the readjusting of the duct or the traversing mechanism is needed. In the experiment, when the relative origin was setup, the hot-wire probe was moved to other corners with a specified distance controlled by the automatic traversing mechanism and the computer, a ruler was used to

check the distance between the probe and the nearest walls on both horizontal and vertical directions. Their accuracies was maintained within ± 0.003 m with respect to the expected locations, otherwise readjustment was carried out. Thus the traverse location uncertainty was ± 0.003 m.

D.5.4.2 The velocity spatial uncertainty

According to the measured velocity profiles at 6.5 D_h or 9.5 D_h, there is higher velocity gradient in the near-wall region than in the central region. Figure 5.23 and 5.24 shows that there are 12 outmost points for the Equal Area method and 16 points for the Log-Tchbycheff methods located in the near-wall region with relatively high gradients. The velocity spatial uncertainty due to the point location errors for these points are higher than those in the central region with relatively lower velocity gradients. Based on a typical velocity profile, the point velocity uncertainty due to the location error in the central region was calculated to be 0.6%. i.e.

$$\left(\frac{\Delta U}{U}\right)_{spatial,c} = 0.6\%. \tag{D-54}$$

According to the measured velocity profiles, those outmost points have a higher velocity spatial uncertainty with the same location uncertainty of ± 0.003 m. To simplify the process, all the 12 outmost traverse points for the Equal Area method were considered to have a same velocity spatial uncertainty $\left(\left(\frac{\Delta U}{U}\right)_{spatial,b,EA}\right)$. At a typical flow condition, the traversing point on the upper-left corner of the cross section according to the Equal Area method was measured, at the same time, two points with both 0.003 m

distance from that traverse points were measured. Several such tests were carried out and the velocity spatial uncertainty was calculated to be,

$$\left(\frac{\Delta U}{U}\right)_{spatial,b,EA} = 1.7\%. \tag{D-55}$$

Similarly, the velocity spatial uncertainty for those 16 outmost traverse points for the Log-Tchebycheff method $\left(\left(\frac{\Delta U}{U}\right)_{spatial,b,LT}\right)$ were tested and calculated to be,

$$\left(\frac{\Delta U}{U}\right)_{spatial,b,LT} = 2.2\%. \tag{D-56}$$

D.5.4.3 The velocity spatial uncertainty for the average velocity

According to the Equal Area and the Log-Tchbycheff methods, the average velocity of the cross section (U_{avg}) was the arithmetic average of the velocities of all the traverse points. Thus the total velocity spatial uncertainty for the Equal Area method was calculated to be,

$$\begin{aligned}\left(\frac{\Delta U}{U_{avg}}\right)_{spatial,EA} &= \sqrt{\left(\frac{\Delta U_1}{U_{avg}}\right)^2 + \left(\frac{\Delta U_2}{U_{avg}}\right)^2 + \ldots\ldots \left(\frac{\Delta U_{16}}{U_{avg}}\right)^2} \\ &= \sqrt{\frac{12}{16}0.017^2 + \frac{4}{16}0.006^2} \\ &= 1.5\%.\end{aligned} \tag{D-57}$$

Similarly, the spatial uncertainty for the Log-Tchebycheff method was calculated to be,

$$\left(\frac{\Delta U}{U_{avg}}\right)_{spatial,LT} = \sqrt{\left(\frac{\Delta U_1}{U_{avg}}\right)^2 + \left(\frac{\Delta U_2}{U_{avg}}\right)^2 + ...\left(\frac{\Delta U_{25}}{U_{avg}}\right)^2}$$

$$= \sqrt{\frac{16}{25}0.017^2 + \frac{9}{25}0.006^2} \qquad \text{(D-58)}$$

$$= 1.8\%.$$

The average velocity for the Equal Area and the Log-Tchebycheff methods was,

$$\frac{\Delta U_{EA}}{U_{EA}} = \sqrt{\left(\frac{\Delta U}{U}\right)^2 + \left(\frac{\Delta U}{U_{avg}}\right)^2_{spatial,EA}} = \pm 2\% \ . \qquad \text{(D-59)}$$

$$\frac{\Delta U_{LT}}{U_{LT}} = \sqrt{\left(\frac{\Delta U}{U}\right)^2 + \left(\frac{\Delta U}{U_{avg}}\right)^2_{spatial,LT}} = \pm 2.3\% \ . \qquad \text{(D-60)}$$

D.5.4.4 The uncertainty of the volume metric flow rate according to the Equal Area and the Log-Tchebycheff methods

According to Equation (D-6), the uncertainty of Q_{EA} and Q_{LT} was calculated as,

$$\frac{\Delta Q_{EA}}{Q_{EA}} = \sqrt{\left(\frac{\Delta U_{EA}}{U_{EA}}\right)^2 + \left(\frac{\Delta A_{SD}}{A_{SD}}\right)^2}$$

$$= \sqrt{(2\%)^2 + (0.52\%)^2} \qquad \text{(D-61)}$$

$$= 2.1\%.$$

$$\frac{\Delta Q_{LT}}{Q_{LT}} = \sqrt{\left(\frac{\Delta U_{LT}}{U_{LT}}\right)^2 + \left(\frac{\Delta A_{SD}}{A_{SD}}\right)^2}$$

$$= \sqrt{(2.3\%)^2 + (0.52\%)^2} \qquad \text{(D-62)}$$

$$= 2.4\%.$$

D.6 Uncertainty of the point velocity using the hand-held anemometer

A TSI 8345 hand-held thermal anemometer was used to measure the time mean velocity within the duct and compare with that measured by the hot-wire system. Its uncertainty comes mainly from the velocity reading and the anemometer positioning errors. The details are as follows,

D.6.1 Uncertainty of the point velocity indicated by the anemometer

The accuracy of the anemometer is ±3% of the reading. In absence of the resolution, the instrumental error could be considered as the bias error, i.e.,

$$B_{anemometer} = 0.03U\,. \tag{D-64}$$

Based on the responses of the last digit of the velocity meter, a digital error of $P_{digit} = \pm 0.05\ m/s$ was introduced as a precision error. In addition, a readability error of $P_{read} = \pm 0.05\ m/s$ was also introduced. Thus the total error related to the indication uncertainty of the anemometer at the velocity of 5 *m/s* was estimated as,

$$\begin{aligned}\left(\frac{\Delta U}{U}\right)_{indication} &= \sqrt{B_{anemometer}{}^2 + P_{digital}{}^2 + P_{read}{}^2}\,/U \\ &= \sqrt{(0.03\times 5)^2 + 0.05^2 + 0.05^2}\,/5 \\ &= 3.32\%.\end{aligned} \tag{D-65}$$

D.6.2 Anemometer spatial uncertainty

The probe spatial uncertainty was estimated by resetting the anemometer to a typical measurement position for 20 times with all the other test conditions remaining the same. Each time, a reading of the time-mean velocity was acquired. The probe spatial uncertainty was estimated as 2 times the standard deviation, as shown below,

$$(\Delta U)_{spatial} = 0.049U\,. \tag{D-66}$$

D.6.3 Total uncertainty for the hand-held anemometer

Same as in D. 5.2.1, an incoming velocity uncertainty was introduced as below,

$$\Delta U_{incoming} = \pm 0.0043U\,. \tag{D-67}$$

Thus the total uncertainty of the time-mean velocity using the hand-held anemometer was estimated as,

$$\begin{aligned}\frac{\Delta U}{U} &= \pm\sqrt{\left(\frac{\Delta U}{U}\right)^2_{indic} + \left(\frac{\Delta U}{U}\right)^2_{spatial} + \left(\frac{\Delta U}{U}\right)^2_{incoming}} \\ &= \pm\sqrt{(0.0332)^2 + (0.049)^2 + (0.0043)^2} \\ &= \pm 5.93\%.\end{aligned} \tag{D-68}$$

VITA AUCTORS

1971	Born in Yichang, China.
1990	Completed high school at Yichang No. 1 High School, Yichang, China.
1994	Received Bachelor of Science Degree at Huazhong University of Science & Technology, Wuhan, China.
2005	Currently a candidate for the degree of Master of Applied Science in Mechanical Engineering at University of Windsor, Windsor, Ontario, Canada.